A Methodology for Numerical Prototyping of Inflatable Dunnage Bags

by

Martin Philip Venter

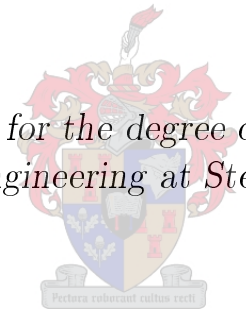

Dissertation presented for the degree of Doctor of Philosophy in the Faculty of Engineering at Stellenbosch University

Promoter: Prof G Venter

March 2015

Declaration

By submitting this dissertation electronically, I declare that the entirety of the work contained therein is my own, original work, that I am the sole author thereof (save to the extent explicitly otherwise stated), that reproduction and publication thereof by Stellenbosch University will not infringe any third party rights and that I have not previously in its entirety or in part submitted it for obtaining any qualification.

Date: .....

Abstract

Dunnage bags are an inflatable dunnage variant, positioned and inflated between goods in multi-modal containers to restrain and protect the goods while in transit. This project endeavours to develop a simple method of generating new numerical prototypes for dunnage bags suitable for simulating operational loading of the bags. Previous research has produced a model that simulates the inflation of a paper dunnage bag using a simple pressure load.

A dunnage bag reinforced with plain-woven polypropylene was chosen as the test case. Woven polypropylene is a highly non-linear, non-continuous, non-homogeneous material that requires specialised material models to simulate. A key aspect of this project was to develop a simple method for characterising woven-polypropylene and replicating it's response with material models native to LS-DYNA. The mechanical response of the plain-woven polypropylene was tested using a bi-axial tensile test device. The material response from physical testing was then mapped to two material models using the numerical optimiser LS-OPT. The response of the calibrated material models was found to correlate well with the measured response of the woven material.

Dunnage bags are subjected to cyclic loading in operation. In order to capture the effects of compressing the contained gas, a gas inflation model was added to the model that calculates the pressure in the bag based on the Ideal Gas Law. A full bag model making use of the calibrated material models and the inflation model was subjected to a cycled boundary condition simulating loading and unloading of an inflated dunnage bag. The two prototype models captured the pressure drop in the bag due to material plastic deformation and the restraining force produced by the bag to within 10 %. The prototype models were also found suitable for predicting burst pressure in voids of arbitrary size and shape.

Opsomming

Stusakke is 'n opblaasbare soort stumateriaal wat tussen goedere in multimodale vraghouers geposisioneer en opgeblaas word om sodoende die goedere vas te druk en te beskerm tydens vervoer. Hierdie projek poog om 'n eenvoudige manier te ontwikkel om nuwe numeriese prototipes vir stusakke, geskik om operasionele lading van die sakke te simuleer, te ontwikkel. Vorige navorsing het 'n model ontwikkel wat die opblaas van 'n papier stusak met eenvoudige drukkrag simlueer.

'n Hoë-vlak stusak versterk met plein-geweefde polipropileen, is gekies om getoets te word. Geweefde polipropoleen is 'n hoogs nie-lineêre, onderbroke, nie-homogene materiaal wat gespesialiseerde materiaalmodelle nodig het vir simulasie. Een van die fokuspunte van hierdie projek is om 'n eenvoudige metode te ontwikkel om die karaktereienskappe van polipropoleen te identifiseer en die gedrag daarvan na te maak met die materiaalmodelle van LS-DYNA. Die meganiese reaksie van die plein-geweefde polipropoleen is getoets met 'n biaksiale/tweeassige trektoets-toestel. Die materiaal se reaksie op die fisiese toets is ingevoer op 'n numeriese optimiseerder, LS-OPT, om op die materiaalmodelle te toets. Die reaksie van die gekalibreerde materiaalmodelle het goed gekorelleer met die gemete reaksie van die geweefde materiaal.

Stusakke word tydens diens onderwerp aan sikliese lading. Om die effek van die saamgepersde gas vas te stel is 'n gas-opblaasbare model bygevoeg by die model wat die druk in die sak bereken, soos gebaseer op die Ideale Gas Wet. 'n Volskaalse sakmodel wat gebruik maak van die gekalibreerde materiaalmodelle en die opblaas-model is onderwerp aan sikliese grensvoorwaardes wat die lading en ontlading van 'n opblaasbare stusak simuleer. Die twee prototipe modelle het die drukverlies in die sak a.g.v. die materiaal-plastiek vervorming en die bedwingingskrag van die sak beperk tot 10 %. Die protoyipe modelle is ook geskik bevind om barsdruk in arbitrêre leemtes te voorspel.

Acknowledgements

I would like to express my sincere gratitude to the following people and organisations ...

Stopak Pty for sponsoring the project, the Technology and Human Resources For Industry Program for their financial support, Livermore Software Technology Corporation for software licenses and, Ferdi Zietsman and the Mechanical Engineering Workshop staff for their patience and advice.

Contents

List of Figures

List of Tables

Chapter 1

Introduction and Project Outline

In 2008 the Department of Mechanical and Mechatronic Engineering at Stellenbosch University was approached by Stopak Pty to perform a numerical analysis of their inflatable dunnage bag products. The Cape Town based manufacturer was looking to begin building a knowledge base for their existing products that would provide an advantage in the development of future products. Over time they would extend their research from commercial dunnage to their other products used to support the transportation industry. As such a collaborative project involving Stellenbosch University has been undertaken with research beginning in 2009.

1.1 Dunnage and Dunnage Bags

Dunnage, in its various forms, are products used to protect and secure goods. Dunnage fills voids, protects from moisture, separates items and restrains the movement of goods. Figure 1.1 shows three common types of dunnage. Processed wood boards are stacked and separated using timber dunnage, raising the wood boards off the ground and increasing airflow through the stack, figure 1.1(a). Steel rollers and large pipes are packaged and shipped using shaped cradle dunnage, figure 1.1(b). Goods transported in a multi-modal container are protected by inflatable dunnage bags, figure 1.1(c). Figure 1.2 shows a woven polypropylene dunnage bag manufactured by Stopak Pty.

1.1.1 Characteristics of Inflatable Dunnage Bags

Dunnage bags are pillow shaped inflatable tensile structures that use a contained gas volume to pre-tension the load bearing structure. Inflatable dunnage has several advantages over conventional solid dunnage. These include;

- Lightweight, low volume construction, with a high stowed to deployed volume ratio.

(a) Timber dunnage (b) Cradle dunnage (c) Inflatable dunnage

Figure 1.1: Common dunnage types

Figure 1.2: Inflated dunnage bag manufactured by Stopak Pty.

- A wide range of voids can be filled, including voids with dimensions that are not known before products are packed.
- Restraining loads are more evenly distributed because the bag moulds to the shape of the void it fills.
- Additional attachment points are not required, reducing the labour required to deploy the bags.
- Inexpensive commodity grade, recyclable materials can be used to manufacture the bags.
- Materials used to manufacture dunnage bags are not subject to the same customs restrictions as organic dunnage, such as wood and paper.

Dunnage bags are cheaper to manufacture and transport. They are easier, cheaper and faster to deploy, while still providing better protection than conventional solid dunnage.

1.1.2 Dunnage Bag Deployment and Operation

When multi-modal containers are loaded there are often voids left between the container and the goods or boxes. If these voids are allowed to remain the goods will have space to move relative to each other. Hard braking or turning could throw products against each other damaging their packaging or the products themselves.

Once goods have been packed into a container dunnage bags are positioned in the voids between the goods and deployed. The bags are inflated to a desired working pressure and sealed with a fixed mass of air contained within the bag. As the bag is filled it presses against the bounds of the void producing a restraining force proportional to the relative pressure inside the bag. The compressed gas is used as a preloaded spring capable of forcibly returning goods to their original position after an impact has dislodged them.

The bag is physically soft allowing a degree of flexibility to conform to the shape of the void into which it is inflated. This means that the shape and size of the void does not need to be accounted for beforehand to ensure sufficient contact area between the restraining dunnage bag and goods. Dunnage bags are typically used in parallel voids. Figure 1.3 shows positioning and use of several bags in a single container.

Figure 1.3: Multiple dunnage bags used to restrain boxes in a multi-modal container

The operating envelope for most dunnage bags is to fill voids with a maximum contact area of 3 m by 2 m and a maximum prescribed void of 300 mm. Working pressures are typically lower than 100 kPa when inflated. The restraining force can exceed 300 kN, depending on the contact area between the bag and the goods it is restraining.

1.1.3 Dunnage Bag Construction

Dunnage bags have a layered construction and are assembled with three major components shown in figure 1.4: A compliant airtight bladder, a non-return valve and a reinforcing cover with a punched hole for the valve. Dunnage bag covers are manufactured from either kraft paper or plain woven polypropylene. Both the kraft paper and woven polypropylene covers are formed as a tube. The polypropylene cover is woven as a continuous tube while the paper covers are folded into a tube and glued, producing a longitudinal seam. Both cover types are folded flat and either glued or sewn along the remaining open ends of the tube.

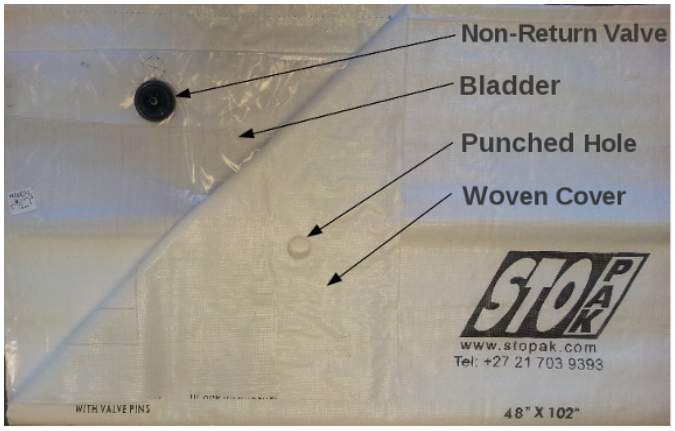

Figure 1.4: Layered construction of an inflatable dunnage bag, bladder, non-return valve and woven polypropylene cover

1.2 Summary of Previous Research

Initial research was centred around analysing the operational stress and strain pattern of a pillow type paper dunnage bag, Venter (2011). The numerical model produced was validated against the results of physical testing. On completion of the first phase of the project in early 2011, a suitable model had been developed. The numerical model was developed for LS-DYNA (Hallquist (2006)) and took into consideration the average geometry of the paper bag, various bag dimensions, material thickness, internal pressure loading, contact with a restraining void, various void sizes, glued seam lines and the rigid valve. The model was then used to investigate the inflated shape of a paper bag as well as regions of failure including high stress areas around the valve.

The research focused on the creation of a stable numerical simulation of an inflated dunnage bag. Several problems were uncovered in this process. Problems associated with the simulation of a dunnage bag were found to be

the large changes in geometry associated with the unknown ultimate shape of the inflated bag, changes in contact conditions and the non-linear nature of the reinforcing materials properties. Model stability, sensitivity to Poisson's ratio and the effect of mass scaling were addressed in the model development.

A series of physical tests was performed with two material thickness values (1 ply and 2 ply paper), four bag sizes (2.2 × 0.9 m, 2.2 × 1.2 m, 1.2 × 1.2 m and 0.9 × 0.9 m) and inflated at three void sizes (unconstrained, 300 mm and 150 mm). Each of these physical tests were matched by a numerical model using an isotropic elastic-plastic material model with kinematic hardening.

The results show a strong correlation between the measured and simulated restraining force, and the stress pattern observed in the numerical simulation was similar to those in literature on plate deformation. No empirical stress or strain results were available for comparison due to the nature of the thin flexible material. Research by this group and others show that the outer reinforcement layer of a dunnage bag is predominantly in tension and should be considered a tensile structure. Figure 1.5 shows a comparison of a simulated and tested paper dunnage bag. The earlier project resulted in a thesis, Venter (2011), and a journal publication, Venter and Venter (2012).

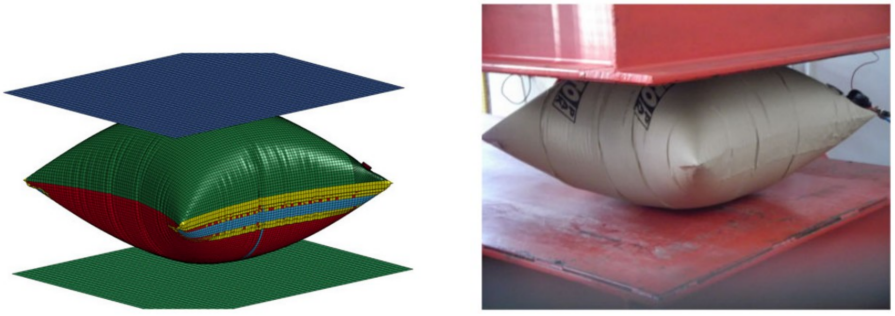

(a) Paper bag simulation (b) Paper bag test

Figure 1.5: Simulated and test paper bags from previous research

1.3 Overview of Presented Research

This project focused on the development of a methodology that can produce a numerical prototype of a dunnage bag that can simulate a real-world load application, suitable for full scale design and testing of new dunnage bag products.

1.3.1 Project Scope

This project straddles several engineering fields. This project endeavours to simulate cyclic testing of the woven polypropylene reinforcing cover of an inflated dunnage bag. The following features are required to realise such a model:

- The numerical model will include the reinforcing cover of woven polypropylene dunnage bags, but not the internal bladder or inflation valve.
- The plain woven polypropylene material will be parametrised in terms of simple engineering properties.
- The compressible nature of the inflation gas will be accounted for, but not the gas dynamics and flow during inflation.
- The void into which the bag is inflated will have variable sizes and profiles that can be dynamically controlled.
- Material changes can include: elongation, thickness and stiffness.
- Bag shapes may be varied in their un-inflated state corresponding to manufacturing tolerance variations and desired design changes.
- Temperature and strain-rate effects are not considered in the material properties.
- Failure and post failure behaviour are beyond the scope of the project.

All testing should be simple and inexpensive and the simulations should make use of commercially available software.

1.3.2 Project Objectives

The objectives for this project can be stated as follows:

1. Develop a test method for characterising plain woven polypropylene.
2. Parametrise woven polypropylene in terms of engineering parameters and select an appropriate material model.
3. Find a method accounting for the work done by the inflation gas under loading.
4. Build a numerical model of an inflatable dunnage bag under cyclic loading.
5. Simulate a certification test for dunnage bags and validate the results with physical testing.
6. Capture the pressure and load drop observed as a result of cyclic overloading of the dunnage bag.

1.3.3 Outline of Research Presented

Following the recommendation of our industry partner the standard test bag chosen for this research is a 48 x 102 inch (1.219 x 2.59 mm) Level 3/4 bag subject to regulation by the Association of American Railroads (AAR). Dunnage bags are classified into five regulated categories, a level 3/4 bag has passed both level 3 and 4 classification. The research conducted for this project is presented as follows:

Chapter 2 gives a short overview of where dunnage bags fit into the various engineering fields borrowed from in this thesis. Chapter 3 gives a short overview of polypropylene and woven textiles, covers the various tests suitable for swatch testing of these materials, discusses a few material homogenisation techniques and available material models. Chapter 4 covers the mechanical testing of woven polypropylene swatches with descriptions of the data processing and interpretation, while chapter 5 describes the parametrization of the material models to match the tested data.

Chapter 6 summarises the available inflation methods and describes the model selected for this research. Chapter 7 covers in detail the full bag model and the test case described by the AAR. Results of physical cyclic bag tests are compared with those produced by the numerical models and the ability of the model to match the results for a representative loading is evaluated. The model's ability to predict failure is discussed in chapter 8.

The research is concluded in chapter 9 with recommendations for future work discussed in chapter 10.

Chapter 2

Dunnage Bags in Context

Although dunnage bags are the focus of this research, there is little literature currently available that directly addresses the simulation or design of inflatable dunnage bags. The literature search was thus extended to include a general study of adjacent research fields. Tensile structures and their related technologies were found to be suitably similar to be used as a starting point for the research conducted here. This chapter provides a brief introduction to tensile structures with an emphasis on inflatable and pressure rigidized structures, air-beams and Tensairity as the most relevant literature surveyed. Literature pertaining to polypropylene, woven textile fabric, homogenisation techniques, photogrammetry and inflation models are covered in detail in later chapters.

2.1 Tensile Structures

Structures where the pre-tensioning of materials is the primary mechanism through which stability and stiffness are attained are known as tensile structures. Tensile components are a construction medium with increasing popularity in areas of design where low manufacturing cost, low weight and a limited life-span are a concern, Luchsinger *et al.* (2004*a*). Tensile structures have grown in popularity in fields ranging from civil engineering and architecture to aerospace engineering. Following this growth in popularity more research is being done on the design, analysis, construction and maintenance of tensile structures. Examples of tensile structures include roofs, coverings, sails, inflated buildings, airships, furniture and air-foils.

The tensile structures of interest here are commonly constructed of thin woven textile composite membranes, where the structural integrity is derived from the continuous state of tension in the structure. On the scale evaluated here most construction materials used will have a low bending stiffness relative to the in-plane strength and are considered to be membranes, not supporting out of plane loading. The disadvantage of using membranes is that they cannot maintain any compressive loads. To generate a state of tension in a structure

using either the membranes or cables there must be a compression element to balance the load. Compression elements are typically rigid struts or mounting points. Inflation can also be used to tension structures that have an internal cavity where the compression element replaced by compressed air in the cavity. Whether compressed gas, rigid struts or fixed mounting points are used the structure can be strengthened by the constructive separation of tension and compression as discussed by Fuller (1975).

Maurin and Motro (2005) state that ideally, a tensile structure should be designed to have no areas that undergo compression. In thin flexible membranes these regions of compression manifest as wrinkles, indicating that the material is no longer being optimally used. In some cases these regions can cause the entire structure to lose stability and fail. From Bletzinger *et al.* (2007), Cerda and Mahadevan (2003) and Stein and Hedgpeth (1961) it can be seen that either a large bi-axial tension ratio or high degree of shear loading can be a root cause of wrinkling in a tensile structure. Blandino *et al.* (2002) and Wong and Pellegrino (2005) show an example of the wrinkling caused by symmetric in-plane loading of a square membrane. Wong and Pellegrino (2006) and Wang *et al.* (2007) show methods of simulating wrinkling numerically and using numerical simulation to predict wrinkling. Each of these papers note the negative effects of wrinkling on the effectiveness of material usage and structural stability, highlighting the need to ensure that the material is optimally loaded.

According to Wagner (2008), in nature there are two means of opposing load. A structure can have a high stiffness and a low deflection or a low stiffness and a high deflection. In the case of large deflection, the stress in the structure is reduced and the material is used more efficiently, leading to a lighter structure. Luchsinger *et al.* (2004*a*) restates that pure tension is the most efficient use of material to bear load. Under pure tension, the maximum load is only dependent on component failure stress and cross sectional area. Compressive components, however, are often subject to failure due to geometric rather than material considerations.

The design procedure for tensile structures is of interest in this project as the ultimate use of the models developed here will be to prototype and design new bags. In this regard Wagner (2005) and Moncrieff (2005) reduce the design of tensile structures to five elements. Wagner (2005) describes a design process while Moncrieff (2005) describes a set of deliverables, Table 2.1.

The two processes described are similar and differ only in the order in which the design is approached. The deliverables defined by Moncrieff (2005), unlike Wagner (2005), shows the calculation of the reaction forces based on the ideal tensioned geometry. The method proposed by Wagner (2005) is of more practical use in cases where the design is subject to practical limitations, because the analysis will provide information on the actual design over the ideal design. Dunnage bags are subject to limitations in their shape determined by the tubular woven material they are constructed from. Both papers state

Table 2.1: Design methods for tensile structures

Wagner (2005)	Moncrieff (2005)
Shape definition	Surface geometry
Development of a cutting pattern	Reaction, support and cable forces
Reassembly of pre-tensioned structure	Textile shear and axial stress
Analysis of structural behaviour	Cutting pattern
Evaluation of the structure	Support structure

that the material properties and seam locations have a significant effect on the stress state of the tensile structure, noting again the detrimental effects of shear in the structure, especially in the vicinity of the seams. With this in mind, the procedure proposed by Wagner (2005) will provide a more accurate analysis phase as it is conducted on a model that takes into account the effect of material orientation and seams.

Wagner (2005) also proposes that the load bearing characteristics of a tensile structure be considered in terms of the desired flexibility of the structure, magnitude of the pretension relative to external loads, orientation of cables and yarns, degree of surface curvature and material stress-strain behaviour. Each of these parameters must be investigated to fully develop a new tensile structure. Following this recommendation woven propylene dunnage bags are highly flexible, high tension structures with yarns in a fixed orientation defined by the material manufacturing restrictions and a degree of curvature defined by the diameter of the bag or the void into which it is inflated. The material is often loaded near its failure limit requiring an investigation into the full non-linear material response.

Linhard *et al.* (2008) discusses the need for a better method of accounting for the inherent non-develop-ability of doubly-curved tensile structures from flat sheet material. The design of double curvature tensile structures require accurate simulation of the material strain in order to determine the best positions for seams, but the difference in the positions of the seams in the ideal structure and a structure manufactured from flat cut components can lead to a miss-match in the two models. This paper presents a method of coupling the shape generation and cutting pattern selection to the FEA to improve the stress prediction of the numerical models. This method uses the cutting pattern to generate the form of the structure as opposed to using the ideal structure to define the cutting pattern. This clearly shows the contrast between the design methods proposed by Wagner (2005) and Moncrieff (2005). A useful observation from this paper is that anticlastic (Chinese hat shaped) structures manufactured from flat sheets have stress peaks along their seams while synclastic (dome shaped) structures have stress peaks in the middle of the material strip, figure 2.1.

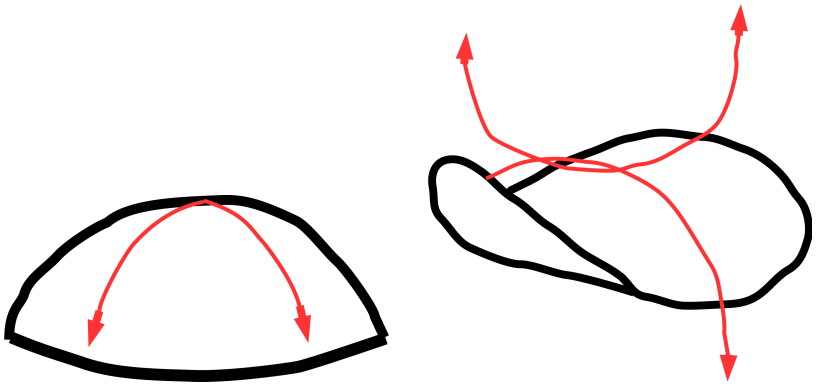

(a) Synclastic curvature (b) Anticlastic curvature

Figure 2.1: Classification of curvature types. Red lines are used to highlight orthogonal lines of curvature for each shape.

2.2 Pressure Rigidized and Inflatable Structures

Kröplin (2005) classifies inflatable tensile structures into four categories. Type one, permanent membrane structures with external pretension, are erected by cables, struts and bearings, figure 2.2(a). Type two, permanent and temporary membrane structures with inflated walls use a pressure ridgidized wall for structural stability; that is, the main volume is not under pressure, figure 2.2(b). Type three, membrane structures with full gas volumes, the main volume is pressurized to give the structure stability, figure 2.2(c). Type four, buoyancy structures use a density difference between the internal and external fluid as the means of structural support, figure 2.2(d). Using these classifications, an inflatable dunnage bag is considered a type three inflatable tensile structure. Other type three tensile structures include air-bags, air-beams and Tensairity structures.

Cavallaro (2006) describes the advantages of structures that are supported or tensioned by an internal fluid or gas volume as light weight, rapidly self erecting, highly mobile, large stowed to deployed volume ratio and no catastrophic failure. Dunnage bags, however, have been shown to fail catastrophically on many occasions.

Luchsinger *et al.* (2004*b*) describes developments in pressure rigidized structures and notes that in order to maintain the shape of a smaller structure a higher pressure is required. Luchsinger *et al.* (2004*b*) agrees with the advantages described by Cavallaro (2006), and notes that typical disadvantages include form restrictions and load limitations, including those described by Linhard *et al.* (2008). The form restrictions of inflated structures can be addressed by the addition of external cables and internal webs, which can be used to create air-chambers and hold shape in critical areas.

(a) Permanent membrane structures with external pretension

(b) Permanent and temporary membrane structures with inflated walls

(c) Membrane structures with full gas volumes

(d) Buoyancy structures

Figure 2.2: Classifications for inflatable structure

Tarczewski (2005) states that structural concepts of pre-tensioning, modular construction and post tensioning can be applied to inflatable tensile structures. Pronk and Houtman (2005) state that the inflated, or pre-tensioned shape of an inflatable structure can be manipulated in three ways, namely by changing the un-inflated shape, adding tension cables and internal compartments. In the construction of dunnage bags there is limited scope to change the un-inflated structure and it is not feasible to add internal compartments due to the additional manufacturing costs. The addition of tensioned cables is as yet unexplored.

Stimpfle (2008) covers the nature of air supported structures. If a membrane is assumed to be a 2D structure in 3D space, the state of stress in a section can be described by two planar axes, x and y. The relationship between the internal pressure, p, the material stress, σ, and the radius of curvature, r, is described as:

$$p \propto \frac{\sigma_x}{r_x} + \frac{\sigma_y}{r_y} \tag{2.2.1}$$

This relationship shows that for a given design stress, as the radius of curvature increases, the curvature of the structure decreases and the maximum pressure that can be contained decreases. This is a similar relationship to that which describes the state of stress in a thin walled pressure vessel. It

then follows that an increase in the curvature of a bag will increase the burst pressure.

Figure 2.3 shows the planar axis on a membrane subjected to a pressure load with boundary conditions representative of those applied to a swatch at the mid-span of an inflated bag. Considering the stress relationship presented by Stimpfle (2008) and figure 2.4 the following two assertions are made: $T \propto p$ and $T \propto r$. Where T is material tension, p is pressure and r is radius of curvature. In the context of a dunnage bag the material load due to tension can be reduced if either the internal pressure or the radius of curvature is reduced. The pressure is required to maintain the restraining force leaving only the radius of curvature of the inflated bag to be modified when designing new bags. An example of this phenomenon is that experimental data shows bags inflated into smaller voids burst at a higher pressure as a result of the reduced radius of curvature in the unsupported regions of the bag, Venter (2011).

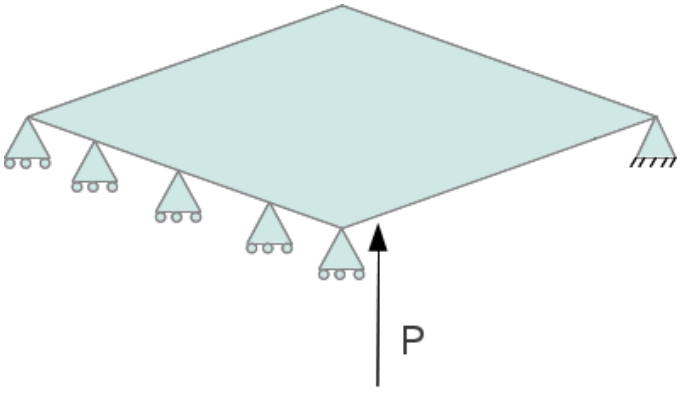

Figure 2.3: A membrane subjected to a pressure load with simple boundary conditions representative of a swatch at the mid-span of an inflated bag

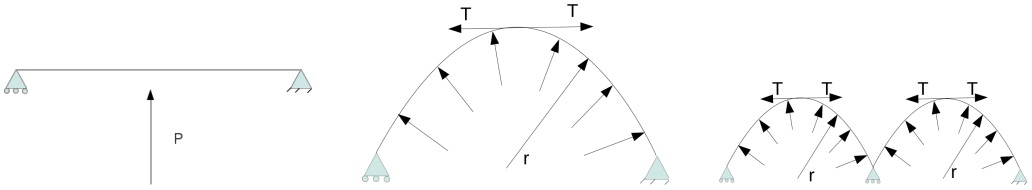

(a) 2D load case for pressure loading of a membrane

(b) Pressure load on a 2D membrane

(c) Pressure load on a 2D membrane where the radius of curvature is halved

Figure 2.4: Relationship between internal pressure, curvature and material tension

Maurin and Motro (2005) also note that in the case of normal pressure the directions of maximum stress correspond with the directions of maximum curvature radius in the membrane.

A critical component in the design of tensile structures is the numerical analysis of the structure. Pedretti (2004) states that although analytical solutions for inflated structures are useful for understanding their mechanics, in general finite element analysis is required to investigate these structures. This is confirmed by Pauletti (2008) who states that the geometric non-linearities presented by taut structures usually overrules the use of analytical solutions.

A description of the simulation of a fluid-supported membrane using finite element methods is given by Rumpel *et al.* (2005). The authors note that the inflation and support of a membrane can be effectively modelled using a pressure load on the inner surface of the structure. For many types of simulations this model is sufficient, but it cannot take into account the change in volume experienced by the structure under loading, as noted by Haßler and Schweirzerhof (2008). The effect of this volume can be achieved by defining a control volume bounded by the inner surface of the structure and supplying an equation of state (EOS) to describe the load applied by that volume onto the surface. The addition of a gas fill described by an EOS increases the model stability even though the gas is not discretized.

The simulation of a slowly inflated membrane is described by Jetteur and Bruyneel (2008). For extremely thin shells, as is the case for the simulation of dunnage bags, the stiffness of nodes in translation is orders of magnitude greater than that of rotation, which leads to a type of numerical instability. This can be overcome by the use of shell elements with no rotational degrees of freedom or membrane elements. These become equivalent when the elements become thin.

A further insight provided by Jetteur and Bruyneel (2008) is that simulating slow inflation using the Newton-Raphson method for integration can result in the development of a large non-physical oscillation leading to a lack of convergence. To prevent this problem an explicit integration method could be used with global damping turned on. However, this method can also lead to unwanted dynamic effects if it is not well managed. A simple method to improve the simulation time, if wrinkle patterns are not crucial, is to use a shell element with a greatly reduced, though non-zero, compressive strength, or a membrane.

2.3 Air-beams

Inflatable beams are being investigated as an alternative to conventional rigid structural elements. The advantage of inflatable beams is their weight and large stowed to deployed ratio. These beams are usually inflated with a gas which puts the outer cover of the beam into tension making the inflation gas

the compressive component. Without the contained gas to rigidize the thin walled structure air-beams are prone to localized buckling or wrinkling which dramatically reduce the effective strength. The higher the inflation pressure the higher the stiffness of the beam, limited by the tensile strength of the material used.

In addition to their low weight and small stowed size inflatable structures may require few, if any, fasteners or connections. This makes them ideal for rapidly deployed structures. Examples currently in use include emergency relief shelters and light aircraft hangers, which can not only be easily transported and deployed but have additional advantages such as being naturally insulated.

Cavallaro (2006) gives an overview of the areas being investigated as potential applications and the basic parameters that are important to designing with inflatable technologies. Inflatable technologies are being investigated in many different fields, for example aircraft wings and space station solar arrays. Two general types of textile fabric are used for inflatable structures, plain woven and braided fabrics. The choice of fibre direction is dependent on the application. Plain woven fabrics allow the best transfer of strength in two primary directions while some knitted fabrics have a higher through-thickness strength.

Inflated structures can also be used to provide axial, bending, shear and torsional stiffness. In the design of an air-beam, the strength comes from the woven textile cover while the bladder is designed to be compliant and conform to the shape of the cover material. Stiffness is a function of the internal pressure. When the beam is loaded the contained mass of air is subjected to a change in pressure and volume. This change requires work to be done on the gas, known as PV-work, in accordance with the ideal gas law. The work done to deform the structure is balanced not only by an increase in internal energy for the structure, but also by the PV-work of the compressed air.

Air-beam research does not usually focus on beam deployment, but rather on the modelling of the inflated beams. Air-beams are modelled as fully inflated or in their final geometry. Simulation of the inflated beam does not require large deformation, as with air-bag inflation. All the deformation is in the form of material strain, avoiding many of the complexities associated with rigid element rotation.

The problem of modelling air-beams has been approached in several ways. Fichter (1966) derived a series of non-linear equilibrium equations, while Davids and Zhang (2008) developed a Timoshenko style beam element that considers cross-section changes and pressure. The most common method of modelling air-beams is to create a 3D shell model of the structure and enforce a pretension in the material.

Apedo *et al.* (2010) discusses the FE analysis of a load bearing inflatable beam made of a textile fabric using two analysis methods. A 3D shell model of the beam using equivalent properties of the pressurized, pre-tensioned material was first used. This method is simple to run and can be used on larger, more

complex structures in much the same way as a conventional truss analysis. Generating material properties for this type of model requires that both the pressure and shear condition of the material be considered when producing elastic properties, because the material stiffness is dependent on both the shear strain and applied pressure in that area.

The second method used was to run a 3D non-linear model of the beam including the pressurization of the material. The challenge here is that a more general material model is needed as the models are used to find stress conditions at different states. This model also runs significantly longer than the analysis of the pre-inflated models. However, the non-linear inflation model captures effects that are not possible in a linear code, most notably local buckling. The strength of a beam is greatly reduced as a result of local buckling or wrinkling.

Cavallaro *et al.* (2003) explored the mechanics of plain woven fabrics to be used for inflatable beams with a focus on the characterization of material properties. The FE model used is continually compared to the results generated from physical testing. A simple 4-point bending test is chosen and the mid-span deflection of the beam is compared to the numerical analysis. The 4-point bending test is used because the mid-span only sees pure bending and there is no contact in that area, which could skew the results.

Cavallaro and Quigley (2007) investigated the relationship between the material strain energy of an inflated beam and the work done by changing the volume and pressure of the contained gas. It was found that the energy dissipated in changing the volume and pressure of the contained gas is much higher than the strain energy induced in the woven fabric of the beam. The higher the pressure, the greater this effect. Dunnage bags have a much larger volume than the inflatable beams investigated but the change in volume is far more significant and produces much the same effect.

While most research done on air-beams is based on pre-inflated beams, some deployment research has been done. In these cases a specific deployed shape is prescribed and the focus is on how best to stow the structure so that it inflates to the desired geometry without becoming tangled. In these cases stress data is of less importance.

Lampani and Gaudenzi (2010) simulated the behaviour of inflatable structures in space. Holland *et al.* (2002) looked into the use of scale models for similar applications, but objectives of simulating an inflatable structure are often twofold. Analysts are often interested in both the simulation of the deployment of the structure as well as accurate simulation of the material state with energy balance on the inflated part. Using scale models it is more difficult to extrapolate the energy balance for the larger structures and exclude the effects of atmospheric loading.

Typically, explicit codes are used to simulate deployment, but due to the large and often rigid deflections of the elements, and the tendency of the element velocities to slow down towards the end of the simulation, the accuracy

of the stress data for the fully inflated part is not as accurate as the overall deformation of the part. For accurate part stress and strain data implicit methods are typically used, but this type of code becomes unstable and does not converge with the large rigid deformations that characterize deployment analysis. With this in mind, a dual explicit/implicit analysis may be the solution. In this case the initial inflation is simulated explicitly, then, as the simulation slows the solver switches to an implicit simulation.

Wang and Johnson (2003) describe the deployment simulation of inflatable structures to be used in space, using control volumes to inflate and deploy parts. Here the inner surface of the model is used to define a control volume that can then be ascribed pressure and volume characteristics. In some cases multiple interconnected control volumes are used, where the relationships between control volumes are described by the numerical solver.

Dunnage bags have a large overlap with inflatable beams, with the most notable differences being that dunnage bags have a much lower aspect ratio than inflatable beams and that the deployment of a dunnage bag is a key aspect of the simulation. This research into inflatable beams shows the importance of a realistic material model and the inclusion of the compressible nature of the inflation media to the simulation of a dunnage bag.

2.4 Tensairity

The conventional method for increasing a beam's critical buckling load is to increase the beam section and, in so doing, the mass of the section is increased. For pressure rididized structures the inflation pressure can be increased with similar effects. The increase in pressure though improving the overall load response of the structure does push the material closer to it's failure limit. Luchsinger *et al.* (2004*a*) state that a good lightweight design should include a constructive separation of tension and compression, such as that described by Fuller (1975).

Tensairty is a method whereby a low pressure inflatable component is added to a structure to constructively separate tension and compression in a load bearing structure. The method is proposed by Luchsinger *et al.* (2004*a*) to increase the strength of an air-beam and results in a hybrid of conventional air-beams and strut/cable systems called tensegrity structures. The theory stems from the fact that a cable under tension is the most effective structural use of material. In this case the strength of the cable is not dependent on its length or shape, only area and material properties. Figure 2.5(a) shows the concept of tensairty where the compression and tension components are separated by an inflated bladder. Figures 2.5(b) and 2.5(c) show two examples of recent tensairty structures.

A Tensairity beam has three major components: a compression element, a cylindrical air-beam, and at least two cables connected to the compression

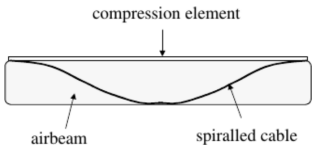

(a) Tensairity concept, Luchsinger *et al.* (2004*a*)

(b) Tensairity beam holds up a car

(c) Tensairity kite, Breuer and Luchsinger (2010)

Figure 2.5: Tensairity concept and examples

element. The air-beam is used to stabilize the compression element by increasing its critical buckling load and to pre-tension the cable elements. The load applied is carried by the compression member and the beam can be made such that the maximum compressive load is only dependent on its material properties. Luchsinger *et al.* (2004*a*) show that with the correct application of Tensairity principles, the pressure required in the air-beam to produce a desired load per meter is independent of the length of the beam. The buckling load can be increased beyond the yield load of the material.

The theory developed in Luchsinger *et al.* (2004*a*) is based on very simple geometry and for practical purposes Tensairity structures must be analysed using numerical tools as described in Pedretti (2004). Pedretti (2004) covers several complications in the simulation of Tensairity structures that are applicable to dunnage bag simulation. These complications include the need for an accurate material model, numerical instability resulting from large rigid displacement and the necessity of including the effect of the air volume under loading. The analysis is separated into an inflation phase and a loading phase for ease of simulation. Cao *et al.* (2011) provide a comparison of numerical and experimental data for a sample Tensairity beam under distributed and point loading, showing fairly good consistency.

Luchsinger *et al.* (2011) provides an overview of the developments made with the simulation of Tensairity structures. In the original Tensairity paper, Luchsinger *et al.* (2004*a*), a cylindrical air-beam was used. Through the information gathered in numerical experiments it was found that a more efficient configuration is to use a cigar or spindle shaped air-beam. It was also found that the positions in the structure are critical with small changes in position having a large effect on the load response of the structure as a whole. In a physical model the cables roll and reorient themselves along geodesic lines on the bag surface, which is not captured in numerical models.

Luchsinger (2006) describes how adaptable structures can be built using Tensairity principles. The paper notes that the stiffness of this type of structure is dependent on the pressure in the air-beam. With this in mind, the stiffness of the structure can be controlled by controlling the air pressure. This type of design will allow the structure to resist loads as they are applied in a

more organic fashion. This adaptivity is shown in an example of an inflatable cantilever lifting device.

The adaptation of the Tensairity principals for beams under bending loads, to columns under compression was approached by Plagianakos *et al.* (2009) and Wever *et al.* (2010).

2.5 Summary of Dunnage Bag Context

Dunnage bags are a type of tension structure with a full gas volume inflation, where the compression component is air and the tension component is the woven polypropylene cover of the bag. Since the compression component is inflated gas this structure is not susceptible to geometric failure such as buckling. Ideally this type of structure should be in pure tension to ensure that the material strength is optimally used.

This class of structure is evaluated in terms of: the relationship between pretension and external load, fiber orientation, degree of curvature and material stress-strain relationship. Dunnage bags are highly pretensioned structures with fixed fiber orientations, a medium degree of curvature and a highly nonlinear material stress-strain relationship that must be accounted for. New structures should be analyzed based on their actual rather than ideal geometries making deployment simulations critical to the evaluation of the structure as a whole.

With the inclusion of an inflation medium that uses an equation of state to update the pressure in the bag the simulations can be expanded to account for dynamic loading of the inflated bag. Deployment simulations of this kind become unstable when run using software that uses implicit integration. Thus an explicit solver is recommended.

Chapter 3

Plain Woven Polypropylene

The dunnage bag reinforcing cover that is the focus of this research is manufactured from a plain woven polypropylene. Woven textiles and fabrics are non-continuous materials with anisotropic mechanical properties, though simple plain woven materials are commonly considered to be orthotropic with a decoupled shear response for practical purposes. The material response of the woven textiles is only partly based on the material properties of the base material. In addition to the material properties of the constituent fibres the material response of a textile is dependent on the mechanics and geometry of the weave architecture. This requires that the textile be considered as a whole when evaluating its mechanical properties. Due to the variation in manufacturing conditions, both in terms of the polypropylene feed stock and the weaving process there is a lot of uncertainty in the response of the material. The generation of more accurate engineering material properties for dunnage bag cover materials will greatly reduce simulation uncertainty. Literature was reviewed to determine the existing methods used to model woven textiles to account for various material characteristics.

3.1 Polypropylene

Polypropylene is a long chain macromolecule containing between 10 000 and 20 000 methyl monomer units attached to every second carbon in a hydrocarbon chain. Figure 3.1 shows the chemical chain for isotactic polypropylene: a polypropylene chain where the methyl groups are attached to the same side of the hydrocarbon chain. Two other polypropylene forms can be made, syndiotactic and atactic polypropylene which either have every second methyl group on the alternate side of the hydrocarbon chain or no pattern to the position of the methyl group along the chain. Only isotactic polypropylene has mechanical properties suitable for use as an engineering material.

Polypropylene is an inexpensive, recyclable, commodity grade, polymer that can be manufactured in large volumes. Advantages of polypropylene

(1)

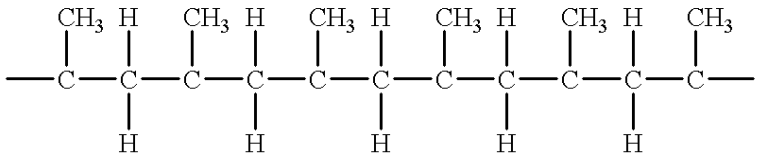

Figure 3.1: Isotactic polypropylene polymer chain, methyl monomers (CH_3) linked to CH-CH_2 chain

over comparable commodity plastics include: lower density, more resistant to heat distortion, excellent fatigue strength, improved environmental stress crack resistance, resistant to degradation caused by most organic and mineral acids and their salts, as well as strong and weak alkalies. Polypropylene also has good machine-ability and can be used for injection moulding and extrusion.

Polypropylene does however have a poor resistance to UV degradation and oxidation, higher mould shrinkage, higher thermal expansion and lower impact resistance. Disadvantages include significant creep, resistant to bonding with adhesives and a low resistance to wear.

These properties can be varied somewhat with the inclusion of chemical additives and filling agents or variation of processing methods. Some general mechanical properties of polypropylene are extracted from Tripathi (2002), and are shown in table 3.1.

Table 3.1: Mechanical properties of polypropylene

Property	Range
Density	0.90 - 0.91 $\frac{g}{cm^3}$
Tensile Modulus	1.14 - 1.55 GPa
Yield Strength	31.0 - 37.2 MPa
Elongation to break	>50 %
Glass Transition	-18 °C
Melting Point	163 °C

The polypropylene tows used in the dunnage bag covers are pre-stretched to increase their stiffness and reduce their elongation to break. This operation makes each tow highly orthotropic. The properties of the warp and weft tows in the weave also differ both in their feedstock and the amount with which they are pre-stretched giving them material properties that are not necessarily related. Further stretching also takes place during the weaving operation. After manufacturing, the bags are seen to shrink as material creep alleviates some of the pretension applied during weaving.

Polypropylene itself has a complex and an uncommon load-unload relationship, further complicated when the material is subjected to multi-cycle loading as shown by Drozdov and Dusunceli (2013). Figure 3.2 shows a stress-strain plot from a uni-axial load-unload-reload test. Drozdov and Dusunceli (2013) notes that the load response for polypropylene changes with each load application and proposes a new model that captures the load-reload characteristic for uni-axial tensile tests of polypropylene. The varying cyclic-response and complex load unload curves for polypropylene will permeate into the properties of the woven polypropylene textile fabric.

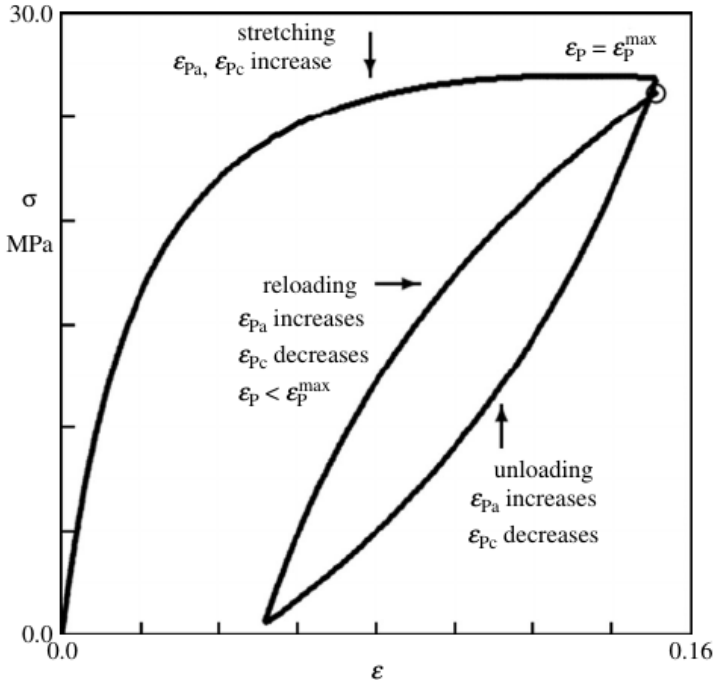

Figure 3.2: Mechanical response of polypropylene to cyclic loading, Drozdov and Dusunceli (2013)

3.2 Woven Textile Fabric

There are six methods of manufacturing fabric: felting, braiding, netting, lacing, knitting and weaving. The material used to construct polypropylene reinforced dunnage bags is of the woven construction. A series of tows are arranged so that they feed in the axial direction of a circular loom. Fibres of this orientation, known as warp fibres, are aligned along the machine direction. Additional tows are interlaced between the warp tows in an over-under alternating pattern to form a spiral around the circular loom as the material is fabricated. Fibres

oriented perpendicular to the warp tows, in the cross direction of the loom, are known as weft tows. Figure 3.3 shows a small plain woven section with four warp and weft tows, representative of the woven polypropylene fabric used to manufacture dunnage bags.

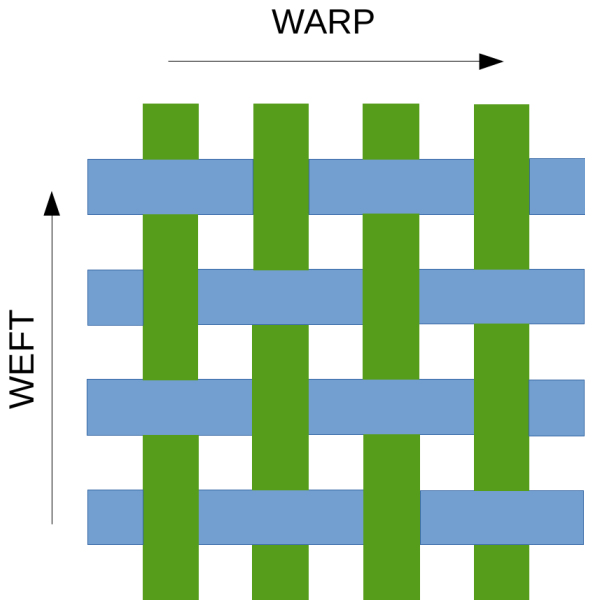

Figure 3.3: Weave architecture for plain woven fabric showing orthogonal warp (MD) and weft (CD) directions

It can be noted that the warp and weft tows can be manufactured from different materials of different sizes and shapes, with unrelated properties. This affords more freedom to develop a material for a specific load orientation and response. However, literature notes that woven materials can have significantly different properties from those of their constituent fibres, most notably that the shear and elastic moduli are dependent on the weave architecture. Tan *et al.* (1997) provide a comprehensive review of the properties of textile composites that will be shown here.

Woven fabric is a non-homogeneous, non-continuous, anisotropic material, which is often modelled as a continuous orthotropic material. This assumption is applicable when the loading is predominantly in-plane in the fibre directions of plain woven materials. In these cases the warp and weft provide the material strength in the primary directions.

Woven textile composite materials and fabrics have a complex material response that is affected by changes in the material properties of the component fibres, the weave architecture and variations in the weaving process such as fibre pretension. There are two prominent mechanical interactions caused by the weave architecture that have an affect on the mechanical response of a

woven textile. These are the non-linear shear response caused by the fibre trellis interaction and the coupled tensile response in the primary and secondary material directions caused by the crimp de-crimp behaviour of the material.

In the construction of a plain woven textile both the warp and weft tows are curved around each other. The weft tow is curved during the weaving process as it passes over and under the warp tows. Similarly the warp tows are curved as they pass over and under the weft tows. The degree to which the warp and weft tows are curved depends on the relative size of the tows, the density of the weave and the tension in the fibres when the material is woven. When the material is loaded in the warp direction the degree to which the warp fibres are curved decreases. These fibres are said to de-crimp, while the degree to which the weft direction fibres are curved increase. These fibres are said to crimp. Figure 3.4 shows a two-dimensional representation of the unloaded fibres, figure 3.4(a), and loaded fibres, figure 3.4(b), as an illustration of the de-crimping effect in a woven textile. West and Adams (1997) describe the de-crimping effect in detail.

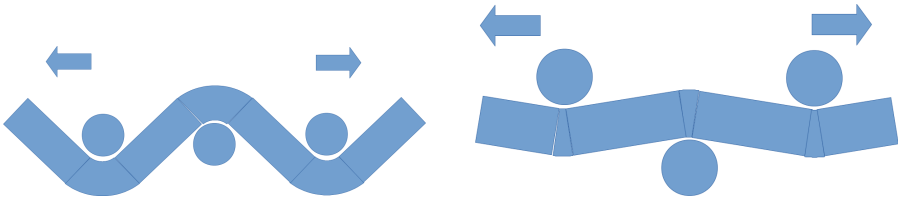

(a) Crimped weave condition (b) De-crimped weave condition

Figure 3.4: Crimped and de-crimped conditions for a simple woven textiles

The other mechanical characteristic of woven textiles related to their weave geometry is the shear response of the material. A woven material undergoing shear is observed to have three distinct phases of shear response. Initially there is little resistance to shear, when a shear load is applied to a woven fabric, the shear is resisted by the de-crimping of the individual tows and the friction between warp and weft tows. As the shear angle increases the tows begin to make contact with each other and are crushed in the plane of the material, increasing the shear resistance. At high shear angles the material begins to wrinkle and the resistance to shear diminishes. Figure 3.5 illustrates the mechanics of the woven material under shear, described in detail by Mohammed *et al.* (2000).

Cavallaro *et al.* (2007) and Boisse *et al.* (2001) show that the material shear and bi-axial load response are dependent on the current bi-axial tension ratio and shear state, making these co-dependent characteristics. Cao *et al.* (2008) reviews the experimental methods and benchmark results used to characterise general woven fabrics. In many cases, such as out-of-plane loading or draping, the primary material directions are no longer the only load directions. Here

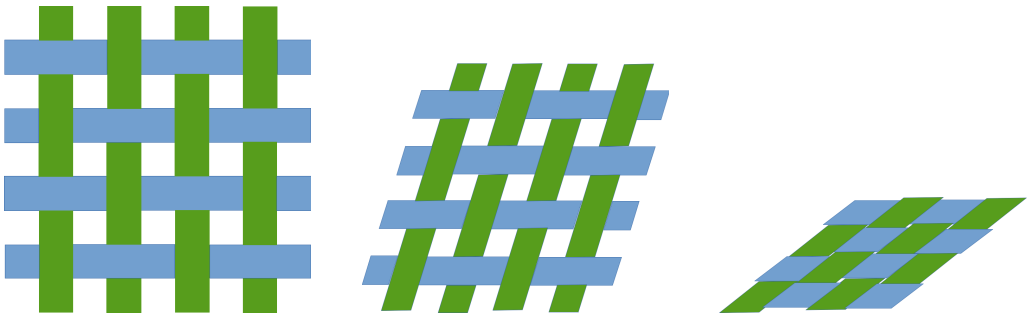

(a) No shear (b) Initial shear (c) Final shear

Figure 3.5: Stages of shear for a woven textiles

the shear characteristics of the woven material become a prominent factor, because the shear strength of a plain woven fabric is not related to the elastic modulus in the primary material directions. This means that a woven fabric cannot be simulated as a continuum, but also cannot feasibly be modelled on a large scale on a fibre by fibre basis.

Lomov *et al.* (2001) gives a hierarchy of textile modelling strategies. Textile modelling strategies are provided at the fibre, yarn, fabric weave and fabric levels. The material mechanics can be investigated at various levels depending on the area of interest of the researcher. Different assumptions are made on each level. For the purposes of this project, only the response of the material as a whole is of interest and the properties will be determined on the fabric level. In this case a property homogenization technique is required to produce an equivalent continuum property that closely resembles the properties of the actual woven material over the domain of interest for an analysis.

3.3 Modelling of Woven Textiles

When using a property homogenisation technique the equivalent property should ideally capture that a woven material has an extremely low shear modulus, at low shear angles. This modulus increases sharply once the material has gone into what is knows as shear locking, at higher shear angles. At low shear angles the shear and elastic properties of woven material are independent. This makes woven materials more drapable than conventional continuum materials. In this research the micro mechanical interaction of the fibres are not of interest and the computational load of simulations at that level on the scale of a dunnage bag is too large to be practical. Several techniques are found in literature that reproduce the response of the mechanical fibre interactions and constituent material properties as an average over an area. The material properties of a representative material section is homogenised and applied to the entire structure.

Three general approaches are evident in literature for modelling woven textiles: meso-scale modelling, parameter identification using unit cells, and material response matching.

3.3.1 Meso-Scale Modelling

Meso scale modelling of woven textiles take into account the mechanics and interactions of individual fibres and tows as well as the material properties of the fibres themselves. This form of modelling is capable of capturing the contact friction, crimp, bending and shear behaviour of a woven fabric, but the computational demand is high.

Lomov *et al.* (2007*a*) investigate the use of meso-scale models of textile composites and propose a road map and data flow for such models. The paper makes use of practical methods of investigating the inter fibre relationships.

Though it is complex to simulate a fabric on the meso scale (yarn scale) Durville (2008) made use of such a model to gain insight into the nature of woven textiles. Inter-fibre characteristics that cannot be measured directly can be investigated by a suitable meso-scale numerical model. This type of simulation can be used to gain insight into the fabric-stitch relationship at seams and folded regions of a dunnage bag. Given the difference in scale between the whole bag and the material weave and stitching the computational requirement of a meso-scale analysis is too high.

Nilakantan *et al.* (2010) and Jin *et al.* (2011) both researched ballistic applications of a woven fabric. In both cases meso-scale solid models are used and each yarn is modelled. Numerical models on this scale are required when the load applied is on the scale of the yarns, such is the case of small calibre projectile impact. On this scale the gaps between the fibres and the true thickness of the yarns are required to accurately predict penetration. In this application the fibre interaction is of critical importance to the calculation of energy transfer from the projectile to the fabric.

Some of the characteristics that must be captured in ballistic simulations include friction, contact and weave kinematics, so a model of each fibre is required in the impact zone. This is possible, but to model a sample that is large enough to give the required results would be too computationally expensive. To work around this, the individual fibres are modelled in the area of the impact as solid fibres. In the zone immediately adjacent to the impact zone, the material is modelled using shell elements, but in this area the individual tows are modelled in their woven state. Then in the zone furthest from the impact the material is modelled as a continuous membrane. The resulting model is divided into three regions, each modelling the fabric on a different scale. The method described constitutes a multi-scale approach that can reduce the computational requirement of a simulation.

Nilakantan *et al.* (2010) makes use of the multi-scale approach in a ballistic impact simulation and notes that care should be taken when connecting the

various meshes. Nilakantan *et al.* (2010) focuses on the coupling of solid, shell and membrane elements to produce a complete model. Also noted are the shortfalls of using homogenized membranes to model general ballistic impact, a complete 3D model of the textile fabric is required to achieve accurate results. Multi-scale solutions are a problem because the solid, shell and membrane elements must be connected in such a way that there is no artificial stress or strain generated and energy is transferred correctly between the different meshes.

An alternative meso-scale mesh was investigated by Jin *et al.* (2011) to simulate the impact of a projectile into a woven textile material. The mesh used for this model is not an exact replica of the physical material, but still produces good results.

Due to the scale differences involved in a dunnage bag simulation meso-scale models are not feasible. A multi-scale approach is also not suitable because of the increased instability of the model due to its more complex energy transfer requirements. The inflation process of a dunnage bag is already numerically unstable.

A multi-scale approach could however be used later to investigate the effect of various stitching patterns on the material. In these areas there are loads and interactions that cannot be represented by an assumed continuous model, such as the stitching fibres penetrating through the weave.

3.3.2 Unit Cell Parameter Identification

The purpose of homogenization is to reduce the number of elements required for a numerical model while still representing the overall mechanics of the system. Numerical unit cells make use of a small repeating, representative area of material where the inter-fibre mechanics can be reasonably accounted for or modelled. The load response of the unit cell is averaged and used to represent the response of the entire area. Two classes of unit cells exist, analytical unit cells and numerical unit cells.

Analytical Unit Cells

Analytical unit cells attempt to account for the micro-mechanical properties of a representative area of material by some analytical means. These models are typically implemented as user-defined materials in commercial software.

Boisse *et al.* (1997) proposes the use of a user-defined material model that can be integrated into an existing FE solution. The material model proposed takes the material properties of woven textiles fabric to be: no shear stiffness, no bending stiffness, no compressive stiffness, no inter-fibre sliding and account for fibre de-crimping. This material model requires a large number of physical tests to calibrate the model. The physical tests are complicated by the need

for an effective method of surface strain measurement, for which the use of photogrammetry is suggested but not implemented.

Apedo *et al.* (2010) and Brueggert and Tanov (2002) used kinematic equations to couple shear loading and displacement. This is done by looking at an individual quadrilateral element for a representative area of the model. This can be visualized as a 4-bar linkage with equal bar lengths and frictionless corner pins. Two non-linear stiffnesses are inserted between opposite corners of the quadrilateral. When a load is applied in one of the two primary directions, the bars of the linkage must extend or compress depending on the stiffness of the bars. However, when a shear load is applied the load is resisted purely by the diagonal stiffeners. This method requires that a user-defined material be used. Using a kinematic representation does, however, not include any component to account for the contact and movement between tows. The point at which two tows cross is represented as a fixed connection between the two fibres. The pin connections used in a kinematic representation do not shift, but in reality fibres are free to shift relative to one another.

Numerical Unit Cells

Numerical unit cells attempt to account for the micro-mechanical properties of a representative area of material by means of a numerical model.

The use of unit cells is discussed by Chung and Tamma (1999). They state that early efforts to find the effective properties of composite materials used an analytical approach. These were later adapted to be analytical models based on some recurring unit cell, and most lately adapted to include numerical simulations on a unit cell geometry. In each case the main problem is that, although the geometry of the unit cell can be chosen to be repetitive, it is difficult to generate boundary conditions that abide by the symmetry conditions required by a unit cell. Despite these limitations, the unit cell method of homogenization is a commonly used and effective technique used on woven textile fabrics.

Cavallaro *et al.* (2003) and Tarfaoui *et al.* (2001) used a numerical approach. Here a sample section of the fabric is fully modelled using accurate material properties and geometries. A single membrane element with a low stiffness is attached to this unit cell such that the edges of the membrane element align with the edges of the numerical unit cell. The virtual fabric model is then loaded in tension and shear, and combinations thereof. The resulting displacement of the membrane will be that of an equivalent homogenized section of fabric. This displacement can then be used to calculate the material properties of the woven material. Cavallaro *et al.* (2007) expanded on the importance of using the unit cell in the correct way when the decrimping behaviour of the fabric is included in the model. This behaviour further separated the properties of the woven fabric from that of the component fibres. The

same homogenized model was used in Cavallaro and Quigley (2007), where the effects of the work done by pressure and volume changes were investigated.

Where the unit cell used by Cavallaro *et al.* (2003), Cavallaro and Quigley (2007) and Cavallaro *et al.* (2007) are made up of four tows and four crossovers, Moncrieff (2005) uses a cruciform unit cell with two tows and one crossover. It is also noted that to produce accurate material properties much calibration is required. Moncrieff (2005) also warns that only the required material properties should be included in any simulation as excessive characterization may lead to an overly complex model that is less stable.

A further investigation into numerically simulated unit cells was undertaken by Bridgens and Gosling (2008), making use of methods for modelling of unit cells. A sawtooth and sinusoidal representation of the tows were compared. It was found that the sawtooth representation was more accurate at representing the overall character of a section of woven material. A shortfall in the model is that the flexural stiffness of the tows is not considered.

Chen *et al.* (2002) used the unit cell approach, but with a much larger material set including samples of different size. Chen *et al.* (2002) discovered that when the results of each test is normalized by the area of the sample, that the correlation between samples of various sizes is found to be good. They warn of the sensitivity of the experimental results to slight variations in the tow alignment during testing.

Gorczyca *et al.* (2002) investigated the simulation of uncured woven composites when producing complex part geometries. Woven materials behave as if their shear and tensile stiffness are not coupled. This means that a shear deformation does not necessarily come with an associate tensile stress. As a result, when a shear strain is applied to a woven material, the material may still be in a stress free configuration. This property makes woven fabrics more drapable than continuous materials. In this model extensive shear testing was done on woven materials and the resulting data was combined with the unit cell method of homogenization to produce a useful material property.

Material homogenization has been implemented on more than just simple plain woven fabric. D'Amato (2001) used a non-orthogonal, though still repetitive, unit cell to find effective material properties for a tri-axially braided fabric. D'Amato (2001) states that the effective properties found using a unit cell homogenization technique can be used to create simulations with a high degree of accuracy for deformation. The author notes that the stress data derived from a simulation using effective material properties is not accurate and can only be used as an indication of areas where a higher stress is likely to be found. The author suggests that in a simulation where stress information is critical, a global-local model should be used.

An alternative to the combination of physical testing and unit cell homogenization is shown in Lin *et al.* (2009). Here the unit cell is used to account for the tensile properties of the woven material only, while the shear properties are provided by a theoretical kinematic model.

3.3.3 Response Matching

The response matching method of material homogenisation does not attempt to account for any micro or meso-scale characteristics, either through direct modelling of the weave or through analogous unit cells. With response matching only the response of a large scale material test is considered with the overall properties of the material transposed on a representative finite element. Grujicic *et al.* (2008) uses this method to develop a continuum model for woven material for use in ballistic simulations.

Galliot and Luchsinger (2009) note that from a practical point of view most material models available for the simulation of woven textile fabrics are too complex for effective use in large simulations. For many applications it has been found that the response of a standard linear elastic orthotropic material model can be used to represent the material properties of fabrics over the region of interest of the simulation. Galliot and Luchsinger (2009) used a trial and error approach to match the response of a fabric measured in physical testing to a simulation of the same test. The results were evaluated and found to be suitable for their later simulations of Tensairity structures.

Based on the success of their earlier work the development of a new shear test rig is proposed and validated in Galliot and Luchsinger (2010*a*) and Galliot and Luchsinger (2010*b*). This new method is well suited to the testing of woven textiles. The test rig is capable of bi-axial tensile testing with independent load ratio and, through the use of a shear ramp load applied along the edges of the material, shear can be induced at any load ratio.

3.4 Strain Measurement for Tensile Structures

Woven textile composites do not lend themselves to direct mounted strain sensors, because the material itself is typically very thin and compliant and a direct mounted device would change the local properties of the material.

Gründig *et al.* (1995) investigated the use of photogrammetry for the in-situ evaluation of tensile roofs. Photogrammetry is the use of optical methods for measurement. In the case of the tensile roofs, datums were attached to the surface of the roof. Digital photographs were taken of the structure from several angles, and the position of the datums were calculated in 3 dimensions. This method was also applied successfully by Moncrieff (2005) as a non-contact measurement tool.

Lomov *et al.* (2007*b*) made use of DIC to track material strain during a physical test. This data was later used to validate the results of a meso-scale FE model. Ehlers and Varsta (2009) show how the use of DIC can improve the material characterization of woven composites. Lee *et al.* (2009) used a different approach for the validation of airbag inflation. In this case sample

airbags are inflated in front of a calibration board and the results over time are directly compared with those from numerical experiments.

Galliot and Luchsinger (2011) recommends the use of DIC to measure full field surface strains that can be directly compared with numerical simulations. Dridi *et al.* (2012) extend the work of Galliot and Luchsinger (2011) to include shear loading of woven fabric.

DIC makes use of images recorded during a physical test of a prepared sample. Images are evaluated sequentially using a least squares method to track the movement of an applied speckle pattern as the average movement of a pixel subset from one image to the next, Sutton *et al.* (1983). Based on the displacement field data produced by DIC the material strain can be calculated. The DIC system supplied by LaVision, and available at Stellenbosch University, is capable of deformation accuracy of 0.05 pixels. This translates to a real world accuracy of 0.01 mm for a 100 mm sample.

The accuracy of the displacement calculation is dependent on the quality of the speckle pattern applied to the sample. Lecompte *et al.* (2006) and Amiot *et al.* (2013) provide a mechanism for the evaluation of the speckle pattern quality that can be used to estimate the relative accuracy of different patterns. A sample pattern is applied using either a spray can or brush and a single photo is taken. The image of the speckle pattern is then mapped to the desired sample geometry in an unloaded state. Finite element methods are used to deform the sample and the original image is mapped to the results of the FEM simulation. DIC software is then used to determine the strain between the two images which is then compared to the FE results. Using this method various patterns and sizes can be compared under various lighting conditions to select the best pattern for a given test.

3.5 Conclusions from Literature

From the literature it can be seen that woven textiles are not conducive to analysis with conventional simulation tools. It is also not feasible or recommended to produce a full-scale model that includes yarn level detail. Most sources recommend that the material be homogenised in an attempt to match the response of the material as a whole to typical loads without being encumbered by the material detail. Unit cells and material swatches are used to ascertain the response of a small scale representative material subset. The response of the unit cell or swatch can then be mapped to a simple element. The new equivalent model homogenises the complex interactions in the weave, producing an average response for an area.

Several papers advocate the use of user-defined material models or element formulations to include more detailed material effects. Unfortunately the development of new material models and element formulations is beyond the scope of this project. For this research it is important to keep the complexity

of the models as low as possible to allow for more models to be run. With this in mind standard rather than user-defined material models will be used. Their ability to approximate necessary physical characteristics of a woven material will be evaluated.

In some cases the material geometry can be homogenised instead of the material properties to match the response of the overall weave. This, however, does not necessarily reduce the number of elements required to adequately represent the material. Using fewer, larger elements also reduces the total computational time. Using a single shell or membrane element to produce the response of a unit cell is therefore most beneficial to the project.

As a result of homogenisation model detail is lost, so it is important to decide on what detail is required. In most cases the homogenised material model will focus only on the in-plane material response. For dunnage bags there is a very large difference in dimensions between the bag's overall length and width, and the material thickness, leading to the assumption that the material can be considered a membrane. This eliminates any requirement for out-of-plane material response from the homogenised material. The shear angle for most of the bag is very low, especially in failure regions, and is only required to be much lower than the elastic moduli of the material

In literature two kinds of homogenisation are mentioned, each capable of capturing various material characteristics: unit cells (based on either analytical or kinematic models) and response matching (making use of inverse analysis and swatch testing). Analytical and kinematic models are not suitable for this project because they both require a user-defined material property.

Numerical models of a unit cell were initially considered but were found to be infeasible for this project because they require a very well calibrated material model for the underlying material, in this case polypropylene, and the weave geometry needs to be accurately accounted for. Figure 3.6 shows the mesh required for a simple unit cell and figure 3.7 shows the results of uni-axial, bi-axial and shear loading of that unit cell.

Producing a high accuracy model for polypropylene requires much the same type of analysis as calibrating the material model for woven fabric, but the equipment required for measuring and generating an accurate weave geometry are not currently available. This leaves response matching using an inverse analysis based on material swatch testing as the only viable homogenisation method for this project.

Photogrammetry and visual methods should be used where possible as a non-contact measurement of material strain to improve validation. Three methods commonly used were discussed and involve the comparison of images taken of physical testing, using stereo camera setups to map large point-to-point deformations using datums and the use of DIC to generate full-field strain data for the materials. DIC is the most promising technology and provides the most detailed results.

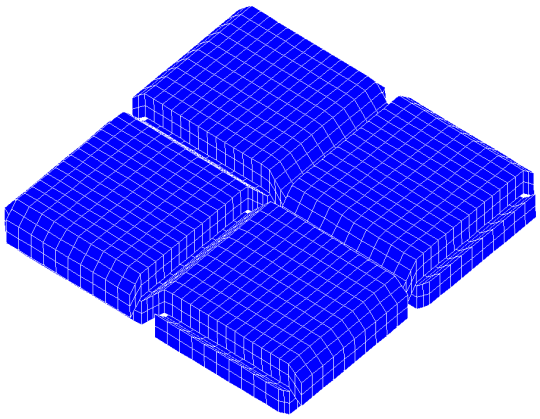

Figure 3.6: Mesh for a numerical unit cell showing a 2 by 2 overlap region

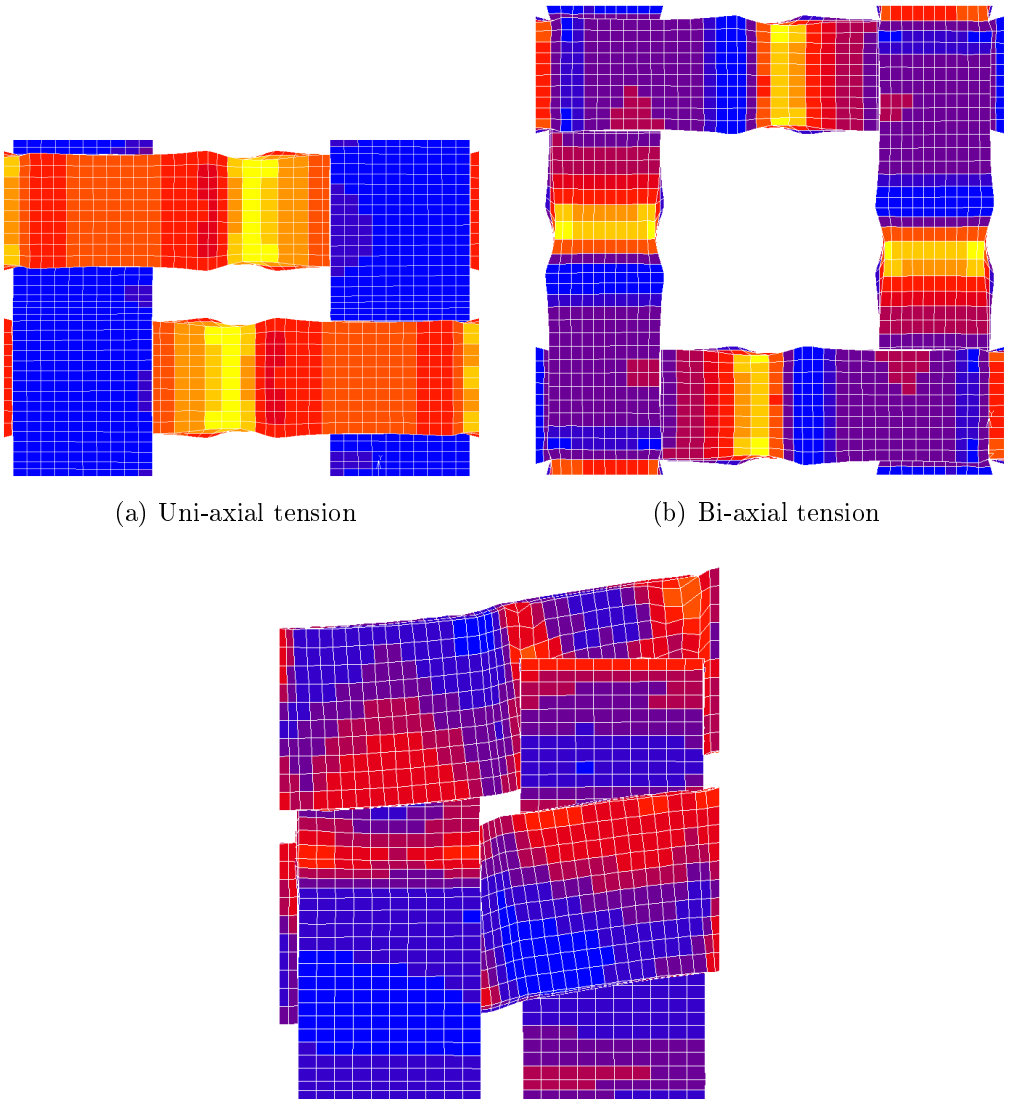

(a) Uni-axial tension

(b) Bi-axial tension

(c) Shear loading (not pure shear)

Figure 3.7: Numerical unit cell response to simple material tests

Chapter 4

Mechanical Testing of Plain-Woven Polypropylene

A key objective of this project is to match the pressure drop caused by overloading a dunnage bag while in operation. To this end the load-unload characteristic of the woven polypropylene fabric must be found. In order to achieve this goal it was required to first find methods to test the operational strain range of the material. With the strain range known, a suitable test device could be selected and built. Finally, the test device could be used to conduct a simple material test for samples that can be easily replicated numerically.

4.1 Experimental Design

In order to capture the response of plain-woven polypropylene the test rig should be designed with the following requirements in mind:

- Perform bi-axial loading
- Record load conditions
- Measure displacement

Additional requirements are that the design must be robust in terms of the range of samples that can be tested and also cheap to manufacture. The material grips should be capable of taking materials of varying thicknesses and weave densities and the number and type of actuators and sensors should be limited. The method of homogenisation chosen for this project is to match the response of the material in physical testing with the response of an equivalent test in the virtual environment. A simple method of deriving the engineering properties for the material is desired.

4.1.1 Available Material Tests

Though dunnage bags undergo large out of plane displacements, the material is predominantly loaded in-plane. It is therefore assumed that an analysis of the planar response of the material will be sufficient for the purpose of this project. The material response tests will be based on planar swatches that are loaded in-plane.

The material response to shear, uni-axial and bi-axial loading will be of interest. Several physical test apparatus and procedures are currently used to evaluate the response of woven materials. Figure 4.1 shows the specimen geometry as well as load cases for most of the available tests which are then described in detail below.

Vibration Test

In a vibration test a sample of known geometry is exposed to an excitation that causes the sample to vibrate. The input excitation to, and output displacement of the sample are recorded. Using mathematical techniques a vibration test can produce a full anisotropic elastic material compliance matrix. In a dunnage bag application the woven material is exposed to loads beyond the limit of a linear elastic model.

Uni-Axial and Bi-Axial Tensile Tests

Uni-axial and bi-axial tensile tests are simple extension tests of known samples. For a uni-axial tensile test a sample is clamped at each end into the test rig and a load or forced displacement is applied in one direction, as seen in figure 4.1(a). In the test the applied load and elongation of an area of interest are recorded. From this data the elastic and plastic response of a material can be found for a given load direction.

A bi-axial tensile test is an extension of the uni-axial test, performed on a cruciform sample, where each of the four arms are clamped into the test rig. Loading is simultaneously applied in both directions and loading can be applied with various load or displacement ratios, figure 4.1(b).

Uni-axial and bi-axial rigs are capable of generating non-linear material response. These tests are used to derive the material response in the primary (E_{MD}) and secondary (E_{CD}) material directions. The through thickness (E_{ZD}) material property will not be directly tested, but is not of interest in this project.

Biased Uni-Axial Tensile Test

The biased uni-axial tensile or biased extension test is an adaptation of the standard uni-axial tensile test. In the case of the biased test the sample is cut so that the primary and secondary material directions (machine and cross

(a) Uni-axial tensile test

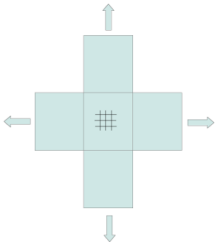

(b) Bi-axial tensile test

(c) Biased uni-axial tensile test

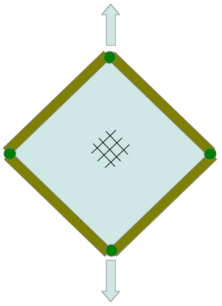

(d) Shear frame test

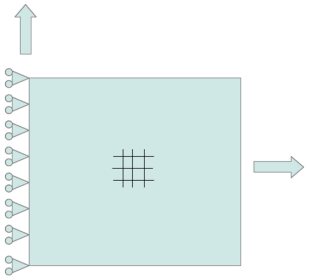

(e) KES-F fabric test

(f) Fabric shear cylinder test

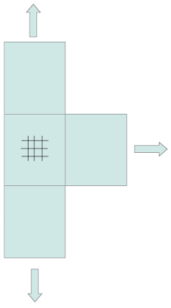

(g) Bi-axial tensile test with T-shaped sample

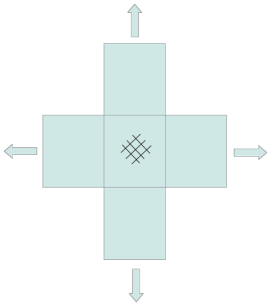

(h) Bi-axial tensile test with offset cruciform sample

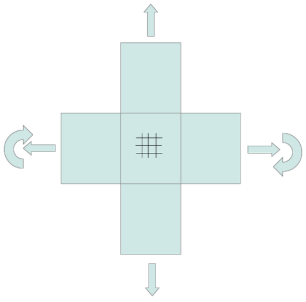

(i) Fabric test patented by Cavallaro (2005)

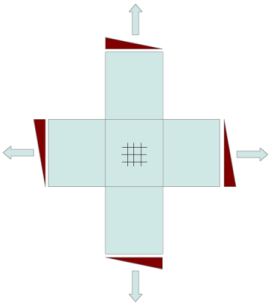

(j) Shear ramp proposed by Galliot and Luchsinger (2010*a*)

Figure 4.1: Material tests for woven textiles showing the loads applied and specimen geometry, material fibre orientation is indicated by cross hatching.

directions) are aligned at 45° to the direction of extension, figure 4.1(c), see Peng and Cao (2005). For a woven textile this produces a region of trellis shear in the centre of the specimen. The shear is then estimated based on the test rig cross-head displacement. This method of testing is often used as a comparison for other shear tests and is also good for finding the material locking angle.

Several disadvantages exist with this method. The shear stress is not homogeneous throughout the sample. There is a triangular region of pure tension at the clamps and a mixed region between the tension region at the clamps and shear region near the centre of the sample. The shear characteristic cannot be measured with reference to the load ratio between the machine and cross directions and, though an estimate for the shear stress in the sample is provided by an analytical equation, accurate shear values can only be obtained by optical measurement.

Shear Frame Test

The shear frame or picture frame test is a mechanism designed to load a square sample in global trellis shear. A sample is clamped into a square frame that pivots at each corner as a four-bar-linkage. The frame is then mounted to a tensile test rig such that diagonally opposite corners are displaced, figure 4.1(d). This test method allows for both positive and negative shear to be applied.

In the picture frame test the shear in the sample is assumed to be homogeneous and the shear angle is evident from the geometry of the frame. The sample is however not loaded in pure shear as the fixed clamping region produces tensile and compressive stresses in the sample. Shear frame and biased tensile tests are often used in tandem to define shear properties for a given sample.

KES-F Test

The KES-F test uses a device designed to apply a load tangential to the primary or secondary material directions, while exerting a constant tensile stress. A square sample is clamped on two parallel sides and a constant tensile load is applied to one clamped edge while a tangential load is applied to the other, figure 4.1(e).

In addition to testing the shear characteristic of a material the KES-F test can also provide: pure tension, compression, bending and surface properties. However, no bi-axial loading can be produced by the device.

Fabric Cylinder Shear Device Test

A test for woven materials exists where a cylindrical sample is clamped to two discs that are attached to a tension-torsion device. Load control is applied to the sample in the axial direction while torque is applied to one of the

mounting discs, generating a shear load, figure 4.1(f). This device requires specially prepared cylindrical samples that must be manufactured for each desired bi-axial tension state.

Bi-axial Test With T-shaped Specimen

A simple method of inducing shear in a sample is to use a T-shaped sample. The sample is clamped on all three edges and a tensile load is applied between the two parallel edges. When a load is applied to the third edge a region of shear is produced in the sample, figure 4.1(g). This test method does not produce a homogeneous shear region and either a FE analysis or optical field measurement is required to evaluate the shear region.

This test method uses an iterative method of tuning an FE model to match the physical data. The method can be problematic for use with loosely woven materials because loosely woven material is likely to pull apart rather than shear.

Bi-axial Test With Offset Cruciform Sample

A shear test can be performed on an alternative cruciform sample that consists of a central region offset by 45° to the loading direction, figure 4.1(h). This has the potential to produce a homogeneous shear state in the central region of the sample that corresponds to the tension-compression state associated with shear. However there is a limitation to the shear state that the test can obtain because the sample must remain in a net tension to avoid any regions of compression which would lead to wrinkling of the sample.

The most prominent disadvantages of this test method are that the preparation of samples is time consuming and that only a balanced bi-axial load can be applied to the sample.

Cavallaro Test

Cavallaro (2005) proposed a linkage set-up that can apply a bi-axial load to a cruciform sample. The Cavallaro test rig is a linkage based mechanism that applies a bi-axial displacement to a cruciform sample in order to pretension the sample. The sample is then loaded in shear by the relative rotation of the linkage, figure 4.1(i). Each of the four linkages are equipped with a load measurement device giving the user the total load applied to each sample arm. This mechanism does not give any indication of how the load is distributed over the sample and does not distinguish between the load due to pretension and that of the applied moment. The benefit of this mechanism is that various pretensions can be applied to a sample and a large range of shear angles can be tested. The device can also be designed to fit on an existing tensile or tension-torsion test device.

Shear Ramp Tests

Galliot and Luchsinger (2010*a*) and Galliot and Luchsinger (2010*b*) proposed an adaptation to an existing planar test rig for cruciform samples. The test rig has five mechanical grippers per arm of the cruciform sample, each gripper can be actuated independently and is fitted with a load measurement device. These independently articulating grippers allow the load applied to the sample to be adjusted so that a load ramp is applied to each arm of the sample, producing a load approaching pure shear, figure 4.1(j). An additional benefit of this mechanism is that the load on each pair of sample arms can be offset, allowing the sample to be pre-tensioned to any load ratio.

4.1.2 Manufactured Test Devices

From the list of available test devices three candidate load cases were selected that provide the ability to test uni-axial, bi-axial and shear load cases as well as mixed mode load cases. Figure 4.2 shows the three load cases selected, a positive only displacement ramp, a displacement ramp with both positive and negative displacement and a positive load ramp.

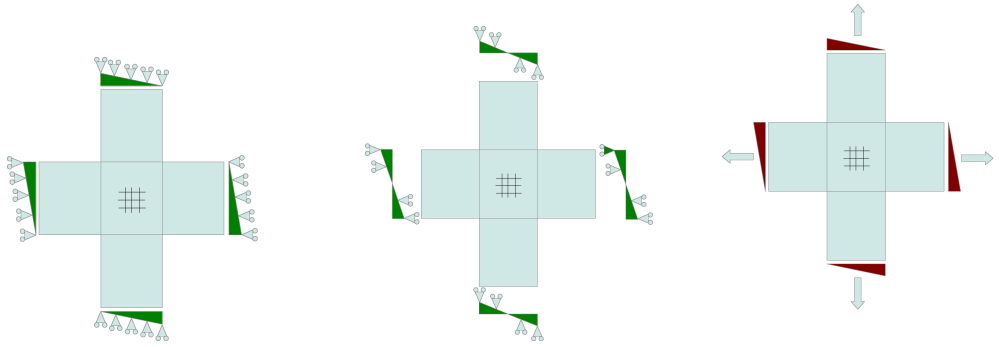

(a) Positive displacement ramp

(b) Positive and negative displacement ramp

(c) Positive load ramp

Figure 4.2: Candidate load cases for physical testing

Preliminary numerical simulations of the three potential load candidates were performed. Figure 4.3 shows the expected deformation pattern for each load case. It is observed that the deformation in the central region of interest is similar for each case.

Each of the candidate load cases have different requirements in terms of actuators and measurement equipment, important because of the cost and simplicity requirements of the project. If a single device is designed for each load case: the positive load ramp will require at least 20 actuators and sensors, the positive displacement ramp and ramp with positive and negative displacement will only require eight of each. For the ramp with both positive and negative

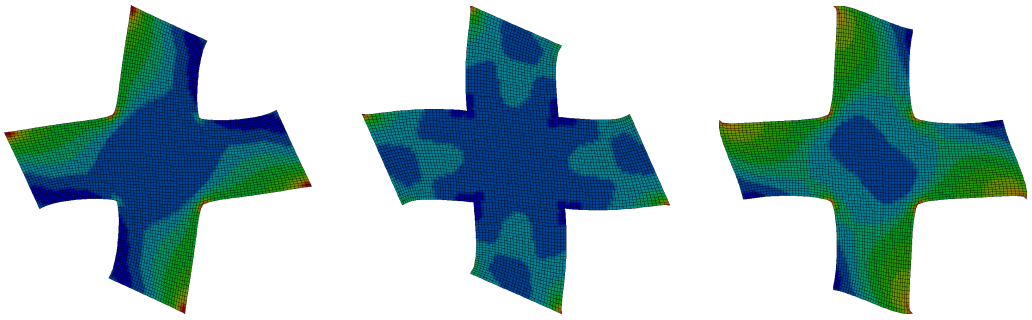

(a) Positive displacement ramp

(b) Positive and negative displacement ramp

(c) Positive load ramp

Figure 4.3: Candidate load case displacements

displacement there is a risk that a membrane subjected to compressive load will produce erroneous results, while the positive displacement ramp requires a more complex mechanism.

If two devices are used, the positive and negative displacement ramp can be reproduced by the combination of a bi-axial tensile frame and a shear frame. The bi-axial frame can be used to pre-tension a cruciform sample before the picture frame test is performed. Using this configuration reduces the number of actuators to four for the bi-axial frame. The shear frame can be designed to connect to an existing uni-axial tensile test device, requiring no additional actuators or measurement devices. If the bi-axial device is limited to fixed displacement ratios using a mechanical driver mechanism, the bi-axial device can also be designed to connect directly to an existing tensile test device. For each of the test fixtures the only actuation required can be provided by a uni-axial tensile test device, this reduces the number of additional actuators required to zero. The two device system will only require four load cells in the bi-axial device.

The driver mechanism based bi-axial device does limit the testing to a fixed displacement ratio between the two sets of clamps. Initial testing will make use of a one-to-one driver ratio, which can be changed by manufacturing multiple driver sets corresponding to various displacement ratios.

A numerical model of the experimental set-up can be created with a geometry equivalent to the physical sample and the loads or displacements measured in the physical experiments can be applied to the numerical sample. By changing the material properties in the numerical simulation the experimental response can be matched and a set of homogenized material properties can be found for any given material.

The purpose of the bi-axial test is to load a cruciform sample in two orthogonal directions, figure 4.1(b). This bi-axial device will impose a known displacement in each of the two material directions. The mechanism is designed so that a fixed displacement ratio is imposed between the two loading

directions. This mechanism can easily be switched so that various displacement ratios can be applied.

Figure 4.4 shows the designed and manufactured bi-axial tensile device. The driver mechanism can be seen in the center of each figure, the sample grippers are rendered in green. The bi-axial test device required the addition of two springs to compensate for gravity, forcing the driver mechanism closed when not in operation. Figure 4.5 shows the picture frame device and figure 4.6 shows the two devices nested together.

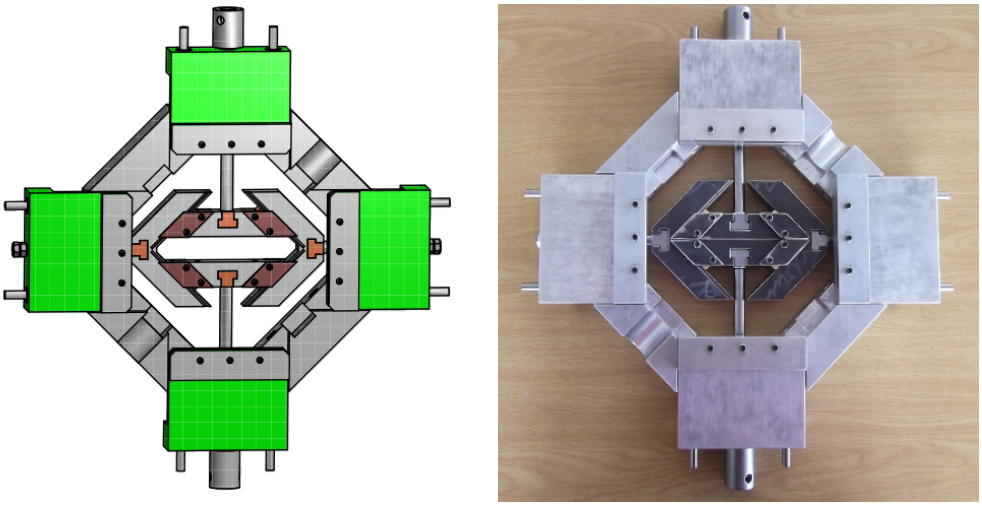

(a) CAD model (b) Manufactured device

Figure 4.4: Manufactured bi-axial tensile device

The test selected to determine the engineering properties of woven polypropylene is a bi-axial tensile test. A picture frame device has also been designed to couple with the bi-axial device for later testing of material shear. The manufactured test devices couple directly to a MTS Criterion tensile test device which drives a mechanism in the bi-axial device that displaces such that the 90° opposed mounting clamps move apart with a one to one ratio. That is if the pair of clamps aligned with the MTS are separated by 1 mm the other pair will also separate by 1 mm. The drive shafts used to actuate the device are gauged so that the load applied to each flap of the sample is measured.

4.1.3 Cruciform Samples

The bi-axial test requires cruciform samples to be cut directly from sample bags provided by the industry partner. Figure 4.7 shows an example of a prepared cruciform sample used in testing. The samples are cut so that a 100 x 100 mm square region is kept intact. The first two fibres in each arm, adjacent to the central region of interest, are removed.

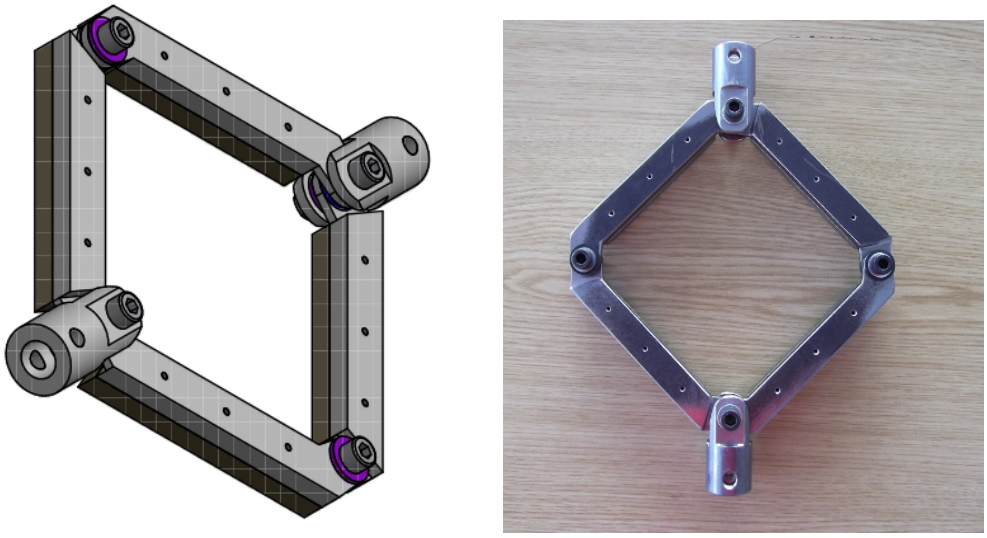

(a) CAD model (b) Manufactured frame

Figure 4.5: Manufactured shear frame

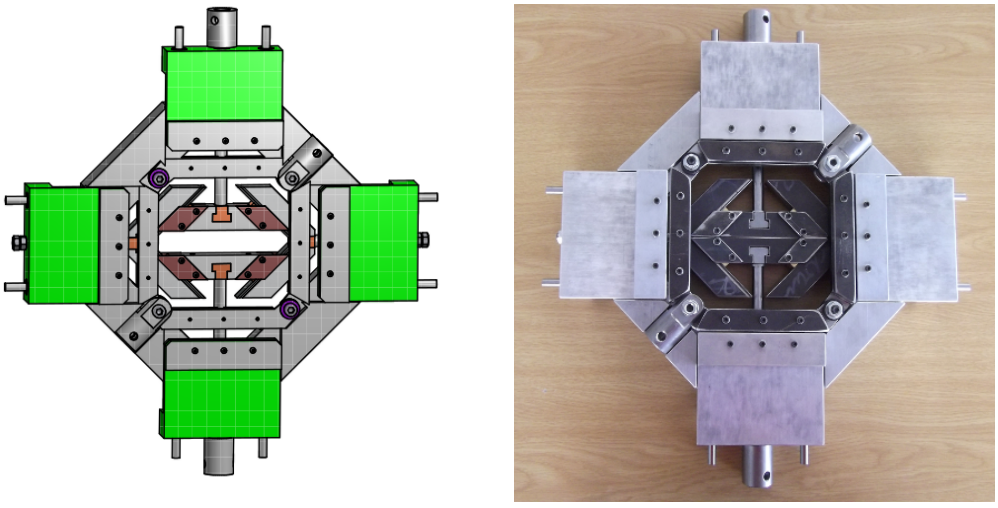

(a) CAD model (b) Manufactured device

Figure 4.6: Combined bi-axial and shear devices

As per a recommendation in Cavallaro *et al.* (2003) the samples are lightly preconditioned by shearing the fibres. This frees the fibres from each other and is more representative of the material under average use. The sample is then sprayed with a speckle pattern to provide contrast for the DIC system used to measure the surface strain of the material. DIC was used to capture the strain field for the center 50 x 50 mm central region of interest, figure 4.8. The region of interest was chosen to be much larger than the individual fibre

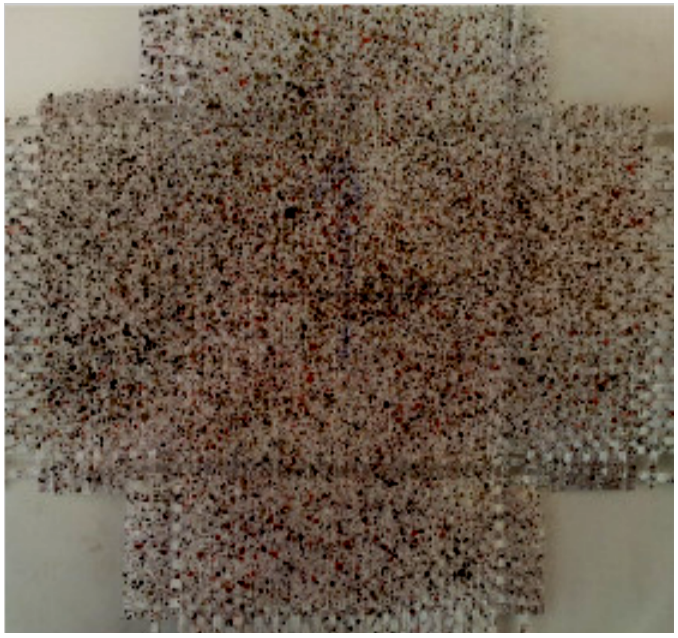

Figure 4.7: Representative cruciform sample, speckled for use with DIC software

tows so that the detail of individual fibre deformation would not be captured.

An important aspect of sample preparation was the selection of the speckle pattern to be used. The speckle pattern quality has an effect on the accuracy of the DIC method, Lecompte *et al.* (2006) and as such requires investigation before any tests can be performed. The speckle patterns for this application were compared by the RMS values of their noise floor, the spurious strain measured between five consecutive images. Ten candidate patterns were created using different paint types and colours. Various application techniques were also considered, including directly spraying the sample from a spray can and splashing paint onto the sample using a paint brush. Figure 4.9 shows the ten speckle candidates.

Two images were taken of each speckle pattern and compared using the DIC software DaVis using the camera system provided by LaVision. That is two different images are taken for each sample pattern without any load applied. The strain between the two images is then analysed using DIC. Figure 4.10 shows the strain measured by DIC from two consecutive images. Considering that the material underwent no strain the strain detected by DIC is erroneous. Figure 4.11 shows a plot of the average RMS value of the strain error for the candidate speckle patterns. Three interrogation window sizes were compared; small (30 pixel), medium (60 pixel) and large (120 pixel). In both cases candidate nine is excluded because the DIC results were the same as candidate eight.

As expected the larger the interrogation window size the more accurately the strain is predicted. Candidate 1 showed the lowest noise floor and was

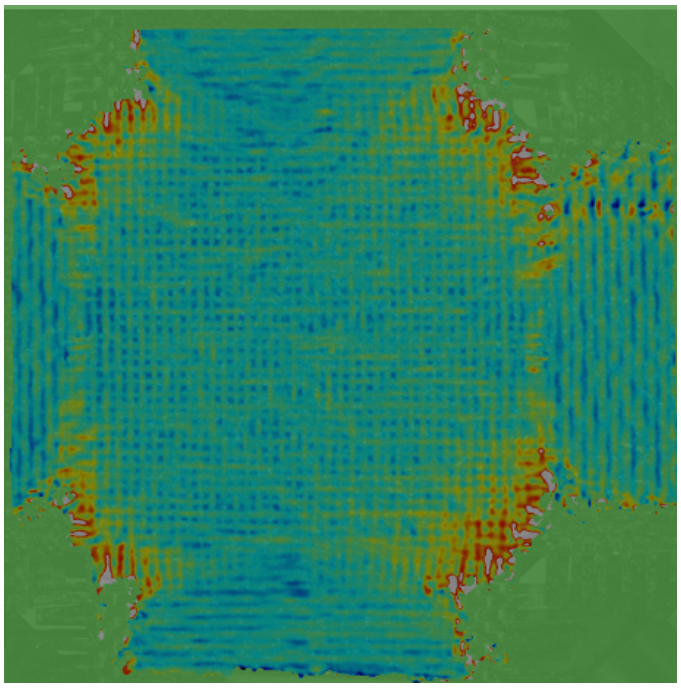

Figure 4.8: Principal strain field measured with DIC

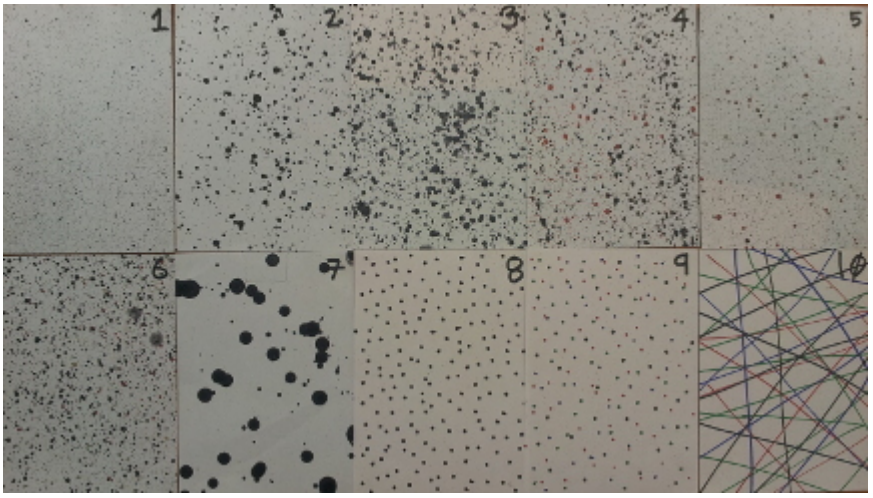

Figure 4.9: Ten speckle candidates for the cruciform material samples

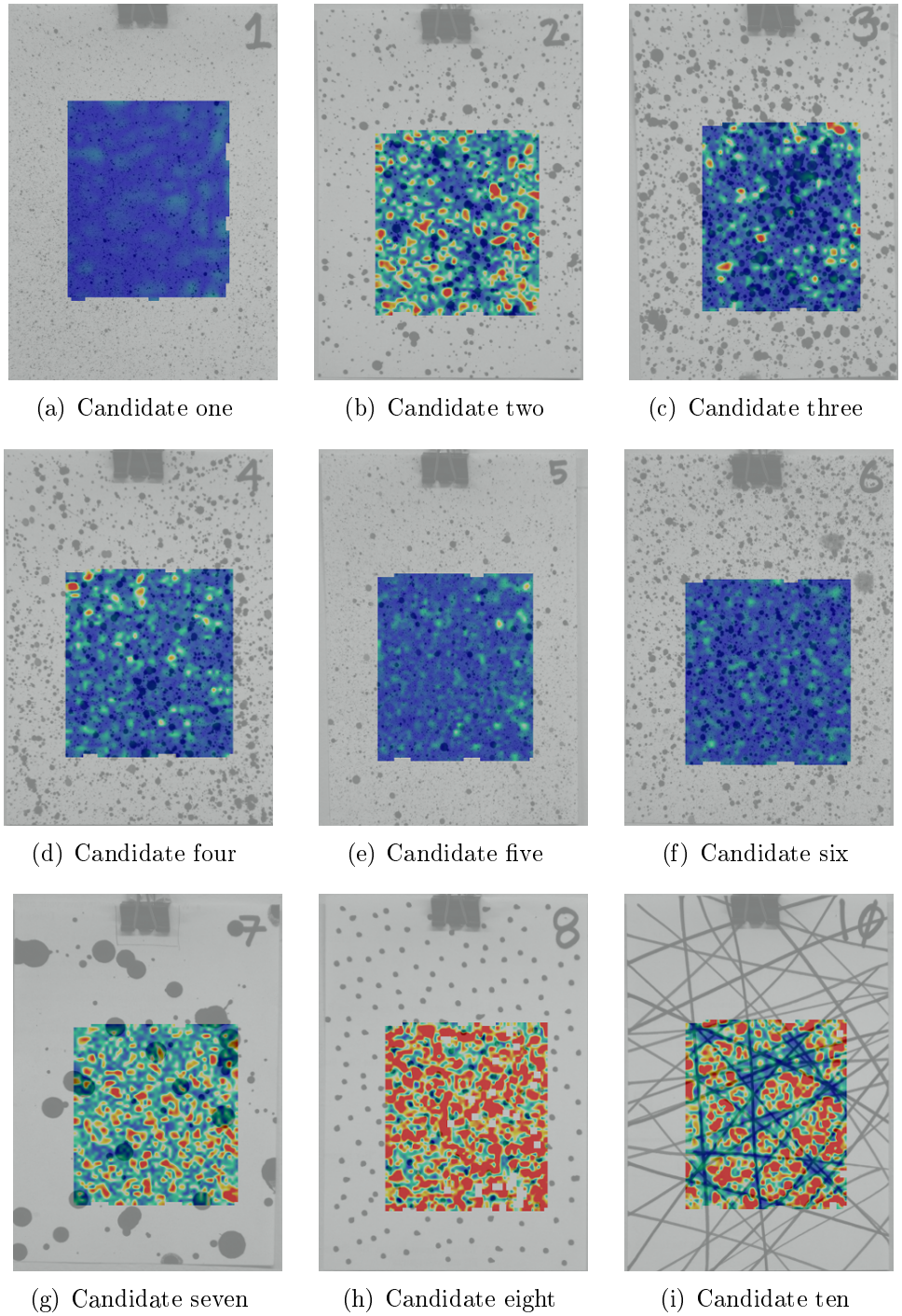

(a) Candidate one (b) Candidate two (c) Candidate three

(d) Candidate four (e) Candidate five (f) Candidate six

(g) Candidate seven (h) Candidate eight (i) Candidate ten

Figure 4.10: Noise floor for all candidate speckle patterns showing displacement magnitude with no load applied

then evaluated for accuracy. A single image was taken of the speckle pattern and elongated by 10 % using photo editing software. The two images were then compared using DIC which measured a 10 % strain in one direction and

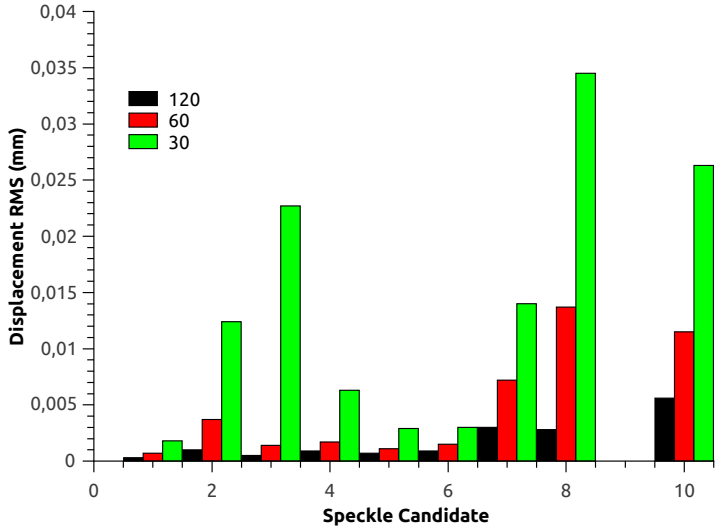

Figure 4.11: Average displacement RMS for the candidate speckle patterns under zero load

0 % in the other. Speckle pattern one is used for swatch tests and pattern three is used for the full bag tests.

4.1.4 Operational Strain Ranges

Due to the complexity of the effective material properties for woven polypropylene it was necessary to clearly define the range over which we intend to simulate the material. This is required both to ensure that the selected test device is capable of producing the desired strain on the sample and to limit the time spent on calibrating the numerical material outside of the desired operating range. The dunnage bags are tested by inflation between two flat parallel plates on a large hydraulic press, constituting an operational void. The bags are inflated to their operating pressure before the void is first reduced and then returned to its initial position, simulating a single load cycle.

The prescribed test case requires a test bag to be inflated to working pressure (70 kPa rel.) and cycled from 305-200 mm. The cycle test was recorded and DIC was used to measure the average strain in the woven material 600 mm from the corner along the longer edge of the bag as indicated by figure 4.12. This position was chosen because the strain state in this region of the bag is representative of the strain state of most of this edge of the bag. The strain state closer to the corner of the bag will be lower and the hydraulic press inhibits measurement at the midspan. Figure 4.13 shows the region used for the strain extraction and the full field strain results in terms of principal strains while figure 4.14 shows the strain field in the material machine and cross directions (MD and CD). The speckle pattern used on the full bag was selected using the same method as for the cruciform samples.

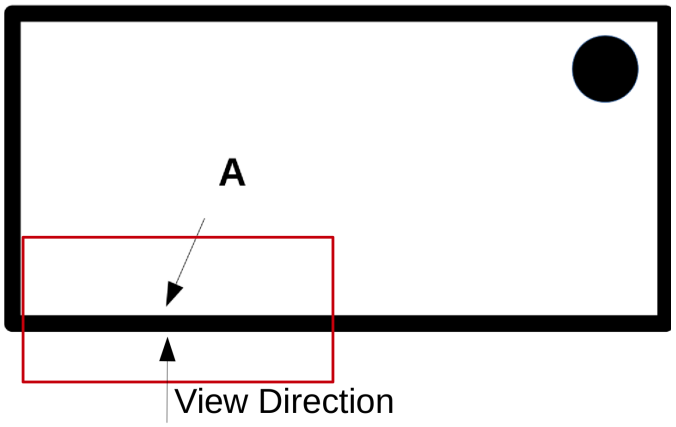

Figure 4.12: Basic geometry of a dunnage bag showing the position of the non-return valve, the strain recovery position (A), and the view window for the DIC strain analysis

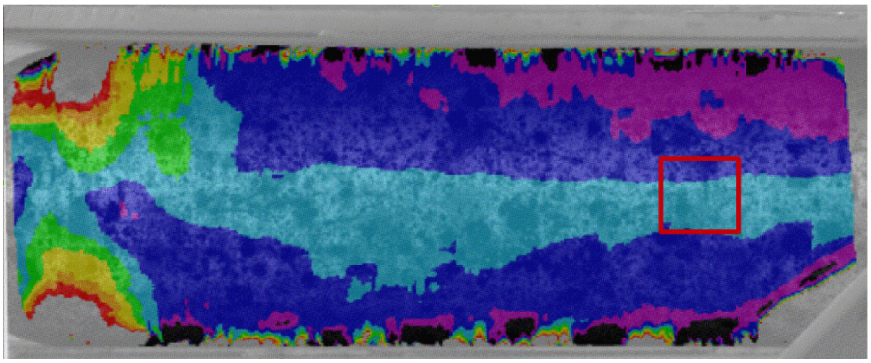

Figure 4.13: Principal strain in an inflated dunnage bag measured using DIC for the view field shown in figure 4.12, the strain extraction position is indicated as a red box

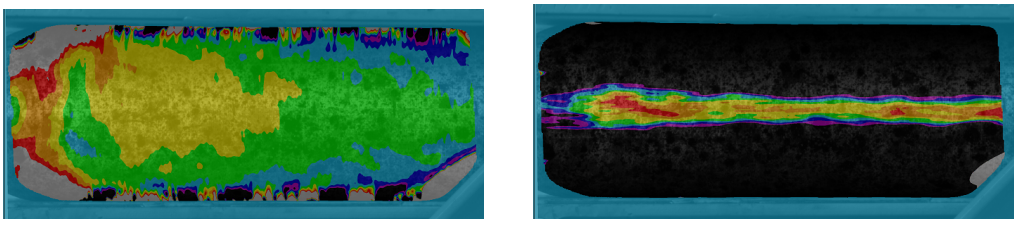

(a) Lengthwise strain (b) Hoop direction strain

Figure 4.14: Lengthwise and hoop direction strain in an inflated bag, measured with DIC, using the viewfield indicated in figure 4.12

Using DIC the material strain in the machine and cross directions (MD and CD) were measured. Table 4.1 shows the maximum strains recorded using DIC in both material MD and CD when the bag is inflated and then cycled. The total CD strain is shown to be much larger than the MD strain though the proportional increase in strain for the MD fibres under cyclic loading is higher than for the CD fibres. In each case the material is assumed to be initially unstrained. The material strain ranges bounding the region of interest are 0-4.9 % for the CD and 0-1.3 % in the MD.

Table 4.1: Maximum strain in material MD and CD

	Inflation Strain	Cycle Strain	Total Strain
CD (hoop)	0.04379	0.00518	0.0490
MD (Length)	0.0046	0.00833	0.0129

4.1.5 Cyclic Loading of Cruciform Samples

The material response in both the loading and unloading phase are required to fully characterise woven polypropylene for a cyclic load test of a full dunnage bag. Cycle tests following a load-hold-unload-hold-repeat sequence were investigated in three load-unload configurations:

1. Loading to a fixed elongation - unload to 90 % of maximum load
2. Loading to a fixed elongation - unload to 10 % of maximum load
3. Loading to a fixed elongation - unload to zero load

The unload to 90 % of maximum load method cannot give the full unload curve.

The unload to 10 % of maximum load method captures more of the material unload cycle than the unload to 90 % of maximum load method, and has the advantage that the sample does not go into compression. This method does, however, not directly capture the amount of plastic deformation the sample undergoes. This could be overcome by unloading the sample until there is zero load. Unfortunately this point occurs at a different displacement for the MD and CD, meaning that compression will occur in one direction.

The unload to zero displacement method captures the entire material unload cycle, but has the disadvantage that the sample does go into compression. This disadvantage was overcome by excluding any data below zero load from the final data set.

Each of the methods are used in two configurations a multi-cycle test over the full range of the bi-axial test device and in a more focused configuration

where the material is only cycled twice, once to the maximum strain range of the material MD and once to the maximum material strain range of the CD. In the multi-cycle case, samples are elongated in 1 mm increments from 1 mm to 15 mm with the unload stage defined depending on the configuration selected.

4.2 Measured Results

Sample swatches were cut from a supplied dunnage bag and a series of preliminary tests were performed using all three load cycle types described in subsection 4.1.5. The preliminary tests were performed with the multi-cycle approach and the final material tests were performed using a single cycle approach.

4.2.1 Multi-Cyclic Loading of a Polypropylene Swatch

Figures 4.15, 4.16 and 4.17 show the load applied to a cruciform sample in the material MD and CD over time for a multi-cycle loading with load cycles unloading to 90 %, 10 % and 0 % of the maximum cycle load respectively. The multi-cycle data shown here corresponds to the full range of the bi-axial test device. In each figure the load peaks correspond to a fixed elongation ranging from 1 mm to 15 mm in 1 mm increments. Each of these three figures show that at lower elongations the CD material is subjected to a higher load than the MD material, but at larger elongations this reverses and the MD material is subjected to higher loads than the CD material. At each point in time the MD and CD fibres are subjected to the same elongation. This indicates that the material properties in the MD and CD are very different over the range of the test device.

The most noticeable characteristic of this woven polypropylene material is that there is a switch in which of the two material directions is stiffer over the tested range. To confirm the results observed the order in which the arms of the cruciform sample are clamped was changed through all possible combinations. Then the sample was oriented first with the material MD aligned with the tensile test MD then with the material CD aligned with the tensile test device MD. In every case this characteristic was maintained and was as such found to be a real characteristic of this particular plain-woven polypropylene fabric. This, however, may not be true in general for this class of material as either or both the MD and CD tows can be varied to get different material properties.

Figures 4.18, 4.19 and 4.20 show the load-elongation curves in the material MD and CD for the multi-cycle tests described above. It can be seen that the load-elongation curves are similar to those described in Drozdov and Dusunceli (2013), see section 3.1. A closer look at the lower edge of figure 4.19 shows that the load on the CD material is higher than that of the MD material. This

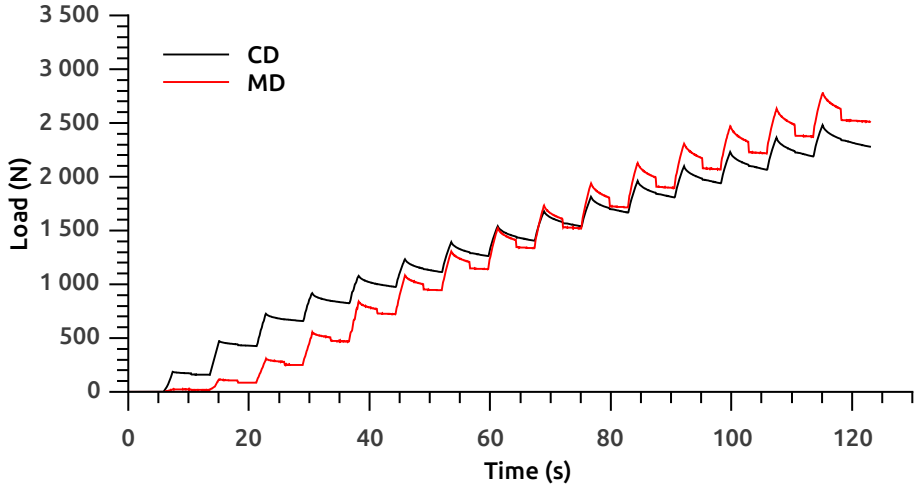

Figure 4.15: Multi-cycle results with load reduced to 90 % of maximum load, 1 mm increments in a multi-cycle configuration

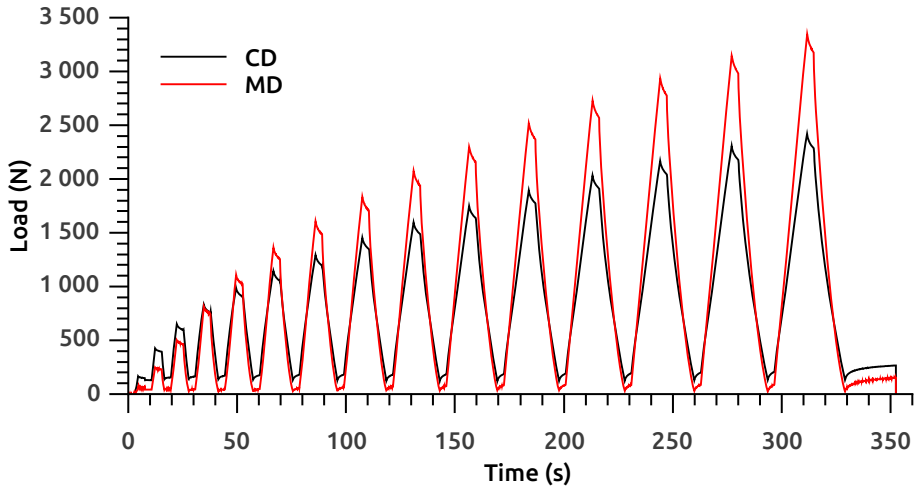

Figure 4.16: Multi-cycle results with load reduced to 10 % of maximum load, 1 mm increments in a multi-cycle configuration

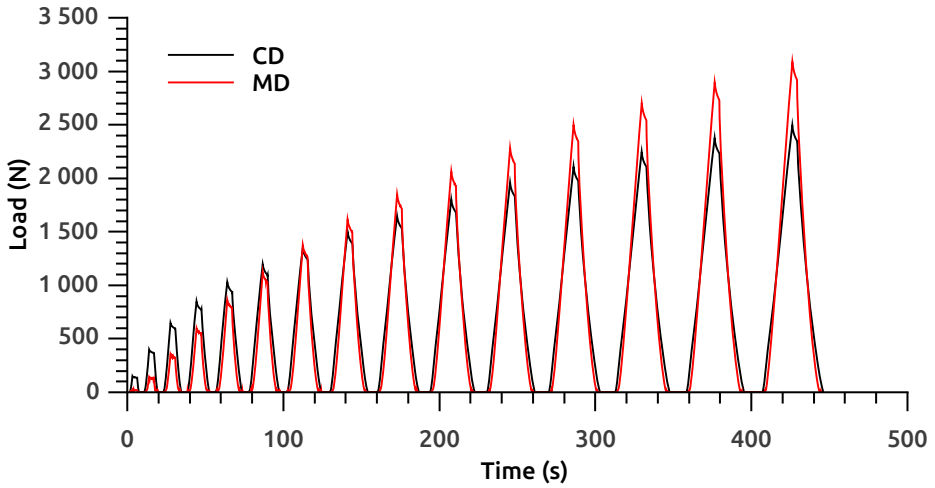

Figure 4.17: Multi-cycle results with load reduced to zero load, 1 mm increments in a multi-cycle configuration

happens because the bi-axial test device used has the same displacement in the MD and CD directions and the load reduction to 10 % is calculated based on the total force input to the bi-axial device. From the figures above it is known that for a small elongation the material in the MD produces a lower restraining load than in the CD. For a given displacement the load applied to each direction of the material is not the same.

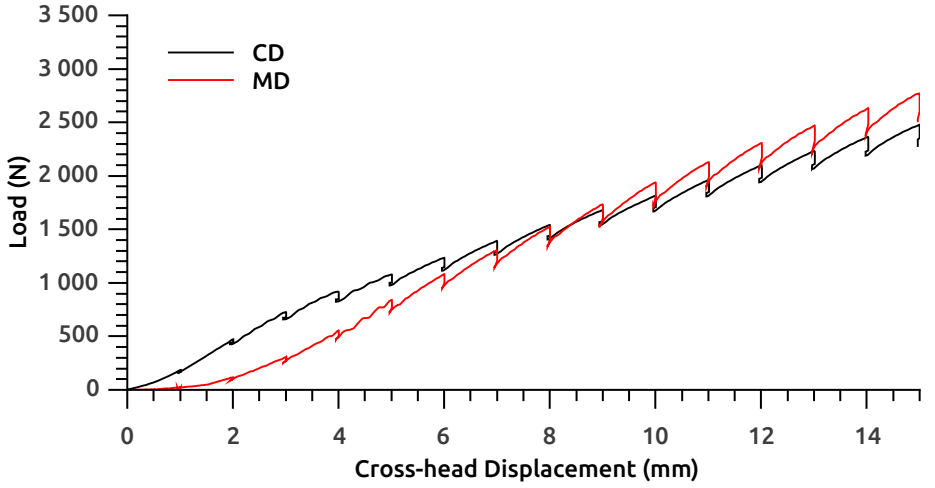

Figure 4.18: Load-elongation curves in the MD and CD for a multi-cycle test to 90 % of maximum load

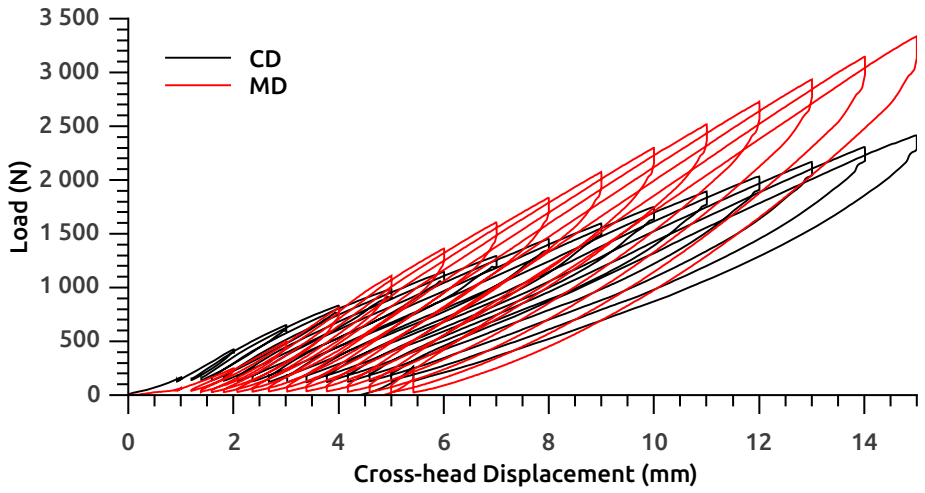

Figure 4.19: Load-elongation curves in the MD and CD for a multi-cycle test to 10 % of maximum load

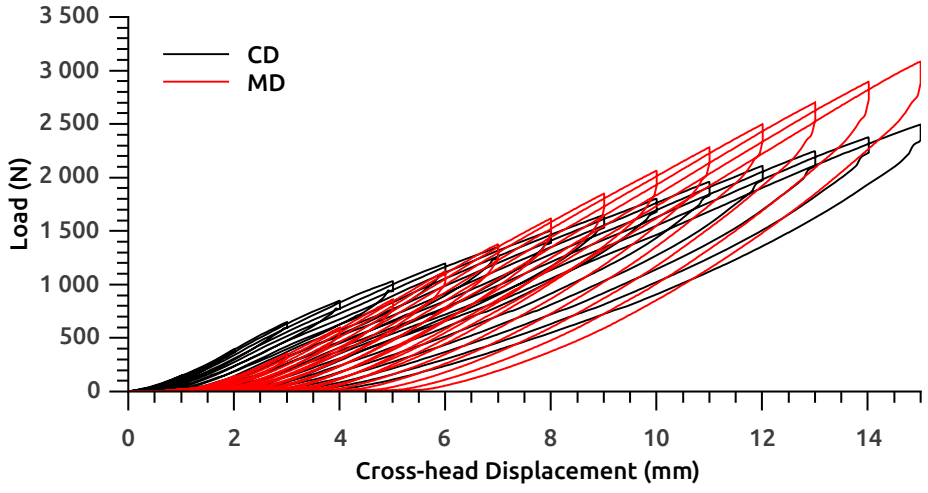

Figure 4.20: Load-elongation curves in the MD and CD for a multi-cycle test to load

4.2.2 Single Cycle Loading of a Polypropylene Swatch

Figures 4.21 and 4.22 show the results of the two-cycle loading. Here the material strain ranges resulting from full bag strain analysis using DIC are used. The maximum strain in the bag hoop and longitudinal directions are translated to material CD and MD respectively. A preliminary set of tests were performed to find the bi-axial device displacement required to generate each the requisite maximum strains. The desired maximum strains are 0.0129 in the MD and 0.049 in the CD. The maximum elongation ranges set on the bi-axial device are 3.5 mm for the MD and 11.5 mm for the CD. These two device elongations correspond to elongations of 1.29 mm and 4.9 mm elongations in the 100 x 100 mm area of interest at the centre of the cruciform sample.

Two single cycle tests were performed to generate the load-unload response for the woven-polypropylene fabric when loaded to the maximum elongation in the MD and CD for the material. Figure 4.21 shows the load-unload curve for the woven material loaded to the maximum MD strain. Figure 4.22 shows the load-unload curves for the material loaded to the maximum CD strain. Unfortunately the bi-axial device used cannot load the woven material such that the MD and CD materials are simultaneously loaded to their maximums strain values. This is a shortfall of the test equipment.

4.3 Evaluation of Results

The purpose of the material swatch testing is to investigate the trends associated with the material response and produce a reliable response curve that will form the basis for material parametrization. The most notable trend observed in the data is that the material CD dominates under low strains while the material MD dominates under higher strains. This trend is not seen with conventional, continuous, homogeneous engineering materials. The transition point, however, occurs outside the expected loading range of the material and thus may not affect the later development of numerical material models.

The load curve that will be used as the basis for the material parametrization is a hybrid case using portions of the material load-unload curves from the two single cycle tests. The MD response will be taken from the MD maximum strain test and the CD response will be taken from the CD maximum strain test. Figure 4.23 shows the material response curves for material parametrization scaled for a 50 x 50 mm sample in the non-SI unit combination of kN and mm used in later simulations.

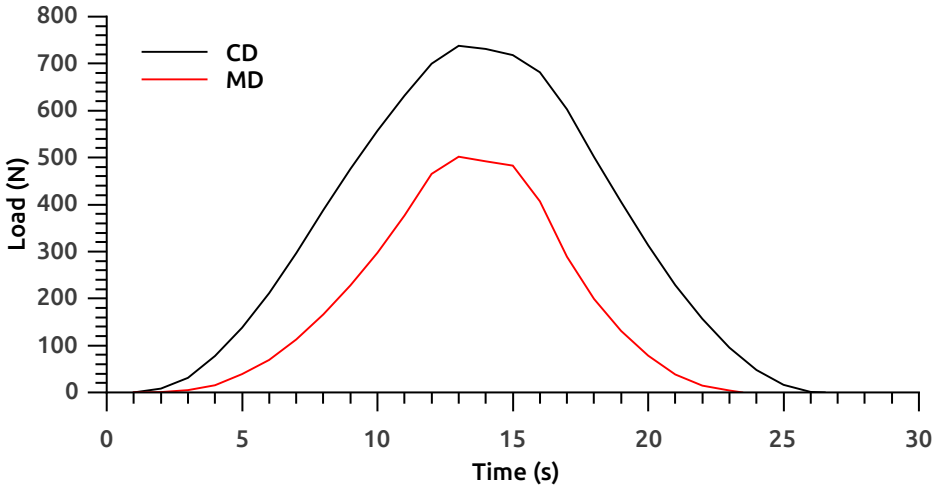

(a) Load-time

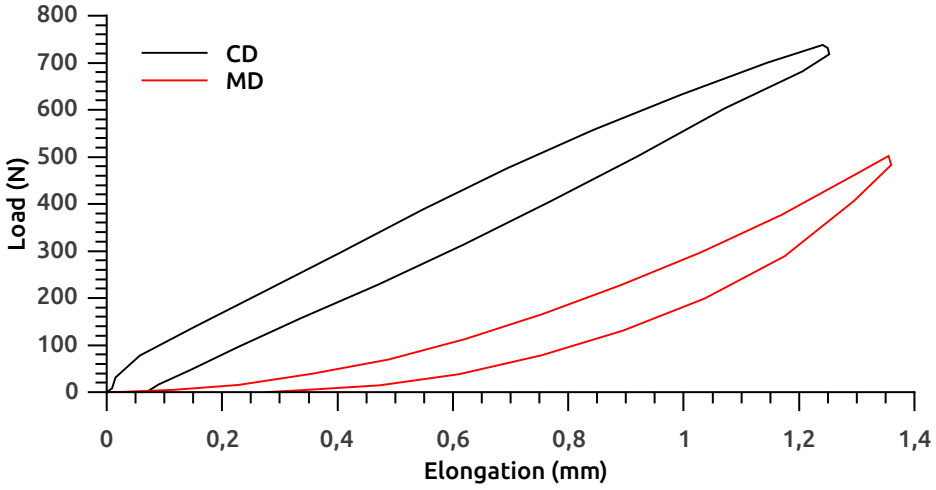

(b) Load-elongation

Figure 4.21: Load cycle to maximum MD strain

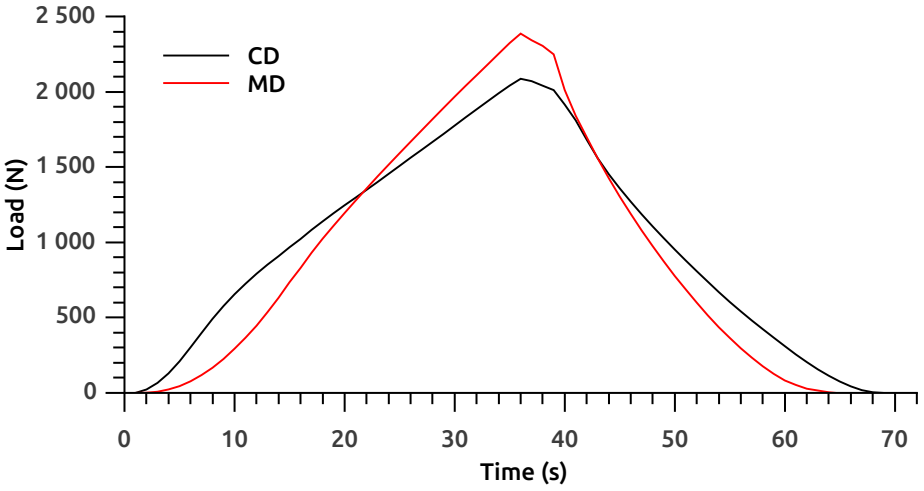

(a) Load-time

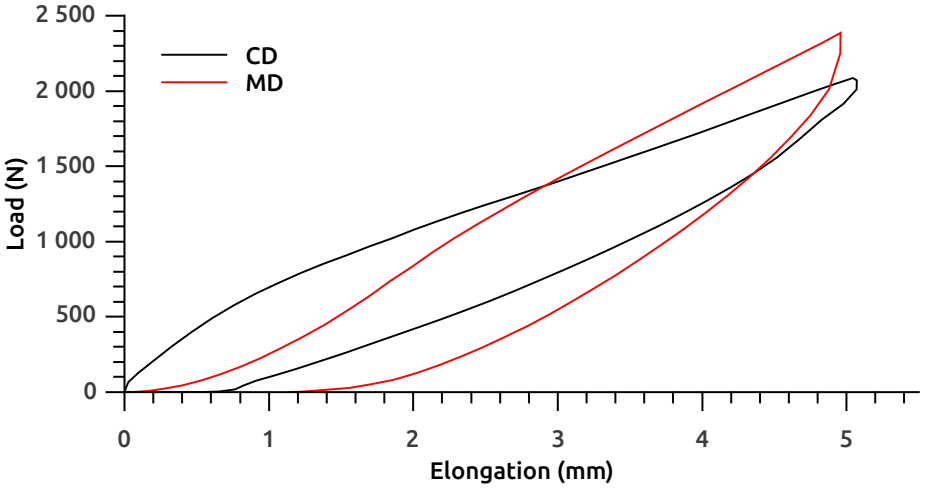

(b) Load-elongation

Figure 4.22: Load cycle to maximum CD strain

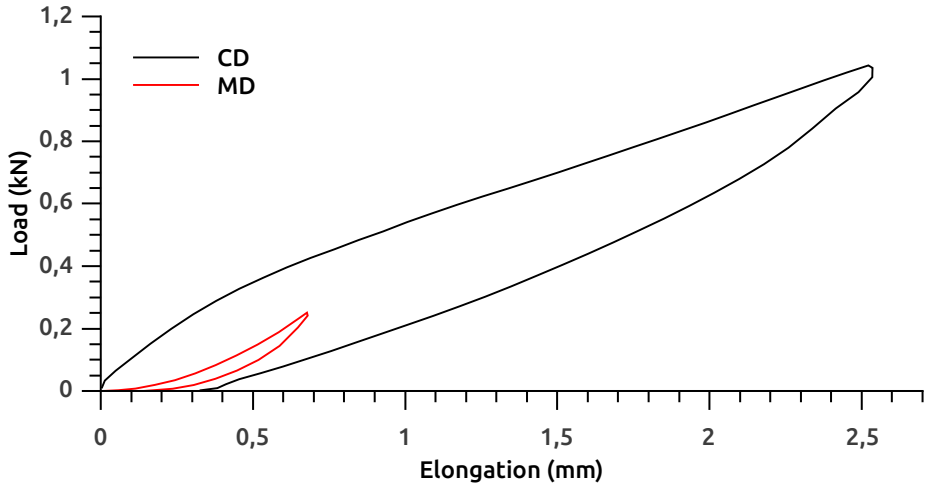

Figure 4.23: Evaluation machine and cross direction load-unload curves for a 50 x 50 mm woven polypropylene swatch

Chapter 5

Material Parametrization

The material properties for plain-woven polypropylene fabric cannot easily be derived based on the properties of the constituent fibres or the properties of the underlying polypropylene itself. The properties of woven polypropylene fabric are a combination of mechanical properties of polypropylene and the mechanical properties of the fabric due to the weave architecture. For a large scale model where the overall dimensions of the structure are much larger than the dimensions of the weave architecture the properties of the woven material should, for practical reasons, be homogenised. For woven inflatable dunnage bags the overall dimensions are on the order of metres while the fibres making up the weave architecture are only about 2 mm wide.

5.1 Material Homogenisation

For the purposes of this project material property homogenisation is the process of describing the average response of the woven fabric to a mechanical load. Furthermore, this average response will be described in terms of a standard material model available in a commercial finite element package.

Literature describes two basic approaches to homogenisation of woven fabrics, one using data collected through physical experimentation (using a fabric swatch) and the other using data from numerical experiments (using a numerical unit cell). A simple trial showed that in order to make use of a numerical unit cell an accurate weave architecture is required as well as an accurate material model for the underling material, in this case polypropylene. Defining an accurate weave architecture that can account for variations in the weave due to manufacturing tolerances requires specialised scanning equipment, not available for this project. Generating an accurate material model for polypropylene is a problem equivalent to generating a material model for the homogenised woven material. Due to these two factors the homogenisation using data from physical swatch tests was selected for this project using the data presented in chapter 4.

Using a homogenised material property has several drawbacks caused by the fact that the homogenised material does not match the mechanics of the true material. As an example the stress in the body being simulated is not representative of the stress in the physical material, meaning that the homogenised material model will make use of a surrogate stress-strain relationship not related to the physical material. Different homogenised material models can also be used to represent the response of the same material each matching different parts of the material response. The errors inherent in the use of a surrogate material can be limited by a clear statement of the desired responses and the range over which those responses are of interest.

For this project the load-unload response of the woven material in the longitudinal (MD) and hoop or (CD) directions are of interest. Material shear response is not evaluated in this project because there is very little shear in the failure regions of the bag and there is no standard material model with the ability to account for the complex non-linear shear characteristic. The decision was made to subject the material to a load similar to that experienced by the material in-situ. The experimental data presented in chapter 4 already accounts for the strain ranges the bag is subjected to in a full cycle test.

The material parametrization procedure presented in this chapter selects a viable material model and formulates an inverse problem that maps the response of a numerical simulation of a material test with the results of the physical swatch tests from chapter 4. The result of the inverse problem is a set of parameter values for the selected material models that best replicates the response of the physical swatch tests.

5.2 Inverse Problems for Material Parametrisation

The use of inverse problems to parametrise materials is not uncommon. Forestier *et al.* (2002) describes the estimation of constitutive parameters of a non-linear material using an inverse method. The response of a non-linear finite element analysis is mapped to the measured results of a physical test. Husain *et al.* (2004) makes use of a similar inverse problem matching the response of a finite element model to test data to determine constitutive tensile behaviour of materials, but makes use of a simple contrived experiment. Milani and Nemes (2004) extends this method to the characterisation of a hyperelastic material model for a textile reinforced thermoplastic making use of a simple biased uni-axial tensile test. Kajberg and Lindkvist (2004) use the inverse method to successfully characterise a material subjected to large strain using in-plane displacement fields. The paper describes how the displacement fields are generated using digital speckle photography, a similar technology to DIC though less accurate. Zhou *et al.* (2006) couples a finite element software package to a

general numerical optimiser to identify constitutive parameters of aluminium oxide at high temperatures. Garbowski *et al.* (2012) uses an inverse analysis to calibrate an orthotropic elastic-plastic constitutive model for thin foils using a bi-axial test device. Surface strain measurements were taken using DIC. In this case the inverse problem was solved by use of a neural network.

The literature available shows that inverse methods are suitable for parametrisation of materials subject to complex interactions of material and geometric properties. DIC systems can be used to generate data sets to be matched by a numerical optimiser. In this project a cruciform sample was subjected to a known displacement at each arm and the surface strain was measured using DIC. A representative material model was selected and a replica for the physical test was created as a finite element model. The measured strain was enforced in the numerical model similar to the physical test. The load-elongation curve from physical testing was then mapped to the numerical model by manipulation of the parameters of the material model.

5.3 Material Models for Woven Polypropylene

The first step in matching the response of the physical testing performed is to select a material model capable of the characteristics observed in the physical test. The physical test showed that the material load-unload curve differs greatly between the material MD and CD in terms of the shape of the curves, and the range of load and elongation values observed in in-situ testing. Of interest here is matching the MD and CD load-elongation curves of the swatch test results. The shear is assumed to be negligible in critical failure regions.

It is known that woven materials are non-continuous, non-homogeneous and have a non-linear shear stress-strain relationship. It is also known that few material models for woven materials have been developed for or implemented in commercial finite element software to date.

LS-DYNA was chosen as the software package most suitable to the simulation of structures that undergo large displacements under an inflation load, such as airbags. Not only does LS-DYNA make use of explicit integration but is extensively used to simulate the inflation of airbags. Using LS-DYNA, two material modelling options were evaluated for this project, existing constitutive models for continuum elements and non-linear discrete elements in the from of a hybrid element. A user-defined material model could also be produced that effectively homogenizes the material properties of woven polypropylene, but that was beyond the scope of this project and is left as recommended further work.

5.3.1 Continuous Constitutive Models

There are several material models available in LS-DYNA that are suitable for representing the homogenised woven polypropylene material. The candidate models were identified using the requirements that the models function with shell elements, support an orthotropic material response and account for plastic material deformation. The list of candidate models is as follows;

- MAT_02 Orthotropic Elastic
- MAT_03 Isotropic Plastic Kinematic
- MAT_24 Isotropic Piecewise Linear Plasticity
- MAT_34 Orthotropic Fabric
- MAT_40 Non-Linear Orthotropic
- MAT_89 Isotropic Plasticity Polymer
- MAT_108 Orthotropic Elastic Plastic
- MAT_187 SAMP-1 Semi-Analytical Model for Polymers (Kolling *et al.* (2005))

It is important to note that there is no model currently available in LS-DYNA that can fully capture the mechanical characteristics and material response of woven polypropylene and each of the candidate models listed above fall short in some regard. Each material model will be compared and evaluated in terms of their ability to replicate the response of a physical test.

Several of the models listed above can be excluded without trial simulations. Even though MAT_02 (Orthotropic Elastic) has been found suitable for modelling inflatable structures in literature it is excluded without trial here because woven dunnage bags inflated to operating pressures are already loaded beyond the yield point of the material. For the purposes of this project post yield material characteristics are required. MAT_03 (Plastic Kinematic) and MAT_24 (Piecewise Linear Plasticity) have similar capabilities in LS-DYNA. MAT_24 can be considered as an extension of MAT_03 capable of replicating a more complex post yield response. MAT_24 is the recommended standard model for simulating plasticity. With the additional features provided by MAT_24 make MAT_03 largely obsolete for this application. MAT_40 (Nonlinear Orthotropic) is not stable, and is not recommended for use by the LS-DYNA user guide. MAT_89 (Plasticity Polymer) is again similar to MAT_24 except that it was developed for materials with a less distinct yield point. This model intern requires additional parameters from physical testing. MAT_89 is excluded because its functionality can be replicated using MAT_24. If MAT_24 is found to be the most suitable material model MAT_89 would be

evaluated in more detail. MAT_24, though able to capture the plasticity in the material well, cannot account for the orthotropic nature of the material.

The remaining models, MAT_34 (Fabric) and MAT_108 (Orthotropic Elastic Plastic), can capture both material plasticity and the orthotropic nature of the weave architecture. Both materials can be calibrated using simple physical tests. MAT_34 was developed for the use with the airbag inflation models and gives additional parameters for airbag permeability as well as the addition of a liner and material coating. The results of uni-axial tensile tests in the material MD and CD are assigned as stress-strain curves (2^{nd} Piola-Kirchoff, Green-Lagrange) to the material primary and secondary direction. MAT_108 is an orthotropic elastic plastic material with an anistropic yield criterion. MAT_108 is capable of capturing plasticity in two orthonormal material directions with plasticity dependent on the material bi-axial tensile state. MAT_34 was excluded from testing even though it is more commonly used for airbag type structures and has more advanced material options because there was no effective mechanism of accounting for the change in material response due to bi-axial loading. MAT_108 was selected as the most likely candidate for replicating the material response of homogenised plain-woven polypropylene.

A recurring problem is encountered when using constitutive material models in that they have difficulty capturing the unload path of the material. The measured response clearly indicates that the material stiffness when unloading is different from the stiffness when loading even at low strain rates. Practically this presents as an over-prediction of the force required to maintain a given elongation during the unload phase of a cycle test.

NOTE: Dubois and Forsberg (2013) have recently proposed a parameter identification method for MAT_34_FABRIC that can capture the strain stiffening effect of woven materials under bi-axial loads. If this method works for the material considered here, MAT_34 will be the better material choice for the homogenised material. MAT_34 gives access to element formulations optimised for use with gas inflation models. This is included at future work.

5.3.2 Non-Continuous Material Models

An alternative to using continuous material models is to create a hybrid element model such as those used by Apedo *et al.* (2010) and Brueggert and Tanov (2002). Here conventional continuum elements are combined to give a net characteristic that is representative of the overall material response. Conventional shell elements can be combined with a cable or beam network to produce an element that is orthotropic and accounts for material shear. Boisse *et al.* (2008) compares discrete, continuous and semi discrete approaches to modelling woven materials and concludes that in general tow overlap points don't shift relative to each other. This means that the tow overlap points can be represented by merged node connections between warp and weft fibres in the numerical model without much loss in accuracy.

The hybrid element model adds four 1D elements to a conventional four-node 2D quadrilateral element to provide stiffness to the element. The new hybrid element still has only four nodes but makes use of five elements. The quadrilateral element is required for inflation using the airbag inflation models available in LS-DYNA and provides some shear stiffness that improves model stability.

Cable, beam and discrete spring elements were investigated as stiffening members for the hybrid element. When cable and beam elements are created using MAT_24 the load-elongation curves in the material MD and CD can be exactly matched when the sample is being loaded. When the sample is unloaded the hybrid element over-predicts the stiffness of the material.

Using a non-linear discrete spring element proved far more successful at capturing the material unload characteristic of woven polypropylene. The chosen hybrid element makes use of a quadrilateral element with a conventional isotropic elastic material model with a relatively low stiffness and four discrete non-linear spring elements using MAT_S06. The non-linear spring model provides the ability to define independent non-linear load and unload load-elongation curves to exactly match the response of the tested material. Unfortunately this comes at the expense of generality for the hybrid element. With the load-unload curve being defined instead of a stress-strain relationship every different size element will require a different load-elongation curve definition. This is not a problem for general simulations of inflatable dunnage bags because the mesh is typically consistent.

5.4 Equivalent Numerical Swatch Tests

The physical test presented in chapter 4 subjected a cruciform sample with a 100 x 100 mm central area of interest to bi-axial edge displacement as shown in figure 5.1. The equivalent numerical model is a simple 4 node unit cell representing a 50 x 50 mm square patch of material. Here the assumption is made that there are two perpendicular symmetry planes at the centre of the physical sample allowing the numerical sample to be split in four along those two lines. The model for a single shell element is shown in figure 5.2, where node 1 is fully constrained and the motions of nodes 2 and 4 are inhibited in the y and x directions respectively. The swatch is subjected to a forced displacement in the x and y directions matching the maximum CD and MD elongations recorded in physical testing. The edges are then returned to the point where the material is no longer loaded avoiding the portion of the simulation that would include wrinkling.

Two candidate materials selected for parametrization each have different parameters. MAT_108 is an orthotropic elastic-plastic material property suitable for use with shell elements. In this case the numerical equivalent model discussed above makes use of only one fully integrated shell element.

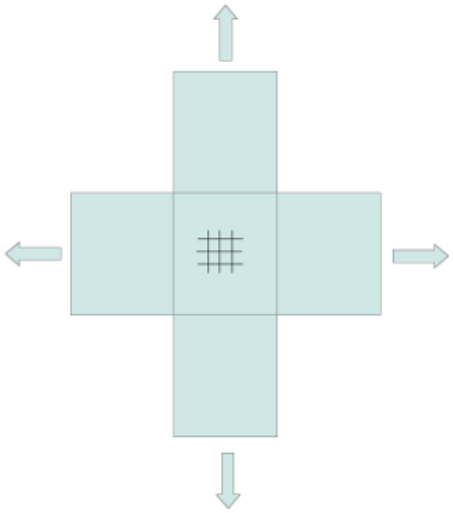

Figure 5.1: Bi-axial loading of a cruciform sample

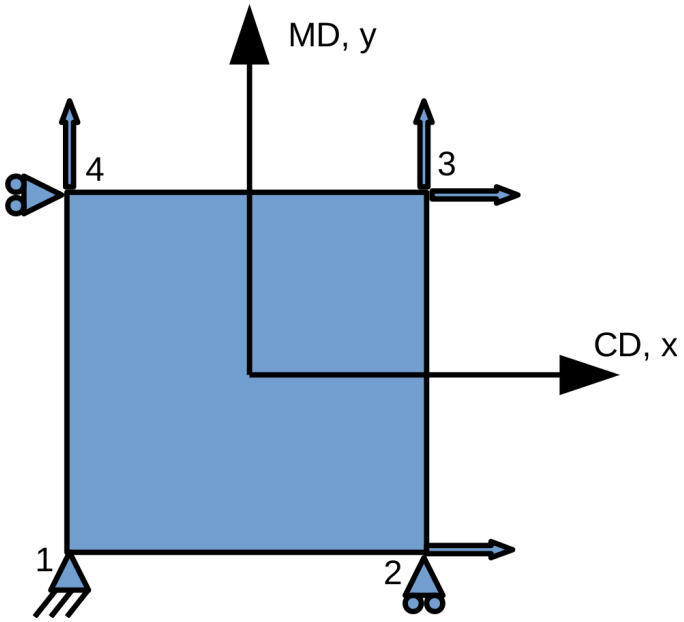

Figure 5.2: Loads and boundary conditions for 4 node unit cell model to replicate the material test

The hybrid spring-shell element equivalent model is similar to that of the MAT_108 model, but material stiffness is provided as a series of 4 non-linear springs referencing MAT_S06. In this case the properties of the shell element are such that it is compliant relative to the springs, providing little stiffness. MAT_S06 allows the software user to define separate load and unload curves for each spring. Two springs are calibrated to the MD response, connecting nodes 1-4 & 2-3, and two springs are calibrated to match the CD response connecting nodes 1-2 & 3-4.

Once the materials have been calibrated these models are checked for robustness through mesh refinement where the number of elements is increased first to four then sixteen while ensuring that the load displacement response of the numerical simulation is maintained.

5.4.1 MAT_108 Material Model Parameters

MAT_108 is an orthotropic elastic-plastic material that makes use of an anisotropic yield criterion. Two orthotropic elastic moduli are used to describe the material response before yield and a nominal effective stress versus effective plastic strain curve is required for the post-yield characteristics of the material. The nominal stress-strain curve is manipulated by the yield parameters to calculate the equivalent stress (σ_{eq}) in the material under various loads.

$$\sigma_{eq} = \sqrt{F(\sigma_{22}-\sigma_{33})^2 + G(\sigma_{33}-\sigma_{11})^2 + H(\sigma_{11}-\sigma_{22})^2} \tag{5.4.1}$$

$$\overline{+2L\sigma_{23}^2 + 2M\sigma_{31}^2 + 2N\sigma_{12}^2} \tag{5.4.2}$$

Where F, G, H, L, M and N are constants normally obtained from testing, defined as

$$F = \frac{1}{2}\left(\frac{1}{R_{22}^2} + \frac{1}{R_{33}^2} - \frac{1}{R_{11}^2}\right) \qquad L = \frac{3}{2R_{23}^2} \tag{5.4.3}$$

$$G = \frac{1}{2}\left(\frac{1}{R_{33}^2} + \frac{1}{R_{11}^2} - \frac{1}{R_{22}^2}\right) \qquad M = \frac{3}{2R_{13}^2} \tag{5.4.4}$$

$$H = \frac{1}{2}\left(\frac{1}{R_{11}^2} + \frac{1}{R_{22}^2} - \frac{1}{R_{33}^2}\right) \qquad N = \frac{3}{2R_{31}^2} \tag{5.4.5}$$

The yield criteria, R_{ij}, are defined as follows where σ_0 is the nominal stress in the element and $\bar{\sigma}_{ij}$ is the stress in each material direction.

$$R_{11} = \frac{\bar{\sigma}_{11}}{\sigma_0} \qquad R_{22} = \frac{\bar{\sigma}_{22}}{\sigma_0} \qquad R_{33} = \frac{\bar{\sigma}_{33}}{\sigma_0} \tag{5.4.6}$$

$$R_{23} = \frac{\bar{\sigma}_{12}}{\tau_0} \qquad R_{13} = \frac{\bar{\sigma}_{23}}{\tau_0} \qquad R_{31} = \frac{\bar{\sigma}_{31}}{\tau_0} \tag{5.4.7}$$

For the purpose of this model the σ_0 parameter is not required. The variable parameters for this material are listed in table 5.1, two elastic moduli, one shear modulus, four yield parameters and three parameters relating to the nominal effective stress-strain curve. The decision was made to go with a simple bi-linear curve for the nominal effective stress-strain. This was done because the material model produces load curves for the primary and secondary material directions that are scaled versions of the nominal curve. The difference between the two load curves is that the onset of plasticity occurs at different points for each direction. Essentially both curves must have the same shape profile.

Results from physical testing show that the character of the load curves for the material MD and CD are very different. If a more complex curve is fitted the response in one direction can be improved, but the response in the other direction becomes less representative. To simplify the model it was assumed that since the MD elongation is much lower than the CD elongation that the MD material can be represented by a linear elastic response only while the CD response includes a non-linear plastic component. In order to force the MD response to remain elastic the yield point in this direction is set beyond the expected stress range for this material.

The nominal stress-strain curve itself is formed using effective stress values at two fixed effective strain values. The strain recovery points are then multiplied by a factor that sets the strain range to an appropriate size. Using this parametrization MAT_108 requires ten parameters.

Table 5.1: Material parameters for MAT_108 material model

Parameter	Description
E_{11}	Elastic modulus in 11-direction
E_{22}	Elastic modulus in 22-direction
G_{12}	Shear modulus in 12-direction
R_{11}	Yield criteria parameter
R_{22}	Yield criteria parameter
R_{33}	Yield criteria parameter
R_{12}	Yield criteria parameter
σ_1	First stress point in nominal stress-strain curve
σ_2	Second stress point in nominal stress-strain curve
$Scale$	Strain scale factor for nominal stress-strain curve

Figure 5.3 shows the parametrized four node element for the MAT_108 model.

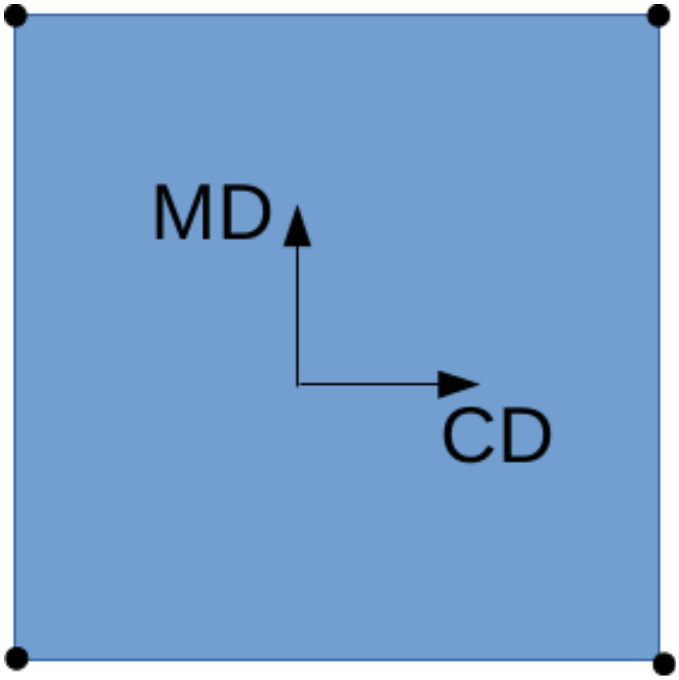

Figure 5.3: MAT_108 element with four nodes and two material directions

5.4.2 Hybrid Element Material Model Parameters

MAT_S06 requires two curves as input, separate force-elongation curves for the loading and unloading of the spring. Arbitrary load and unload curves can be set for the material MD and CD. Though this model does not directly take into account tow interaction due to bi-axial loading it is somewhat accounted for by Poisson's ratio of the isotropic shell. Figures 5.4 and 5.5 show how the load and unload curves for MAT_S06 have been parametrized.

The curve for loading is defined with ten parameters that define the force-elongation curve. There are eight force parameters, one elongation parameter and one scale factor for elongation.This is a similar configuration as the one used for the stress-strain curve in the MAT_108 model. The force-elongation curve comprises of eight points, one of which has both force and elongation components. This is because the observed material response appears to be somewhat bi-linear and there is a lot of advantage to having a point directly at the point of change. The remaining forces are at fixed, evenly distributed intervals. The first nine parameters are used to change the shape of the curve and the tenth, the elongation scale factor, is used to stretch the curve to its best fit.

The unloading curve is similarly constructed to the loading curve and has six force parameters, one elongation parameter and one elongation scale factor. A description of all the hybrid element parameters is given in table 5.2. There are a total of 44 parameters in the hybrid element material. Considerably

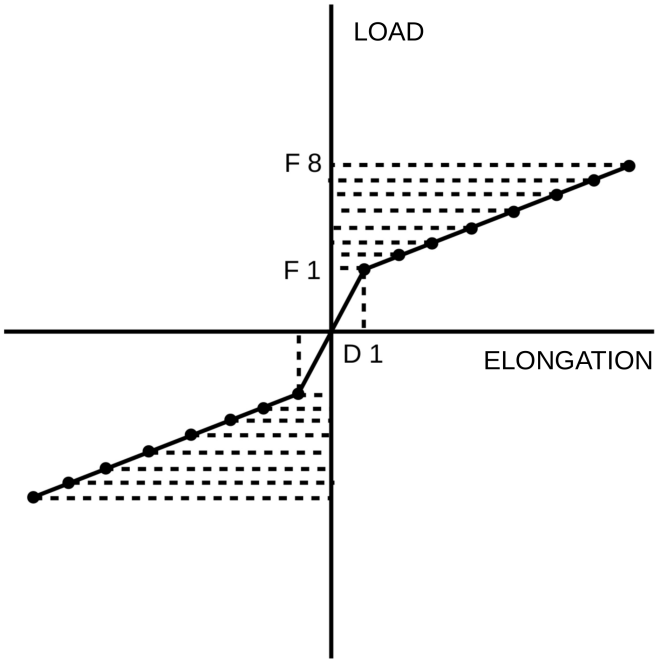

Figure 5.4: Parametrized Load-elongation curve under loading for a non-linear spring MAT_S06

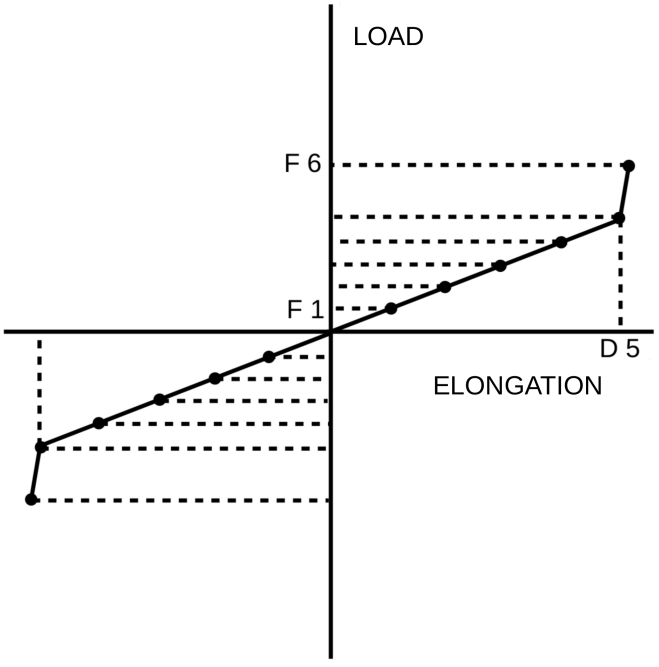

Figure 5.5: Parametrized Load-elongation curve when unloading for a non-linear spring MAT_S06

more than for the MAT_108 model.

Table 5.2: Material parameters for hybrid element material model

Parameter	Description
$L_{CD}F01$ to $F08$	Force Component for CD loading
$L_{CD}D01$	Elongation Component for CD loading
$L_{CD}ScaleE$	Scale factor for elongation for CD loading
$U_{CD}F01$ to $F06$	Force Component for CD unloading
$U_{CD}D01$	Elongation Component for CD unloading
$U_{CD}ScaleE$	Scale factor for elongation for CD unloading
$L_{MD}F01$ to $F08$	Force Component for MD loading
$L_{MD}D01$	Elongation Component for MD loading
$L_{MD}ScaleE$	Scale factor for elongation for MD loading
$U_{MD}F01$ to $F06$	Force Component for MD unloading
$U_{MD}D01$	Elongation Component for MD unloading
$U_{MD}ScaleE$	Scale factor for elongation for MD unloading

Figure 5.6 shows the parametrized four node element for the the hybrid element model.

5.5 Parameter Mapping Using LS-OPT

For each of the two candidate materials the optimization problem works the same way. In each case the optimizer is asked to run the equivalent numerical swatch model with given parameter values and extract histories for the load applied to each edge of the numerical swatch and the displacement of each edge of the swatch. The x- and y-forces are the sum of forces applied in the x and y directions at nodes 2 & 3 and 4 & 3 respectively. x- and y-displacements are recorded at nodes 2 and 4 respectively, see figure 5.2. The software then cross-plots the load-time and displacement-time curves in the x- and y-directions to generate two load-elongation curves for the MD and CD. The load-elongation curves generated by LS-DYNA are then compared to those selected in figure 4.23. The optimizer is tasked with minimizing the difference between the response curves produced by LS-DYNA and the response curved generated in physical tests, by varying the parameters defined in the LS-DYNA models.

The optimizer selected is LS-OPT (Stander *et al.* (2012)) which is an integrated optimizer for LS-DYNA. The inverse problem described above was solved using a genetic algorithm as a direct method using the curve matching metric described by Witowski *et al.* (2011). The method described by Witowski *et al.* (2011) delivers a single value describing the area between two

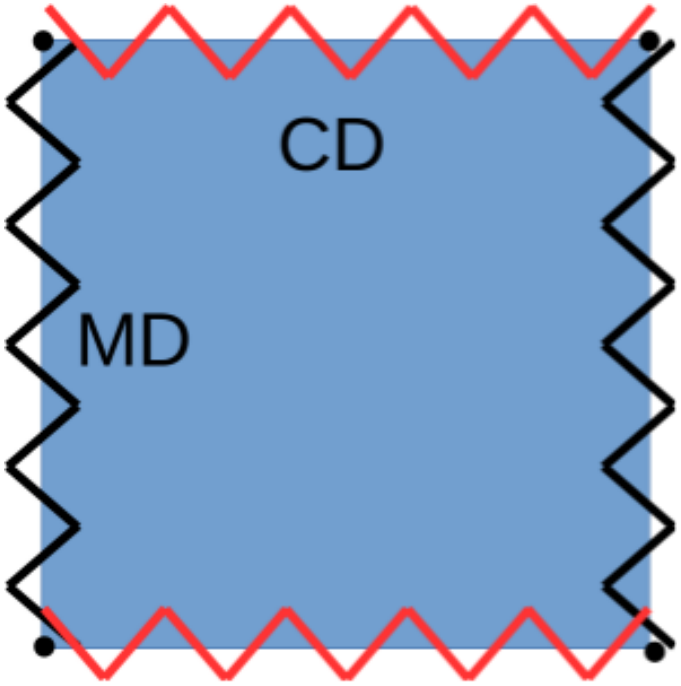

Figure 5.6: Hybrid element with four nodes and two material directions. Four springs are attached to a four node membrane element, two springs for the MD material response and two springs for the CD response

curves. This method has been recommended over the traditional least squares method because of its superior ability to deal with curves that double back on themselves as the load-elongation curves do here.

This allows the following optimization problem to be formulated.

$$MINIMIZE : f(\mathbf{X}) = W_1 + W_2 \tag{5.5.1}$$

(5.5.2)

Where W_1 is the area between the tested material CD load-elongation response and the simulated load-elongation response. Similarly W_2 is the area between the tested material MD load-elongation response and the simulated load-elongation response. $\mathbf{X}$ are the parameters specified for each material model discussed in sections 5.4.1 and 5.4.2.

A preliminary trial and error process is used to define the starting values for each parameter. Here LS-OPT is used as a model builder, scheduler and post processor to streamline the evaluation of the curve comparison, figure 5.7. During the trial and error phase on optimisation is performed. The user changes the variable values in LS-OPT which in turn makes the required changes to the LS-DYNA input deck and runs the simulation. LS-OPT then imports the results and plots the load-elongation curve in the MD and CD and displays them on a graph with the curve recorded during physical testing. The

relative size and shape of the curves is then used to evaluate the parameter values. New values are input and the process is repeated until starting values have been found for each parameter.

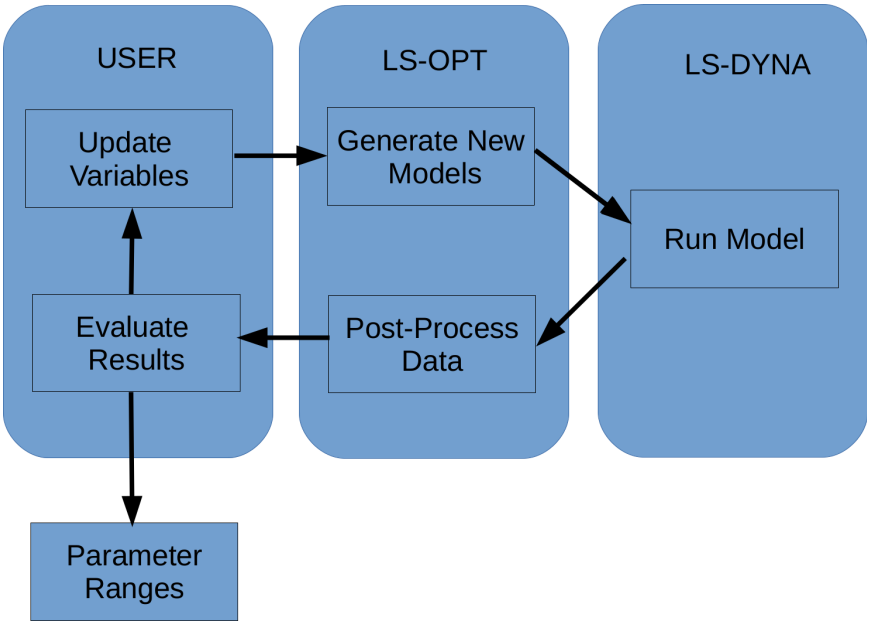

Figure 5.7: Trial and error approach to finding parameter ranges

Once the initial values are found LS-OPT is used to run a genetic algorithm to find the optimum parameter values for each model, figure 5.8. The genetic algorithm runs 300 generations with a population of 150 for the hybrid element material and a population of 50 for the MAT_108 material.

5.6 Numerical Material Response Results

LS-OPT models were created and run for both the MAT_108 and hybrid element models and the robustness of the results was confirmed through mesh refinement. The resulting load-elongation curves for each model are presented below. Each model is calibrated to a specific load path and the effects of over and under loading are not directly modelled, these are rather evaluated in terms of how well they maintain the general trends associated with the calibrated model.

5.6.1 MAT_108 Material Response Results

When working with MAT_108 several problems arise. MAT_108 requires both the primary and secondary material responses to be of similar shape.

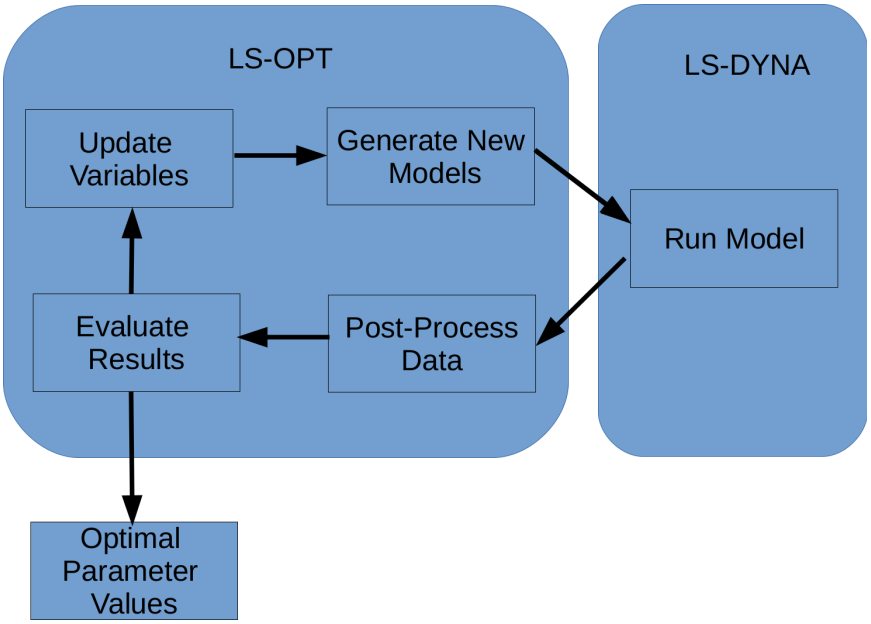

Figure 5.8: Finding optimal parameter values with LS-OPT

This is because both material responses share a common stress-strain reference curve. With this in mind it was decided that the CD response would be the focus of the material calibration. This is done by weighting the CD response more heavily than the MD response in the objective function for the optimization loop. With this philosophy the MD response was made purely elastic. This is a reasonable assumption since the MD material did not undergo as much plastic deformation in physical testing as the CD material, and as such is expected to play a smaller role in the overall geometric change caused by loading.

Figure 5.9 shows the material response of the physical bi-axial testing of cruciform samples as seen in figure 4.23 and the response of the numerical replica of that test that makes use of MAT_108. It is seen that the response of the numerical model is similar to that of the physical test for the loading of the material in the CD, but does not capture either the unload response in the CD nor the load or unload responses in the MD.

Figure 5.10 shows the effect of increasing or decreasing the maximum strain on the element by 25 %. This is done to get an idea of how the material responds outside it's calibrated range. Again the material maintains the general trend associated with the median curve.

5.6.2 Hybrid Element Material Response Results

The results generated for the hybrid element material are shown in figure 5.11. Here it can be seen that the material model captures all key components of the load-elongation curve generated in the bi-axial tensile test. Both the load

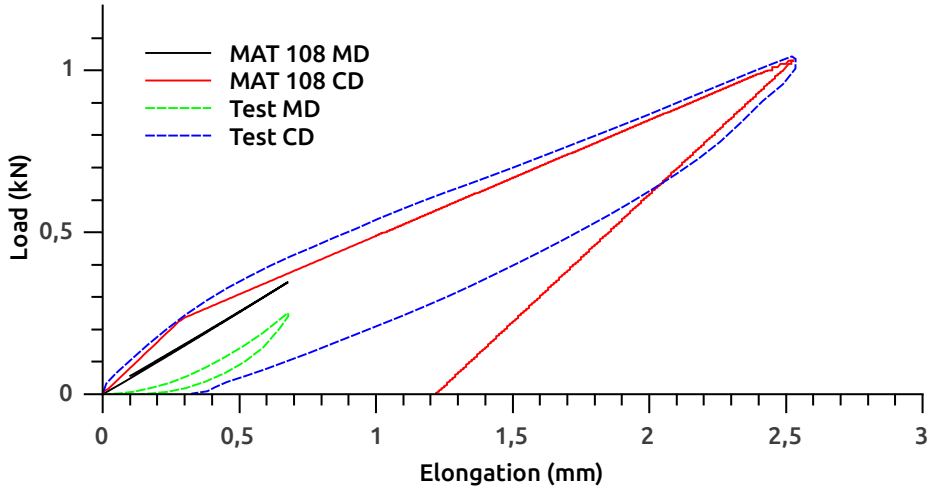

Figure 5.9: Optimised load-elongation curve for numerical swatch with MAT_108 material. MD and CD response for the numerical equivalent model (solid lines) and the physical test results (- lines)

and unload curves have been matched. The model is capable of capturing the different MD and CD trends and the degree of plastic deformation is well captured.

Figure 5.12 shows the results of two simulations used to compare the load-unload trend of a model using the best parameter results shown above when the maximum elongation in each direction is first increased by 25 % then decreased by 25 % from the elongation at the design point. This is a concern because there are parts of the material that may be loaded to a lower strain state or due to material wrinkling go beyond the range over which the numerical material model has been calibrated. It can be seen that the material model is stable in both cases with the general shape of the curves being maintained.

5.7 Material Model Evaluation and Selection

When considering the selection of which material model to proceed with three main items are considered: the accuracy of the material response, the computational requirements of the model and the robustness of the model.

In terms of accurately replicating the material response the hybrid element models is greatly superior to that of MAT_108. The hybrid element model accurately captures both the loading and unloading characteristic of the woven polypropylene material. MAT_108 can be adapted in such a way that a more accurate material response can be obtained under loading. For some materials the material response under loading can be comparably accurate to that of the hybrid element model. There is however a problem in that MAT_108 is restrictive in it's unloading response. MAT_108 is only capable of a constant

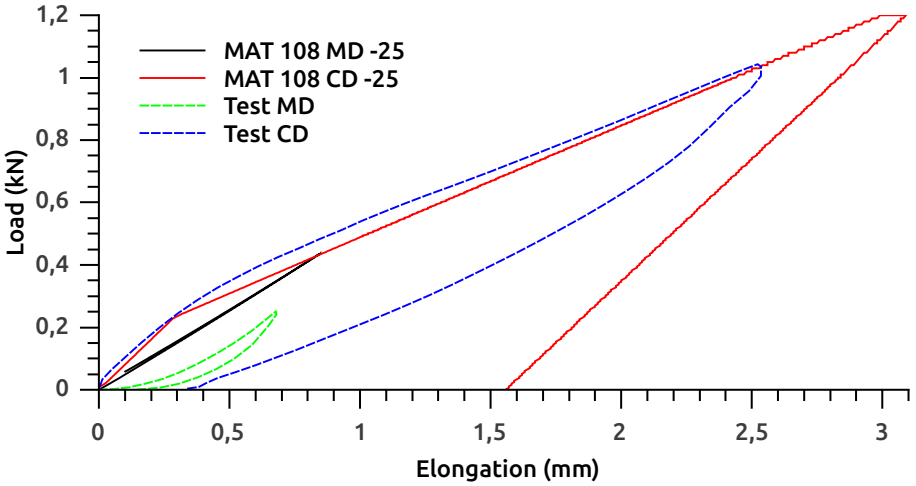

(a) Increased elongation

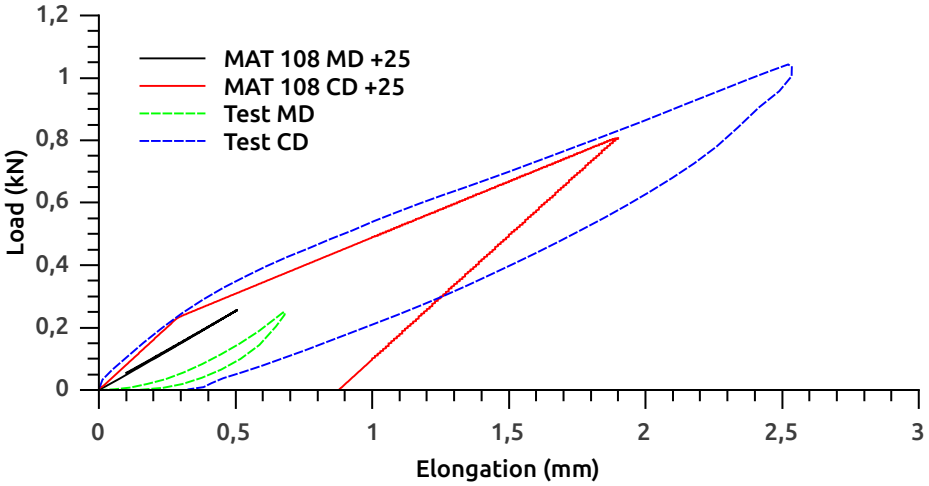

(b) Decreased elongation

Figure 5.10: Load-elongation curves for optimised MAT_108 material swatch with increased and decreased maximum elongation. The maximum elongation is increased or decreased by 25 % from the elongation at the design point

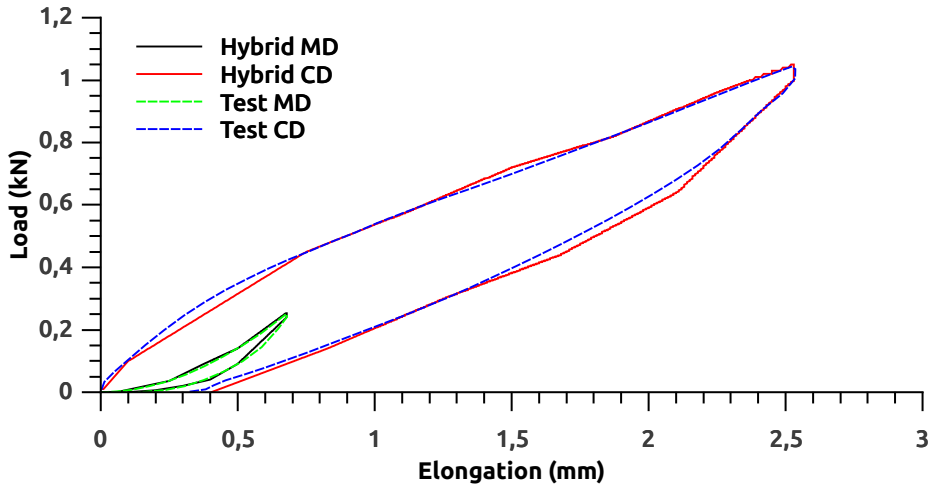

Figure 5.11: Optimised load-elongation curve for numerical swatch with hybrid element material. MD and CD response for the numerical equivalent model (solid lines) and the physical test results (- lines)

slope unload curve, not representative of the curve measured during materials testing.

With regards to both computational requirements and robustness MAT_108 is superior. For a comparable number of elements a model constructed using the hybrid element material will require on average 10-15 times more time to solve than a model using MAT_108. In terms of robustness, MAT_108 has the advantage that the material is the same irrespective of the size and shape of the elements used to construct a bag model. Unlike MAT_108 the hybrid element model requires a different load-elongation curve for each element of a different length. In a simple bag model this can be easily implemented, but if more complex geometries are investigated, or if shape optimization is attempted the number of load curves required to define each individual spring will become impractical.

With the accuracy, computational requirement and robustness of the material models in mind both options should be selected for use depending on the requirement of the final full model. If an accurate unload characteristic is required then the hybrid element model is required. Though the accuracy of the MAT_108 model is reasonable under loading-only cases.

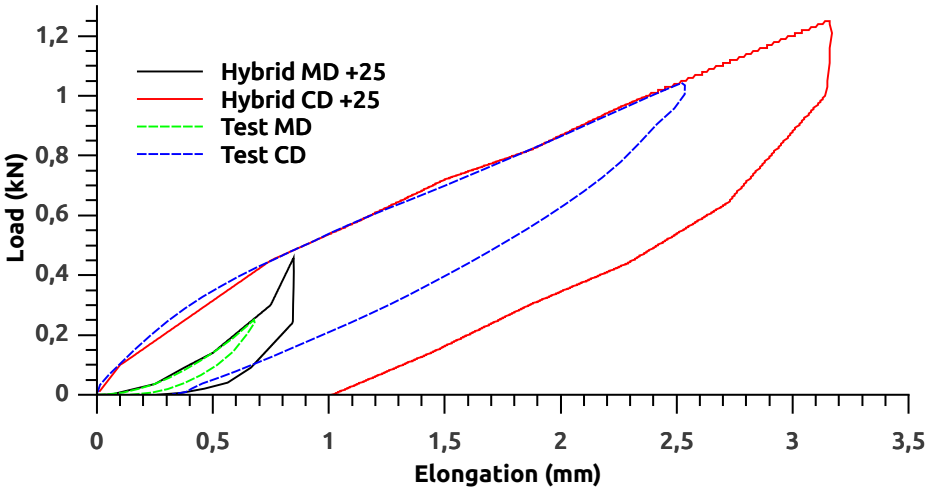

(a) Increased elongation

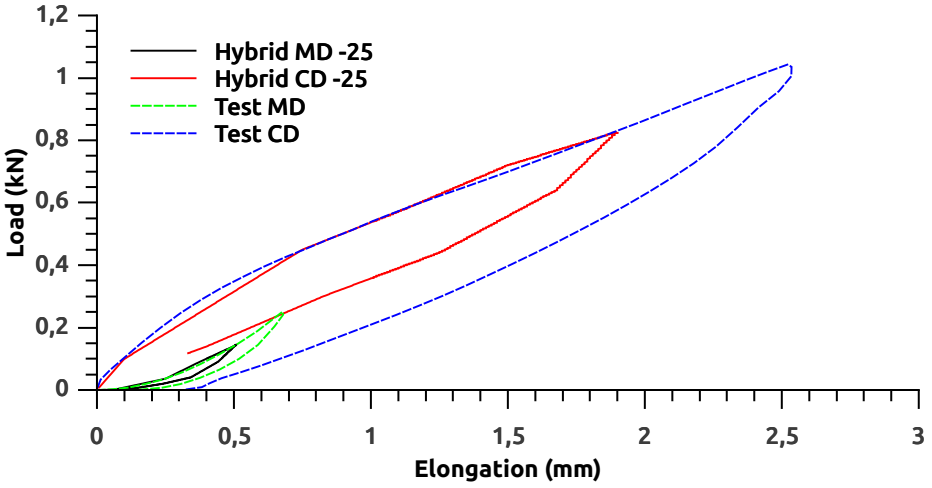

(b) Decreased elongation

Figure 5.12: Load-elongation curves for optimised hybrid element material swatch with increased and decreased maximum elongation. The maximum elongation is increased or decreased by 25 % from the elongation at the design point

Chapter 6

Inflation Methods for Dunnage Bag Simulation

Inflatable dunnage bags are inflated with compressed air to a desired working pressure. In earlier dunnage bag research the compressible nature of air was not considered. Instead a pressure load was applied to the inside surface of the bag. This method is simple and suitable for investigations where the void size is static. Even though the method is simple, care should be taken when applying a pressure load to a large flat surface to avoid unwanted dynamic effects. The drawback of using a pressure load is that the pressure in the numerical dunnage bag is not dependent on the void size. That is if the numerical model is subjected to a void reduction the pressure in the bag will remain at the value set by the pressure load.

6.1 Inflation Models in Literature

A desired outcome for this project is that the compression of the inflation medium be considered such that the rise in pressure caused by a reduction in void size is captured. The system to be replicated has a dunnage bag inflated to a desired working pressure by a fixed mass of gas. Once the initial inflation is completed that mass should remain the same. As the void is reduced the pressure in the bag will increase. Therefore, in order for the model to simulate operation of a dunnage bag the compressible nature of the inflation media must be considered. The research field closest to inflatable dunnage bags with this regard is that of automotive airbags.

Airbags are similar in that they are made from soft flexible materials that are supported by a full gas volume. In the case of airbags the gas volume serves two purposes, it is the mechanism through which the airbag is deployed and provides the resistance to impact required of the deployed device. Dunnage bags also require an inflation medium to deploy, but unlike airbags the strength of the stiffness of the system is derived from the preloaded material, not PV-

Work in the gas.

Airbags have additional features not seen in dunnage bag simulations. Airbags are inflated through combustion that produces the inflation medium. The temperature of the inflation gas is important in simulations to determine the restraining force provided by the bag. Airbags are also designed with gas vents and the material itself is typically porous to allow gas to escape after the initial impact in order to reduce the likelihood of a vehicle occupant suffocating in the now deployed safety system.

A key difference between the operating conditions of airbags and dunnage bags is the rate of deployment and the duration of operation. Airbag deployment happens on the milli-second scale while it takes several minutes to inflate a dunnage bag. Airbags are designed to function for a few seconds while dunnage bags can be in operation for up to a month. This difference in operation duration becomes important in simulations because the recommended explicit solvers become very computationally expensive when long operation times are of interest.

Automotive airbags are rapidly deployed restraining devices designed to reduce the speed of impact experienced by a vehicle occupant in a collision. A slower impact produces less peak energy and consequently less damage and reduces the risk of serious injury. Due to the nature of airbag rapid deployment, simulations are focused on matching deployment rate, deployed geometry and energy transfer rate. Several techniques exist to perform this type of simulation, some of which have been developed with the capability to analyse so-called 'out-of-position impacts', which requires an accurate deployment simulation.

There are three main methods commonly used to model the inflation of airbags. These methods include the airbags being inflated by a constant pressure over the inner surface defined by a control volume, excluding the dynamics of any internal gas; modelling both the fluid flow and the structure in a coupled analysis know as the Arbitrary-Lagrange-Euler approach; and modelling the structure of the bag with conventional finite elements and inflating the model using a particle representation of the fluid known as a corpuscular method.

The overlap between airbags and dunnage bags is the inflation, during which both undergo massive deflection. For the most part, airbag inflation simulations are done using explicit finite element methods. High inflation of thin membranes has difficulty converging due to the Newton-Raphson method applied by implicit solvers. This is exacerbated in the presence of large shear areas as seen in inflation of square pillow shaped dunnage bags. The drawback of explicit FEM is that it is only conditionally stable with the assumption that if the time-step remains below a critical value the simulation will be representative of the physical problem. No energy balance is performed as part of the solution algorithm, without which the error in each iteration is compounded. Explicit methods are used because they run quickly, allow for better parallelization, and the simulation method is stable even when large

deformations occur.

Explicit solvers such as LS-DYNA are the recommended finite element solvers for modelling the inflation of thin shell or membrane structures. This class of tension structure is prone to wrinkling and when wrinkling occurs the body undergoes an apparent rigid body movement that could cause an implicit analysis to terminate, see Suhey *et al.* (2005). A similar effect is observed when the period of the wrinkle changes. Wrinkling is a multi-scale phenomenon that is dependent on the tension state of the material as well as the relative density of the material and surrounding media. As the tension in the membrane increases a point is reached where a wrinkle changes period to drop to a lower energy state causing the apparent rigid motion.

An additional benefit of using LS-DYNA is that the code has an extensive list of methods developed for airbags through decades of commercially backed research.

Two examples of particular interest are that of Brueggert and Tanov (2002) and Hirth *et al.* (2007). Brueggert and Tanov (2002) investigated the use of LS-DYNA to model an automotive airbag. The airbag they investigated is used to protect passengers from side impact. This type of airbag has an inflating bladder covered with a loosely woven fabric. The fabric serves to reduce the effective length of the airbag as the contained volume is increased. In this case, the loosely woven fabric is used as a mechanism to change the geometry of the airbag. Brueggert and Tanov (2002) made use of a user-defined subroutine that accounts for the material properties of the woven covering.

Hirth *et al.* (2007) followed the development of airbag simulation tools in LS-DYNA. The paper gives an overview of the three main methods used in LS-DYNA to model airbags, namely the uniform pressure technique (UP), Arbitrary-Lagrangian-Eularian approach (ALE) and the newly developed corpuscular method (CP).

The UP technique is the simplest and fastest airbag inflation method. This method assumes that a pressure is applied uniformly to the inner surface of the airbag. This method produces reliable fully inflated shapes for airbags, but falls short of accurately representing their shape during the interim stages of inflation. These interim stages are used to analyse out-of-position impacts, which are impacts that occur before the airbag is fully deployed. Another shortfall of the UP technique is that it does not automatically take into consideration the volumetric effects of the gas contained by the bag. Simply put, if the bag is inflated fully and is then impacted by a body, the change in volume and geometry of the airbag will have no effect on the pressure within the airbag. Volumetric effects can be included by using the hybrid-airbag methods shipped with LS-DYNA or a control volume method that uses an equation of state to account for the varying internal pressure.

The ALE approach requires the use of a coupled Eularian, Lagragian mesh. The finite element approach typically uses a Lagrangian mesh while computational fluid dynamics uses an Eulerian mesh. A Lagrangian mesh representing

the structure is submerged in an Eulerian mesh representing the gas. The Lagrange mesh is free to move in the Eularian mesh and the two systems are coupled. In the ALE approach, both mesh types are used to represent the problem. An Eulerian mesh is used to model the fluid and a Lagrangian mesh is used to model the structure. The outer edges of the structure are defined as dynamic boundaries to the Eulerian mesh using a penalty method, whereby the flow of material across that boundary is resisted. The force required to maintain that boundary in the Eulerian mesh is then calculated and applied to the Lagrangian mesh. When the structure is deformed, a new boundary is defined in the Eulerian mesh and the process is repeated.

Compared to the uniform pressure approach, the interim inflation shapes are more accurate, the volumetric effects of the contained gas can be accounted for, and the action of flow into the airbag can be simulated. This method does, however, require many more elements than the uniform pressure technique and as such requires far more processing time. The ALE method has also been found to be less suitable for tightly folded or close packed airbags because in order to capture the fluid flow correctly there needs to be a number of Eularian elements between the structures of the bag. This requires a large number of small elements adding to the computational burden of this approach.

The final method discussed is the CP method of airbag deployment. This method stems from the idea that the airbag is being inflated by molecules of gas that collide with the surface material of the airbag. The sheer number of molecules contained by an airbag precludes modelling them individually. Typically gases are modelled as a continuum, but this does not represent the physics of the problem. CP methods rather lump the properties of the gas molecules together and simulates the movement of the resulting larger particles. In this way, the number of elements simulated becomes manageable. The theory of corpuscular method methods is described by Wang (2010).

The advantage of the CP method over the ALE approach is speed. The CP method is much faster than the ALE approach and more accurate in some test cases. The speed difference between a CP or particle and ALE approach can be further enhanced by the degree to which explicit particle methods can be parallelized. The CP method also has an increased ability to model an airbag that has been tightly folded. Using the ALE approach, there must be elements defined between two sides of the airbag in its folded state. Using CP methods the gas mesh can penetrate voids inside the airbag where no mesh was initially defined.

Lee *et al.* (2009) investigated how to validate a numerical model of an airbag. The results of physical bag tests are compared visually with the results of numerical simulation at various points during inflation. Images taken with a high speed camera are overlaid with a grid, and a similar grid is placed over scaled images from numerical tests. The grids are then used to compare the shape of the two bags at that point in the inflation process.

Airbag study has lead to the development of many tools to evaluate infla-

tion. A short-falling of the previous dunnage bag model, Venter (2011), was that it did not have the capability to easily simulate the volumetric effects of the air contained in the bag. From the discussion by Hirth *et al.* (2007), the use of control volume, ALE and CP methods for inflation will add those characteristics. With the inclusion of the volumetric effects of the contained gas, the dunnage bag model can be expanded to include dynamic testing of the models and at a later stage the inflation from folding of the bags for specialist applications.

6.2 Modelling of Air Volume for Dunnage Bags

The hybrid airbag model available in LS-DYNA was selected for the numerical simulation of a dunnage bag. This model makes use of a control volume defined by the user through a parts list. The user must ensure that the shell normals all point out of the control volume. The software then detects and calculates the internal volume of the bag. The inflation model requires the mass of air in the bag at each point in time. This is defined through a curve for the rate at which mass is put into the control volume over time, figure 6.1. The software automatically calculates the volume of the defined control volume. The inflation gas makes use of simple gas properties, shown in table 6.1, and the Ideal Gas Law to calculate the pressure in the bag using the calculated volume and mass of the gas in the bag. This pressure is then applied to each element in the next time-step. This process is repeated each time step.

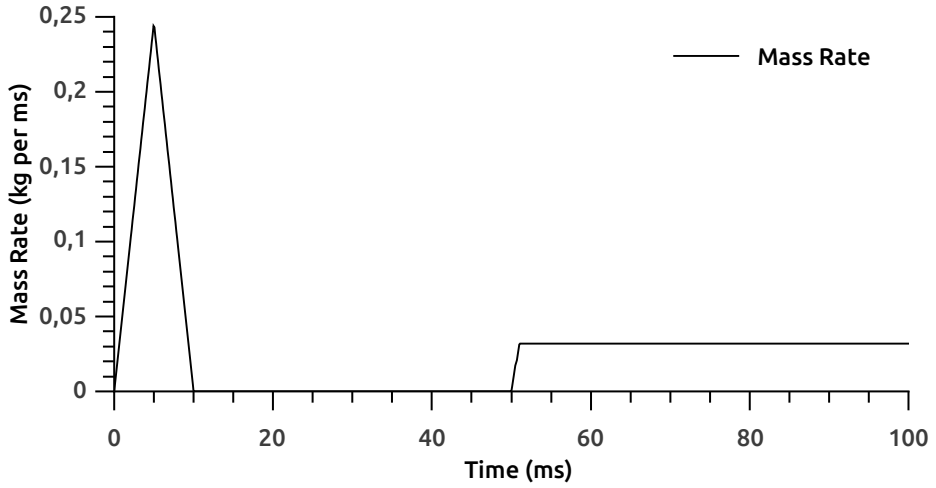

Figure 6.1: Dunnage bag mass inflation rate over time. A two phase inflation model is used. An initial inflation to working pressure, the pressure is held static while the void is cycled, then the bag is inflated to burst

Table 6.1: Properties for air

Property	Value
Mass	1.04 kg
Cp	1004 $\frac{J}{kg}$K
Cv	717 $\frac{J}{kg}$K
T	300 K
Air density	1.164 $\frac{kg}{m^3}$

As an illustration of this inflation method, a 48 × 102 inch (1.219 x 2.59 m) level 3/4 bag is modelled in a parallel void, of 305 mm. The dunnage bag is inflated by defining the mass input to the bag using the mass rate over time curve shown above. Figure 6.2 shows the mass in the bag over the inflation time. The bag is gradually inflated to 1.30 kg and the mass is then kept constant for 10 ms, allowing all numerical dynamic effects to die out. This mass of air was selected because it generates a pressure of 170 kPa (abs), where the desired relative pressure is 70 kPa when the ambient pressure is 100 kPa. The mass of air required to produce a specific desired pressure is not initially known, as it depends on the volume of the contained gas. The volume is dependent on the material strain, which is dependent on the pressure in the bag. LS-OPT is used again to minimise the difference between the pressure resulting from the simulation and a desired pressure by varying the mass of air used to inflate the bag. These models make use of time scaling to reduce the computational cost of each simulation, further details of the time scaling are given in chapter 7.

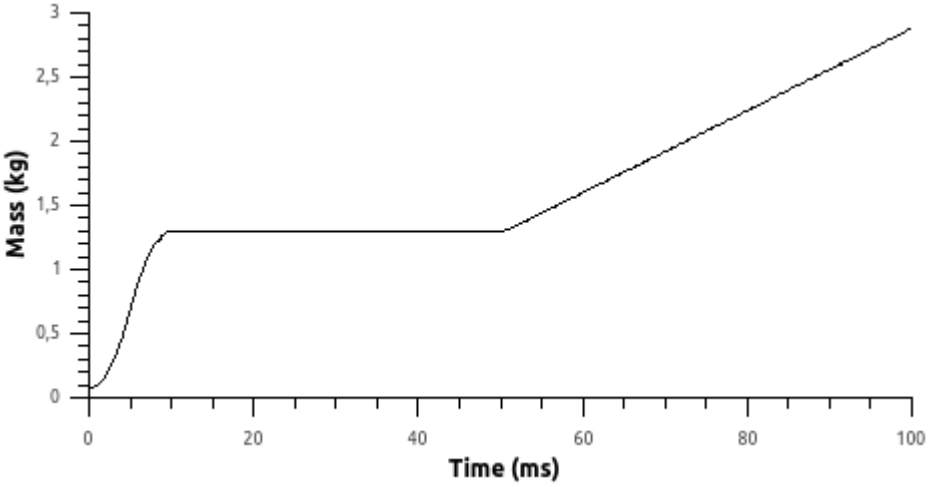

Figure 6.2: Dunnage bag inflation mass over time

If the void is then decreased from 305 to 200 mm from time 20 ms to 25 ms, without any additional air pumped into the bag, the internal volume should decrease, while the internal pressure, gas energy and restraining force should increase. Figures 6.3 and 6.4 show the contained volume and absolute pressure of the air in the bag over time. These figures show that as the void is decreased the contained volume of the air decreases and the pressure in the bag increases. Figures 6.5 and 6.6 show the PV-energy or internal energy of the gas and the restraining load generated by the inflated bag over time. Both the internal energy and the restraining load increases as the void decreases. The restraining load increases more rapidly than either the internal pressure or the internal energy.

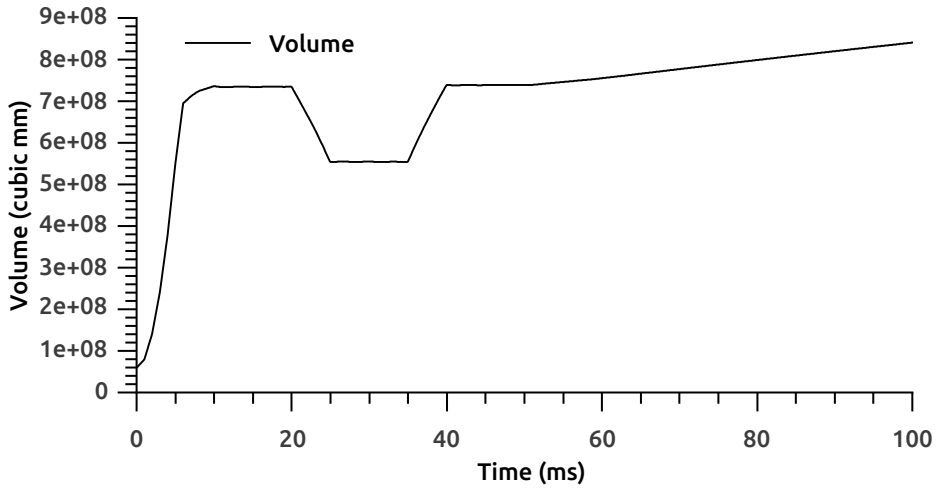

Figure 6.3: Dunnage bag volume over time

The alternative methods using ALE and CP methods are both more computationally expensive, and with the quasi static dynamic loading that the model is subjected to there is no need to capture the internal gas dynamics or the intermediary inflated shapes of the bag. The data shows that the use of a hybrid airbag model that makes use of a fixed mass of air and the ideal gas law captures all the desired features of an air filled dunnage bag and is suitable for use in this numerical model.

6.3 Comparison of Mass Inflation and Simple Surface Pressure Methods

Previous models make use of a pressure load applied to the inside of the bag. The new airbag model with the same pressure should produce the same result as the pressure inflation model. Figure 6.7 compares the inflated shapes and

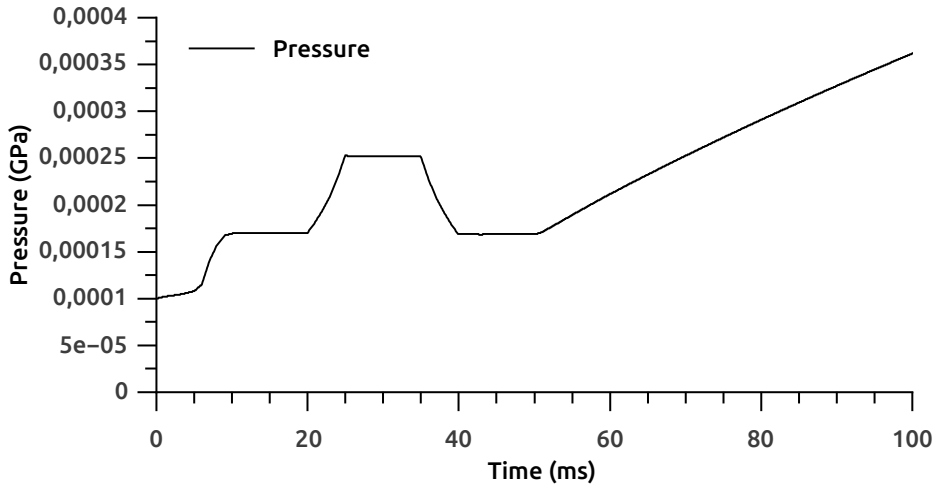

Figure 6.4: Dunnage bag absolute internal pressure over time

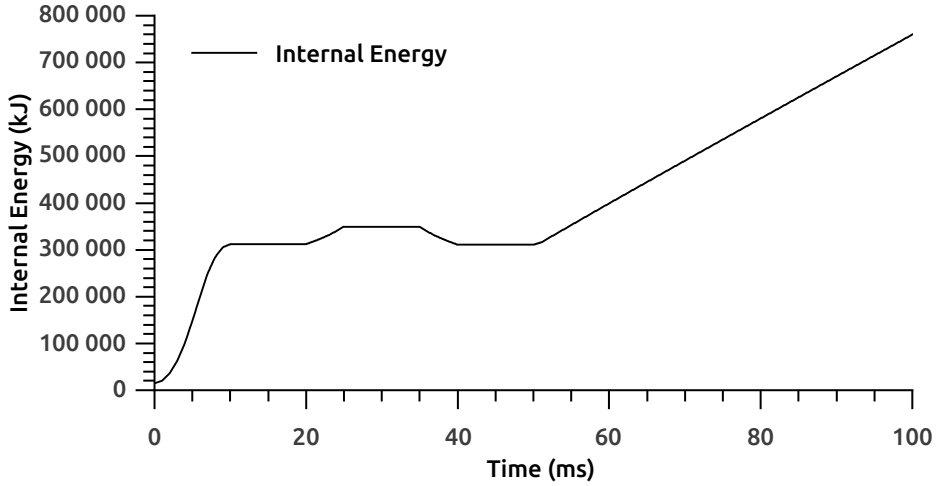

Figure 6.5: Dunnage bag gas energy over time

the effective stress for a standard bag in a 305 mm void inflated to 70 kPa. It can be seen that the results are the same. The gas inflation model and a conventional pressure load can be interchanged depending on the desired outcome of the simulation. If only the loading phase is required then a pressure load is suitable but if a dynamic load is required then the use of the airbag inflation model is recommended.

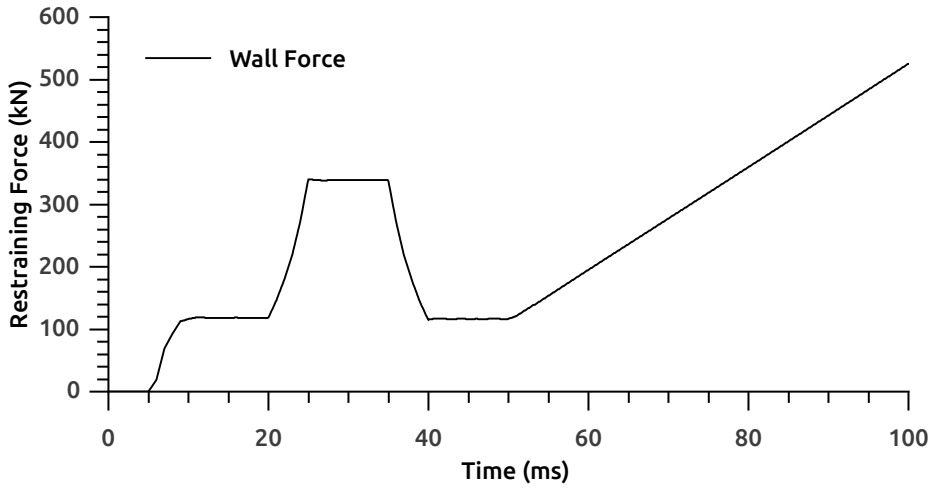

Figure 6.6: Dunnage bag restraining force over time

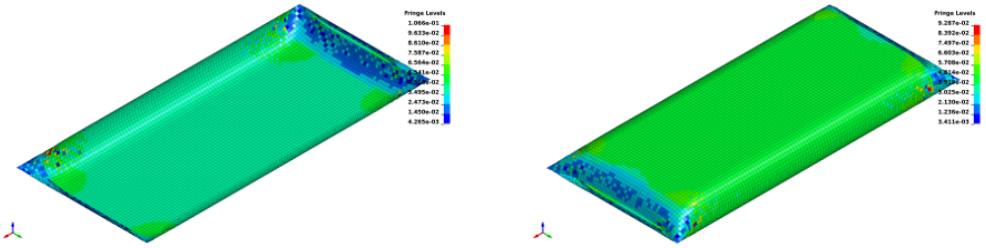

(a) Gas inflation model (b) Pressure load

Figure 6.7: Inflated shape of a dunnage bag using gas inflation and simple pressure load

Chapter 7

Test Case for the Full Model

So far each of the components required to build a complete dunnage bag model have been identified and evaluated, but the full model has not been described. This chapter covers the details of the numerical model of a full-scale dunnage bag, used to evaluate and validate the proposed numerical prototype. The evaluation of the full dunnage bag numerical prototype model starts with the selection of a test case, followed by physical testing of dunnage bags according to the test case then the replication of the test case using the numerical prototype. Details of the numerical prototype are also included.

7.1 AAR Test for Pneumatic Dunnage

It was decided to evaluate the numerical prototype with reference to an industry standard test. The industry partner for this research (Stopak Pty) has recommended that the 'Product Performance Profile for Pneumatic Dunnage' published by the Association of American Railroads, AAR (2004), AAR (2012) be used for this purpose. This test standard is a simple pass/fail test for certification of pneumatic dunnage for use on rail-roads in the USA. This test will be replicated in physical testing using a large hydraulic press and numerically using the material models and gas inflation model described in chapters 5 and 6.

The AAR performance profile for pneumatic dunnage covers three areas of consideration for certification: application, performance level and performance measures. It is noted that the AAR certification is performed with physical tests only and only on a standard 48 x 102 inch (2590.8 x 1219.2 mm) dunnage bag.

7.1.1 Applications for Pneumatic Dunnage

The AAR test defines two principal applications for pneumatic dunnage. Dunnage bags can be used either as lateral void fillers or lengthwise void fillers.

In lateral voids dunnage bags are used to press goods against the sides of the container, perpendicular to the traveling direction of the vehicle. In lengthwise deployment the dunnage bag is used to restrain goods against fore/aft movement in the container. Dunnage bags used as lengthwise void fillers are typically subjected to greater operational loads. Dunnage bags used as void fillers require the the following attributes:

- Lateral void filler
  - Must be capable of maintaining 0.5 to 3.0 psig (3.44 to 20 kPa gauge) in voids from 4 to 12 in (101 to 305 mm).
  - Must not leak or lose significant air pressure.
  - Must meet minimum burst strength requirement of 8 psig (55.15 kPa gauge).
- Lengthwise void filler
  - Must be capable of maintaining 5.0 to 8.0 psig (34.4 to 55.15 kPa gauge) in voids from 4 to 12 in (101 to 305 mm).
  - Must not leak or lose significant air pressure.
  - Must meet minimum burst strength requirement of 17 to 30 psig (117.21 to 206.84 kPa gauge).

7.1.2 Performance Levels for Pneumatic Dunnage

Five performance levels are defined by the AAR and reproduced in table 7.1. The performance levels define the suitable applications and maximum cargo weight it can restrain.

Table 7.1: AAR performance level application guide

Performance Level	Application
Level 1	Lateral voids, primarily in inter-modal loads
Level 2	Lengthwise voids with loads up to 75 000 lbs (34 020 kg)
Level 3	Lengthwise voids with loads up to 16 0000 lbs (72 575 kg)
Level 4	Lengthwise voids with loads up to 205 000 lbs (92 986 kg)
Level 5	Lengthwise voids with loads up to 205 000 lbs (92 986 kg) and horizontal applications in approved roll paper loading methods.

On the request of the industry partner involved in this porject, all testing will be performed on a level 3/4 dunnage bag in a parallel void. Level 3/4 bags are designed to be suitable for both level 3 and 4 application.

7.1.3 Performance Measures for Pneumatic Dunnage

The performance of level 2-5 dunnage bags is measured according to the results of three sequential tests: a leak test, a cyclic test and a burst test. The standard for certification is to make use of ten samples.

Part A: Leak Test

All ten samples are inflated into a 12 inches (305 mm) void to the required pressure in table 7.2 and held for 19 days. At the end of the 19 days no individual bag may have lost more than 1 psig (6.89 kPa) and the standard deviation for all ten samples cannot be more than 0.15 psig (1.03 kPa).

Part B: Cyclic Test

Five samples from part A are then randomly selected for dynamic testing. For the dynamic testing the bag is inflated in a 12 inches (305 mm) void to the pressure listed for part A. The bag is then loaded a minimum of 10 times with the load described in table 7.2 for part B. The sample should not burst and the final pressure in the bag once returned to the 12 inches void should be within 10 % of the initial pressure. A full cycle is performed in 0.4 seconds.

Part C: Burst Test

At the completion of the dynamic test in part B, each of the five bags tested in Part B is then further inflated to the pressure specified in part C of table 7.2 while maintaining the 12 inches void. The bag should maintain the pressure for at least one minute without bursting.

Table 7.2: Performance requirements for level 2 to 4 dunnage bags

Level	Inflation Pressure psig (kPa) Part A	Maximum Load lbs (N) Part B	Inflation Pressure psig (kPa) Part C
Level 2	5 (34.47)	21 900 (97 416)	17 (117.21)
Level 3	8 (55.15)	46 500 (206 842)	25 (172.37)
Level 4	10 (68.95)	59 600 (265 114)	30 (206.84)

NOTE: As of January 1^{st} 2012 Part B of the 2004 performance profile has been excluded. The load method used by the AAR which required that a bag be loaded to a set load at high speed was found to deliver no useful results. The test was initially included in an attempt to replicate the load seen by a dunnage bag during a typical shunting operation, a high speed operation. The 2004 AAR standard test, however, did not capture the displacements observed

during the shunting operation. During shunting the dunnage bag void can be reduced from 12 to 4 inches, an 8 inch void reduction, while the AAR test equipment only generated about a 1 inch void reduction. Even though they have now been excluded from the AAR requirements, cycle testing of dunnage bags is still a valuable test and is still performed by all major manufacturers. However, a static equivalent cyclic test is now used. The static equivalent test will be included in the new European standard by industry recommendation.

7.2 Proposed Modified AAR Test

The AAR tests are not all suitable for this project and can be structured differently to be better suited for simulation. Material permeability is beyond the scope of this project. Part A of the AAR test is a leak test and is excluded from testing here.

Time dependent effects are also beyond the scope of this project. In Part B of the AAR test a load rate is defined but will not be replicated by any effect in the numerical prototype. The modified AAR test used for this project rather makes use of a quasi-static cycle test cycled at 0.1 Hz to exclude time dependent effects from the test data. The cycle test is also modified so that it is no longer load controlled. The void is cycled from 305 to 200 mm and returned to 305 mm each cycle. Static testing of dunnage bags show that a standard size bag inflated to the prescribed working pressure in a 305 mm void reaches the AAR recommended load of 59 600 lbs (265 114 N) when the void is reduced to between 8 and 9 inches (200 to 229 mm). Eight inches being the lower bound was chosen as the minimum cycle size for the modified AAR test.

Related to time dependencies, creep is not accounted for in this project. Once the material in the numerical prototype model has plasticly deformed in the first load cycle no further plastic deformation will occur in the second cycle. The test will as such be modified to have only a single cycle, not the ten cycles proposed by the AAR.

In Part C of the AAR test, static inflation, the bag is inflated into a fixed 305 mm void to the prescribed pressure. In the AAR test the pressure is maintained for one minute, but as any time or rate dependent material properties are beyond the scope of this project there can be no difference in the response over this time. Instead the proposed test procedure proceeds directly to the inflation to burst stage of the test. The numerical prototype does not directly account for material failure, so the bag will be inflated to a pressure just beyond the burst range recorded in physical testing.

The modified AAR test performed for this project can then be summarized as follows:

1. Inflate the bag to working pressure

2. Reduce the void from 305 to 200 mm and hold for ten seconds

3. Return the void to 305 mm

4. Continue inflation until burst

In practice the 19-day leak test allows the bag to be preconditioned negating some of the effects of creep. In the 19-day leak test the bag is inflated to working pressure, left for 1 hour, topped up to working pressure then left for 19 days. It has been observed that the rate of creep decreases greatly over the first hour and becomes nearly zero after that. All physical test samples are preconditioned by inflating unconstrained bags to working pressure and holding the samples for at least 1 hour.

7.3 Modified AAR Test Results

Ten modified AAR tests were performed on standard level 3/4 dunnage bags using the hydraulic press at Stellenbosch University. Figure 7.1 shows representative pressure, load and void size measurements over time for the modified test. The three test phases can clearly be seen: inflation, single cycle test and inflation to burst.

Figure 7.2 shows the test results over the single compression cycle in more detail. When the void reduces the pressure in the bag increases as does the restraining load. A loss in pressure at the apex of the cycle is observed. The pressure drop is around 1 kPa at maximum pressure, caused by creep. Creep occurs even in the preconditioned bags because the bags are only preconditioned at their working pressure.

The average results for the modified physical tests are shown in table 7.3. All test bags surpassed the required minimum burst pressure of 30 psig (206 kPa relative) and, as per the test requirement, the maximum load is above 256.9 kN. The MD (lengthwise) and CD (hoop) strains at minimum void were measured using DIC as 4.9 % and 1.29 % respectively.

Table 7.3: Test results for modified AAR test

	Cycle Start	Maximum	End	Drop	Burst
Pressure (kPa)	70.1	144.4	62.2	7.9	237.0
StDev (kPa)	0.272	3.11	1.88	1.88	14.9
Load (kN)	115.845	307.811	101.077	14.778	459.569
StDev (kN)	2.696	10.647	4.560	3.755	37.206

Figure 7.3 shows both the load displacement and pressure displacement curves for the cycle test. This information is useful in predicting the restraining

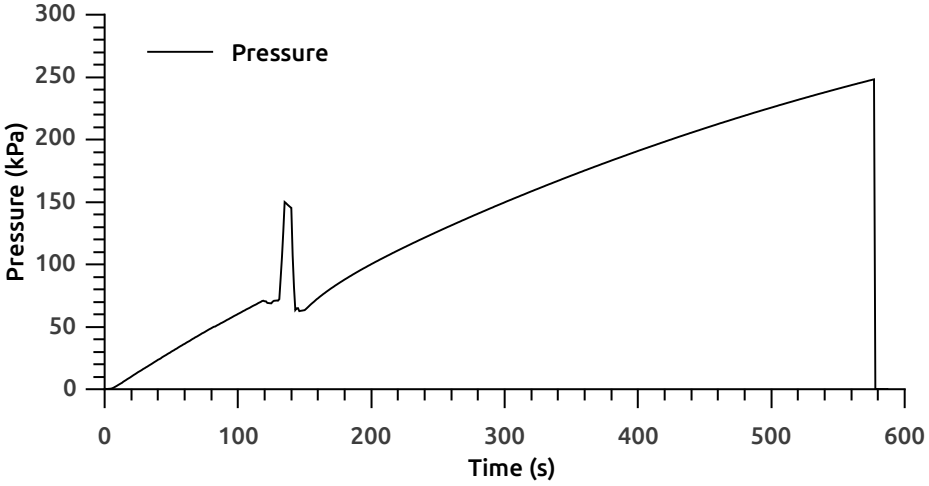

(a) Pressure over time

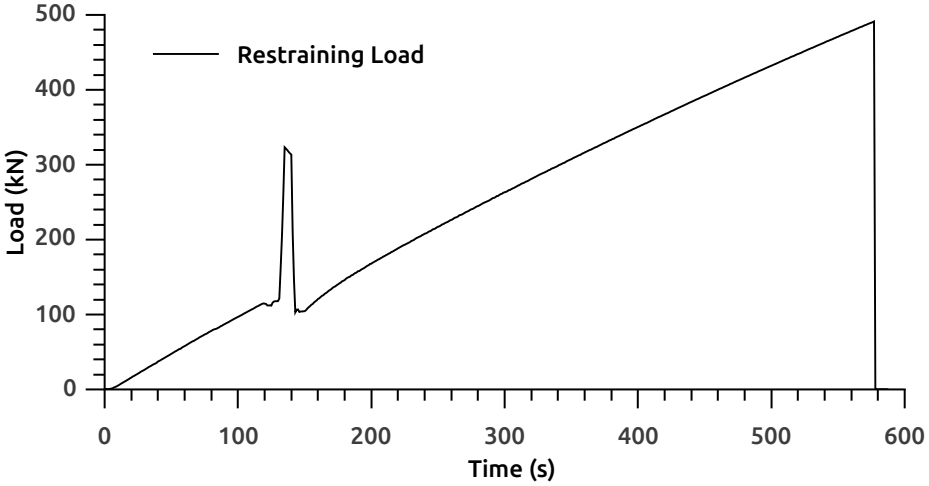

(b) Load over time

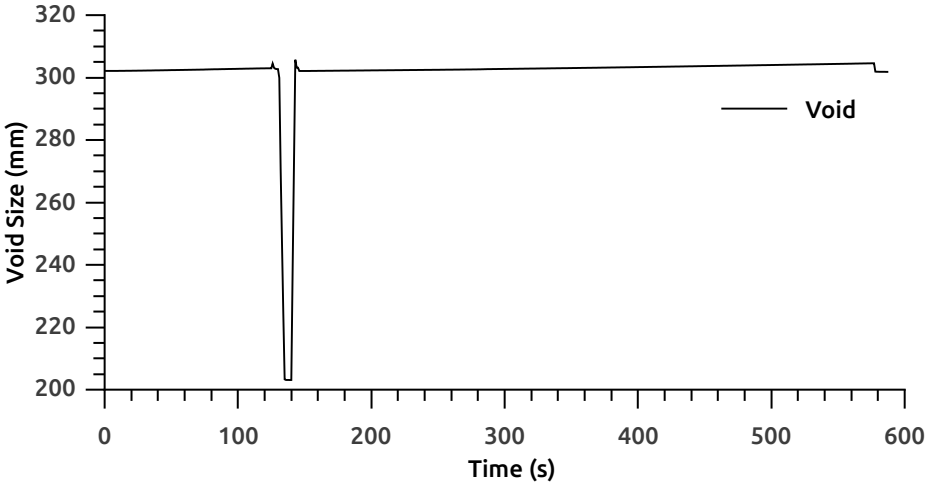

(c) Void size over time

Figure 7.1: Physical test results for inflatable dunnage bags over time, showing the inflation of the bag, a single compression cycle and inflation to burst

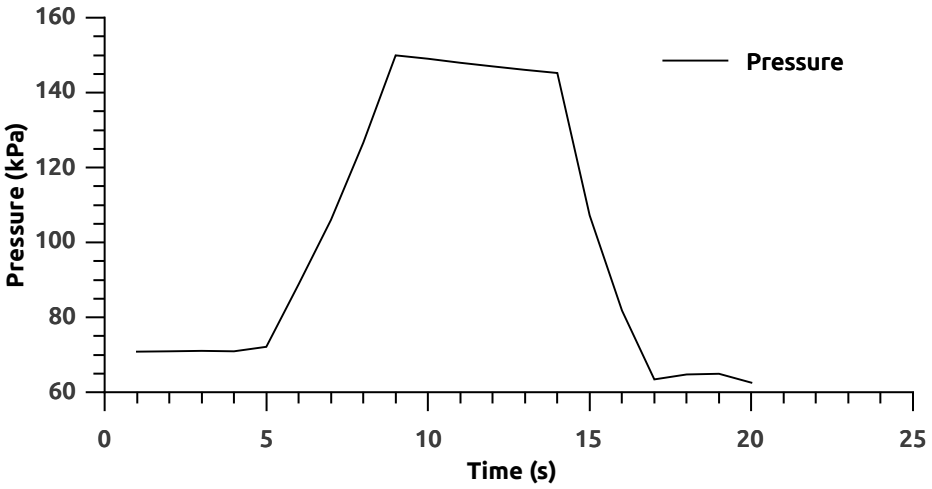

(a) Pressure over time

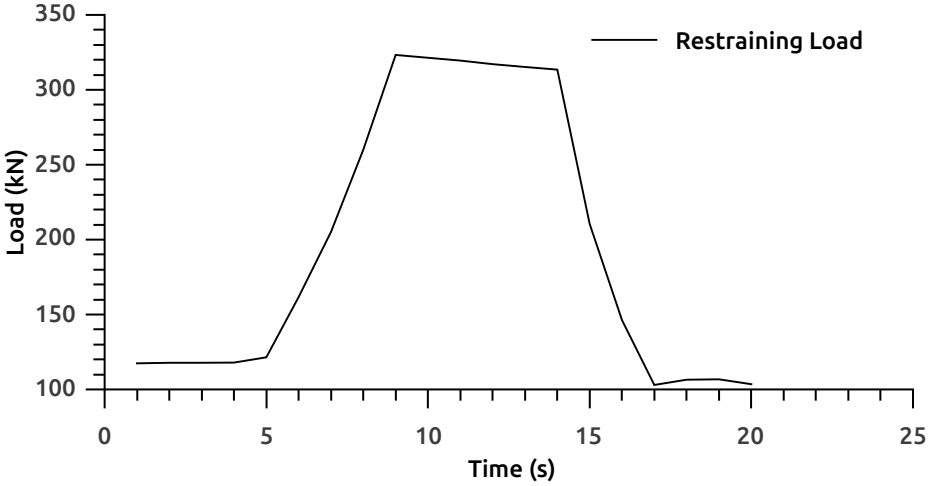

(b) Load over time

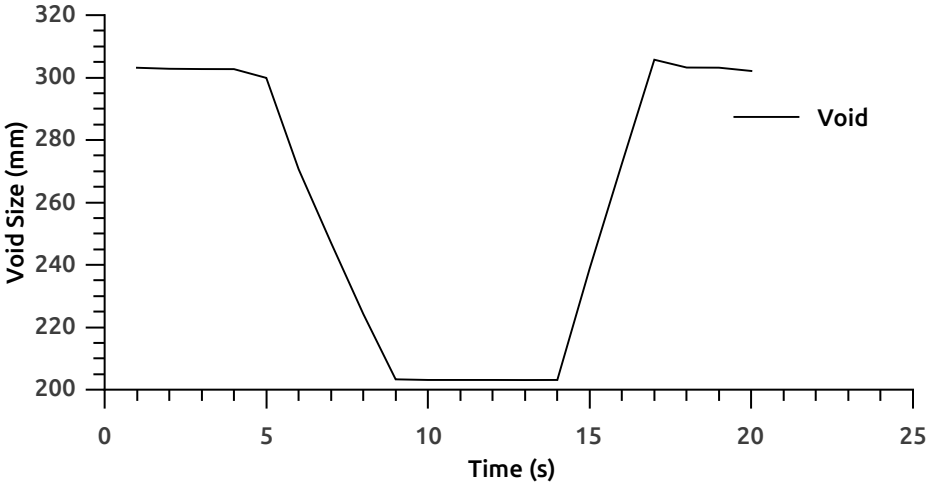

(c) Void size over time

Figure 7.2: Physical test results for inflatable dunnage bags over time for the void cycle only

force produced by a dunnage bag when the void is reduced as well as identifying how close a bag is to failure in a given void.

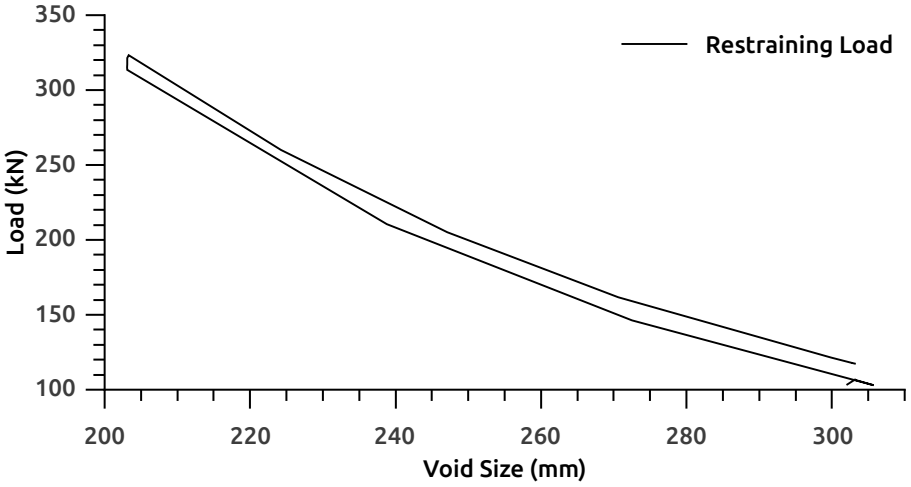

(a) Force vs void size

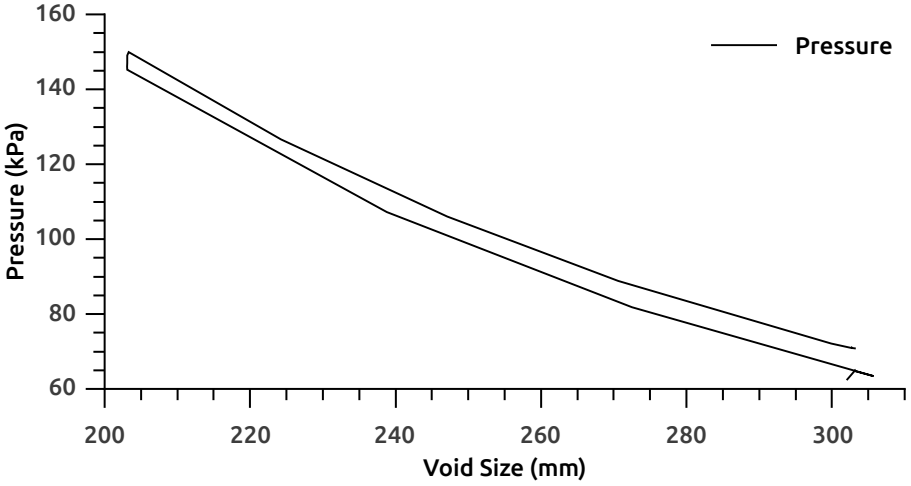

(b) Pressure vs void size

Figure 7.3: Physical test results for inflatable dunnage bags related to void size

7.4 Numerical Equivalent Modified AAR Test Results

The dunnage bag chosen for evaluation is a 102 x 48 in (2 590.8 x 12 19.2 mm) level 3/4 for use in a parallel void. The bag is fabricated as a woven polypropylene tube which is cut to length and stitched to form a flat pillow shaped bag

around a compliant inner bladder. This bag is designed to be used in a maximum 12 in (305 mm) void with a maximum inflation pressure of 10 psig (70 kPa gauge). The modified AAR test is reproduced using a numerical model with a representative geometry using the homogenised material properties defined in chapter 5 and the inflation model discussed in chapter 6. Neither the seam nor the valve are modelled here as they do not affect the ideal burst condition for this dunnage bag. The dominant failure mode for this bag is a mid side material failure.

7.4.1 Geometry and Meshing

Figure 7.4 shows the overall dimensions of the evaluation bag selected. Also seen in the figure are two 200 mm overlap regions where the woven polypropylene is folded back onto itself producing two double-thick sections, indicated by the dashed lines in the figure.

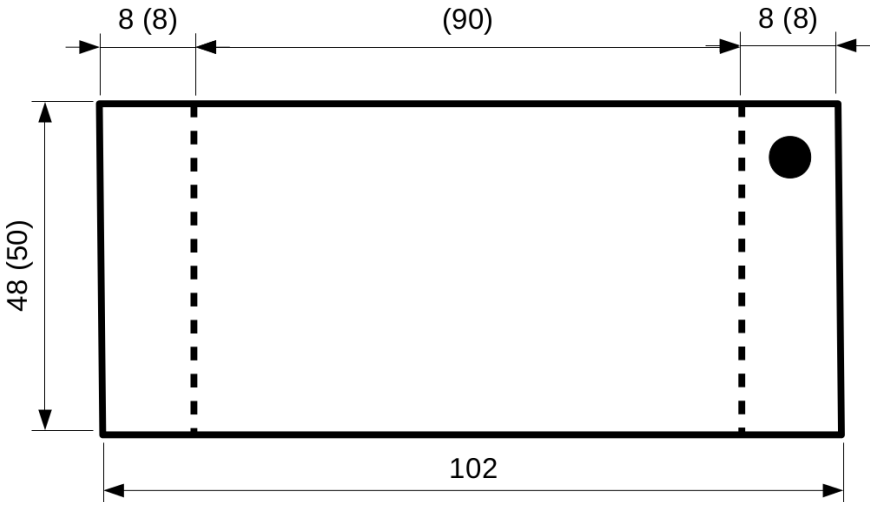

Figure 7.4: Dimensions of the a level 3/4 dunnage bag. Length values are in inches and the number of elements along each edge are shown in brackets

The bag is meshed with fully integrated membrane elements. Membrane elements are selected because the resistance of the material to bending is very small relative to the in-plane strength, and neither of the material models are calibrated with bending stiffness in mind. The shell thickness used in all the models is 0.23 mm, this thickness has no bearing on the material response, it is only important to ensure that the same thickness is used in both the material calibration and the full bag model. The density used for the woven material is $900 \frac{kg}{m^3}$

The mesh itself has an orthonormal, two-layered construction with the top layer defining the top surface of the bag and the bottom layer the bottom surface of the bag. The element normals are reversed on the bottom layer such

that all the element normals point away from the central cavity as required to define a control volume for the airbag type inflation.

The stitching and bag seam are not modelled here because they do not affect the pressure inside the bag which is the focus of the test case.

7.4.2 Load Case and Boundary Conditions

The dunnage bag is loaded in four phases: inflation, settling, compression and burst. The bag is loaded by an internal pressure due to inflation and constrained by two analytical surfaces defined for contact that does not require any elements. These analytical surfaces represent the two parallel plates of the test device. The bag is further constrained by two orthogonal symmetry conditions to limit unwanted rigid displacement of the model. These constraints are not required but are used for convenience.

Inflation

The dunnage bag inflation is simulated using a simple airbag model that calculates a pressure load based on the mass of air and the volume of the defined control volume. Mass is injected into the control volume during the first part of the full simulation. Figure 7.5 shows the rate of mass inflation defined in the airbag model. Figure 7.6 shows the mass of the gas in the bag over time. The pressure calculated by the airbag model is then applied to the surface of each element. The bag is inflated into a static void until a desired pressure is met. Depending on the material used the mass of air required to produce a desired pressure will differ due to varying degrees of stretch in the material. LS-OPT is used to minimise the difference between the desired pressure and the simulated pressure in the bag at the end of the inflation phase. The simulation requires that the bag be inflated to 170 kPa (absolute) in the initial 305 mm void.

Settling

Before and after the compression stage, the bag is left in a constant void with no additional gas mass being added. During these phases a global numerical damping attenuates any unwanted dynamic effects that might produce erroneous results. A global damping factor ($VALDAMP$) of 0.5 is applied throughout the simulation to ensure that the system kinetic energy is suitably low relative to the internal energy of the material. This global damping applies a force opposing acceleration equal to $VALDAMPma$, where m is the nodal mass and a is the nodal acceleration.

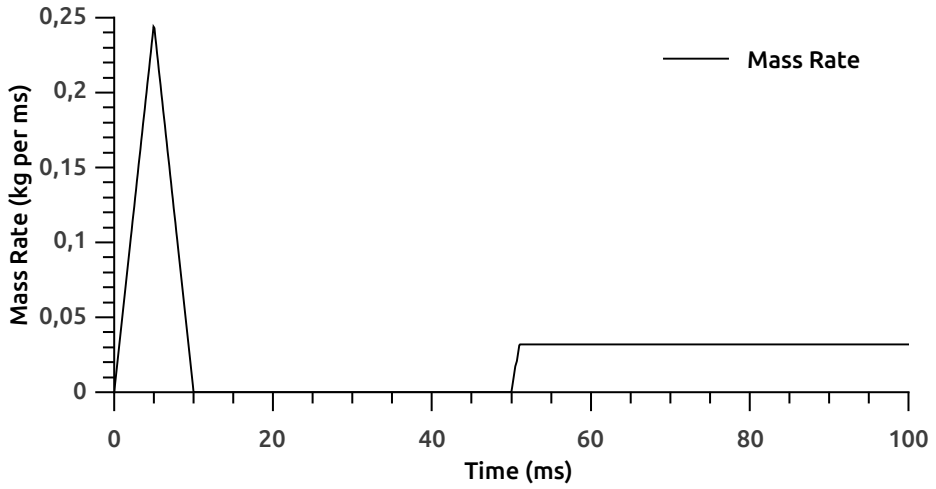

Figure 7.5: Mass inflation rate over time for the full bag simulation

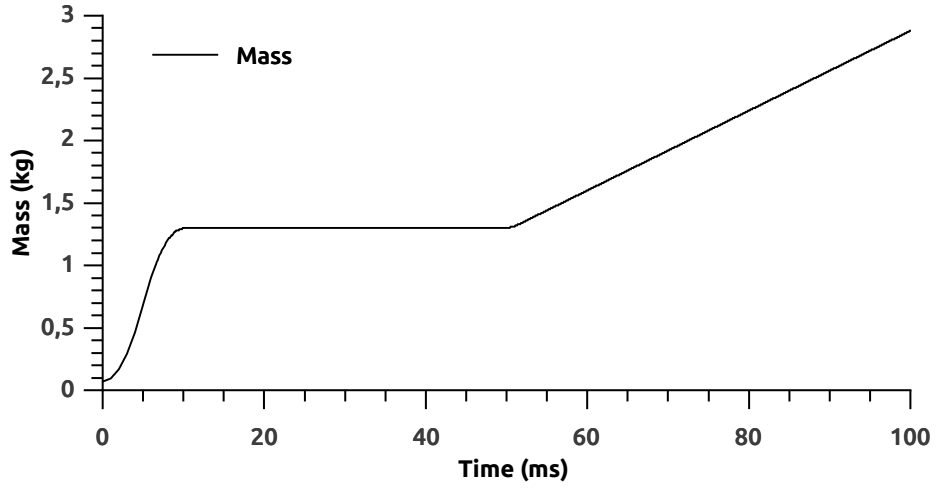

Figure 7.6: Inflation mass over time for the full bag simulation

Compression

Once the bag has been inflated to the desired working pressure and the kinematic effects have dissipated, the parallel void into which the bag is inflated is reduced from 305 mm to 200 mm, held there for some time and then returned to its initial position at 305 mm. The parallel void used in this simulation is created using a rigid wall, an artificial analytical construct in LS-DYNA that allows the user to define a contact boundary without requiring additional elements. The void for this problem is created using two planar rigid-walls defined parallel to each other, set apart to create the desired void size. Each of the parallel rigid-walls is given a motion profile that moves each plate closer to the other by half the desired reduction in the void size (52.5 mm), figure 7.7.

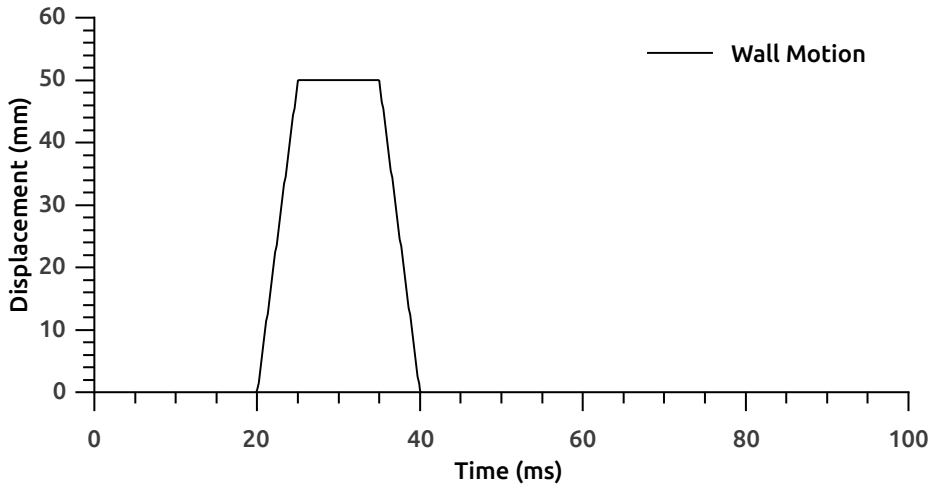

Figure 7.7: Motion of the rigid walls during a full bag simulation

Burst

After the compression load the bag is held to allow dynamic effects to dissipate. The mass of air in the bag is then increased until the pressure in the bag is 350 kPa (absolute) to ensure that the pressure in the numerical model exceeds the tested burst pressure. This value is chosen because it is sufficiently above the average burst pressure to allow the strain in the bag to be evaluated at the average burst pressure recorded in the full bag tests, 237 kPa (relative).

7.4.3 Model Optimization and Scaling

Though LS-DYNA is capable of simulating most kinematic and structural events, emulating the real-world physics often requires extremely long computation times. The computational time can, however, be improved in many cases by restructuring components of the problem or making assumptions that neglect components or the real problem. The simulation of a dunnage bag deployment is an example of a case where components are excluded for the sake of computational efficiency.

Finite element codes using explicit integration such as LS-DYNA are only conditionally stable. The integration is stable if the time-step is kept below some critical value, calculated by the software. When using an explicit finite element solver the internal loads propagate through the body being analysed over time. If the time-step used is too large the rate at which the load front is propagated can be delayed leading to spurious results. The critical time-step should be smaller than the minimum time a sound wave would take to pass through the critical element, which is the element requiring the smallest time-step. The critical time is calculated based on the numerical values of the shortest edge length of an element, the stiffness and mass of the material.

The computational time required to solve a finite element model using explicit integration is defined by the minimum critical time-step for the model and the total duration of the simulation. For example, a model with a critical time-step of 1 and a duration of 1 000 will require a minimum of 1 000 steps. The LS-DYNA solver does not make use of any units so whether time is measured in seconds or milliseconds in the simulation 1 000 steps are required. This can potentially result in extremely long computational time.

Computational time of the finite element model can be improved by manipulating the critical time calculated for the model or reducing the simulation time or both. Changing any of the values of element edge length or material mass and stiffness changes the critical time-step.

The numerical value of the smallest edge length was considered. The numerical prototype requires a high element density to capture the fine model details, which necessitates small elements. The smaller the elements the smaller the smallest edge-length and the lower the critical time-step. The numerical value of the minimum edge length was increased by using non-SI units for the numerical prototype. The unit system used is kg, mm, kN, GPa, ms and kN-mm. This leads to a drastic decrease in the computational time required for one simulation.

Material mass and stiffness are both related to the critical time-step in the same way and could be scaled to improve computational time. The critical time-step is $\propto \sqrt{\frac{M}{K}}$ where M is mass and K is stiffness. Increasing the mass of the system increases the critical time-step and increasing the stiffness of the material decreases the-time step. Neither mass nor stiffness was scaled in these numerical simulations. The stiffness is not scaled because of the effort required to calibrate the material stiffness and mass scaling was found to be less effective than time scaling.

Time scaling is done by reducing the simulation duration. If the simulation time is halved so is the computational time. The effect of time scaling is evaluated by comparing the kinetic and internal energy of the system. If the internal energy is much greater than the kinetic energy the effect of time scaling is assumed to be minimal, especially when no time dependent phenomena are being investigated. Using time scaling the total time in the numerical simulation was reduced to around 100 ms.

7.5 Modified AAR Test Simulation Results

Two numerical prototypes were constructed to simulate a modified AAR test using LS-DYNA. The two models differ only in the material model they use, one prototype for each model described in chapter 5, MAT_108 and hybrid element materials. The numerical prototypes each record pressure, restraining load, volume, void size and strain data over the duration of the simulation.

7.5.1 Prototype with MAT_108 Material

Figures 7.8, 7.9 and 7.10 show the pressure, restraining load and contained volume of the numerical dunnage bag over time using the MAT_108 material. As per the modified AAR test, the bag is inflated to 170 kPa (abs) and the void is cycled between 305 and 200 mm. Pressure increases through mass inflation, then again through the load phase of the compression cycle with constant mass. During the unload phase the pressure decreases. After the compression cycle is completed, the pressure is lower than before the cycle, which corresponds to plastic deformation in the material. The load curve has a similar shape to the pressure curve and the restraining load is typically proportional to the internal pressure for constrained bags. The volume curve shows the expected reduction in internal volume associated with the compression cycle and an increase in volume under the burst inflation at the end of the simulation.

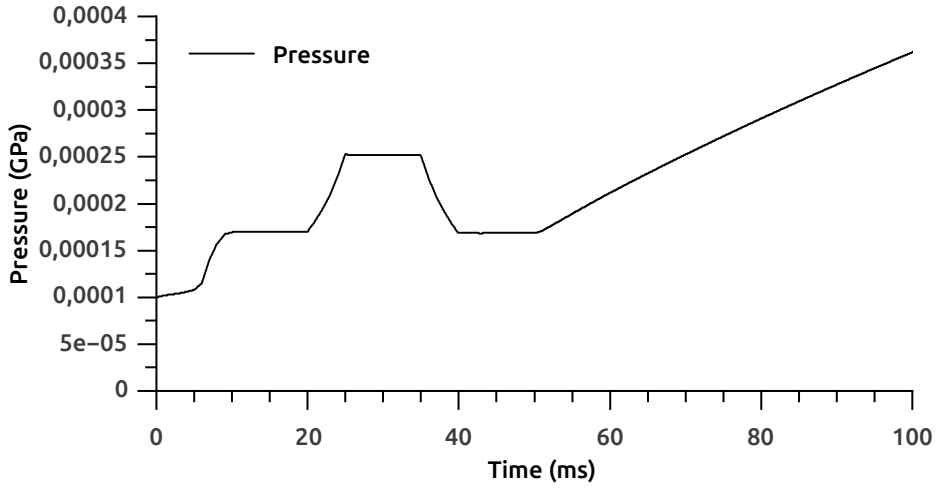

Figure 7.8: MAT_108 material simulation pressure over time

Figure 7.11 shows the relationships between pressure and void size then restraining load and void size. These load curves can be used to replace a full dunnage bag simulation in a simplified loading operation simulation that can be used to get more accurate load cases (see chapter 10 for more details).

Figure 7.12 shows the comparison of the internal and kinetic energy in the simulation that shows internal energy much larger than kinetic energy. This simulation is not dominated by dynamic effects and the time scaling is found to be suitable.

The shape of the simulated dunnage bag after the compression cycle is shown in figure 7.13. Also shown are the overlays of effective true strain and effective stress. It can be noted that the high strain areas of the bag are along the edges of the bag. This is the most common failure region observed in bag burst testing and is also observed in data generated by DIC. The average

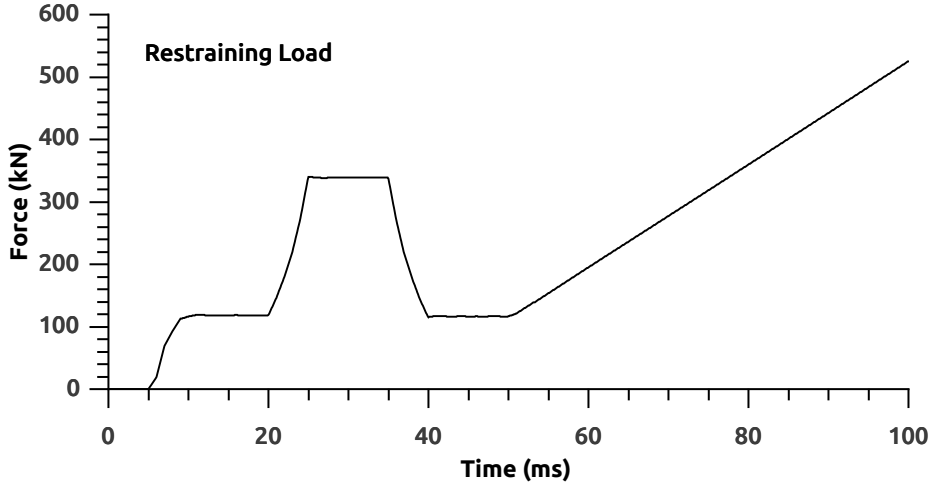

Figure 7.9: MAT_108 material simulation load over time

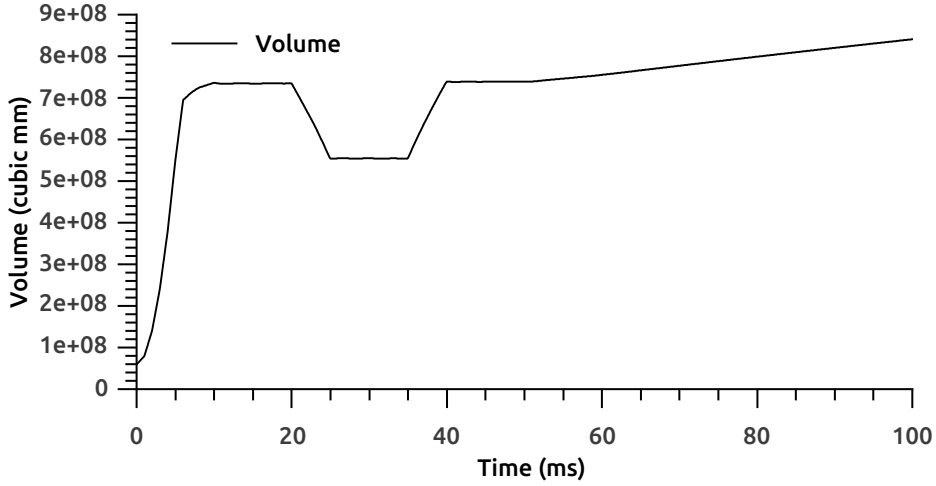

Figure 7.10: MAT_108 material simulation volume over time

strain of the middle third of the bag is presented in figure 7.14. It can be seen that with this material model the strain is largely constant after inflation making it unsuitable for prediction of failure. Figure 7.15 shows the effective stress over time, which increases over the burst component of the test allowing for a suitable failure criteria to be found. Physical bags burst at an average of 237 kPa (rel.). The corresponding stress in the numerical model was recorded as 142 MPa. It is reiterated that the stress values calculated using a homogenised material model have no physical meaning.

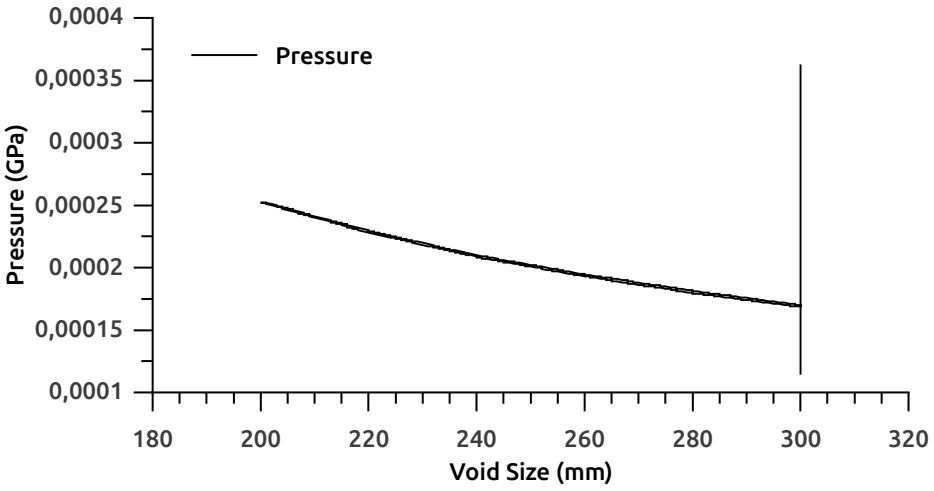

(a) Pressure vs void size

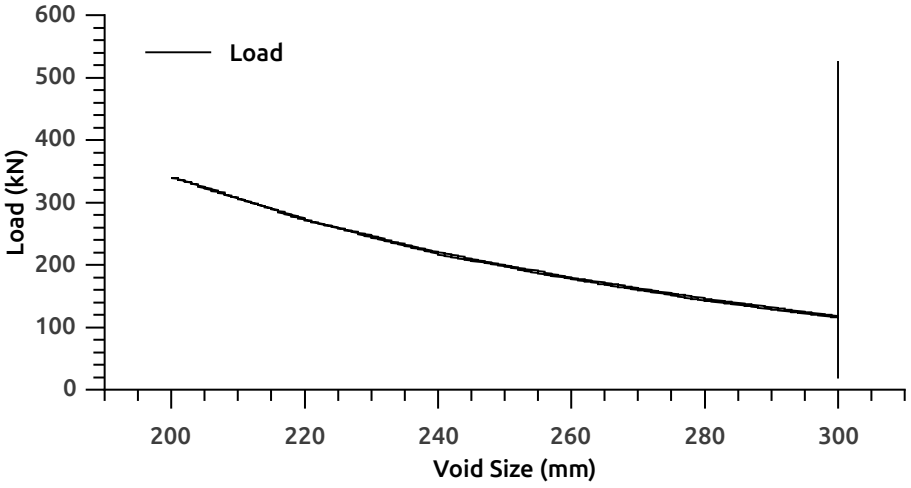

(b) Load vs void size

Figure 7.11: MAT_108 material simulation void cycle results related to void size

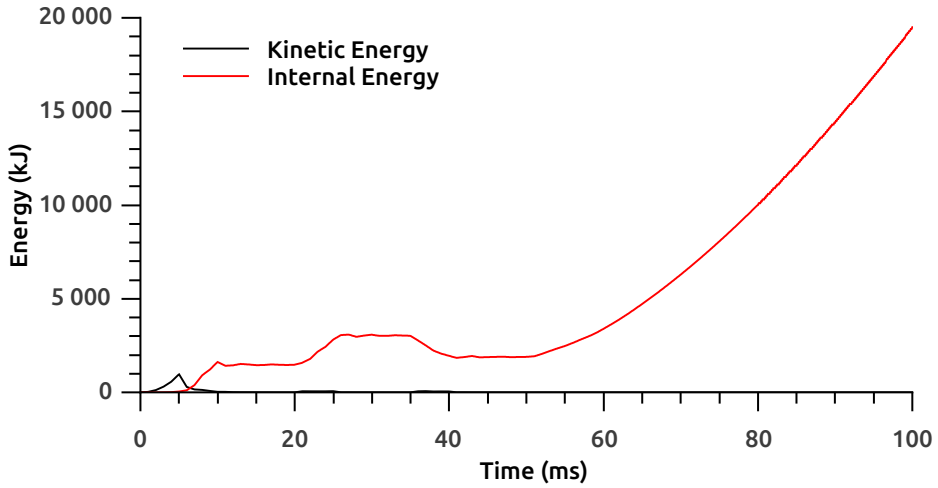

Figure 7.12: MAT_108 material simulation system energy over time

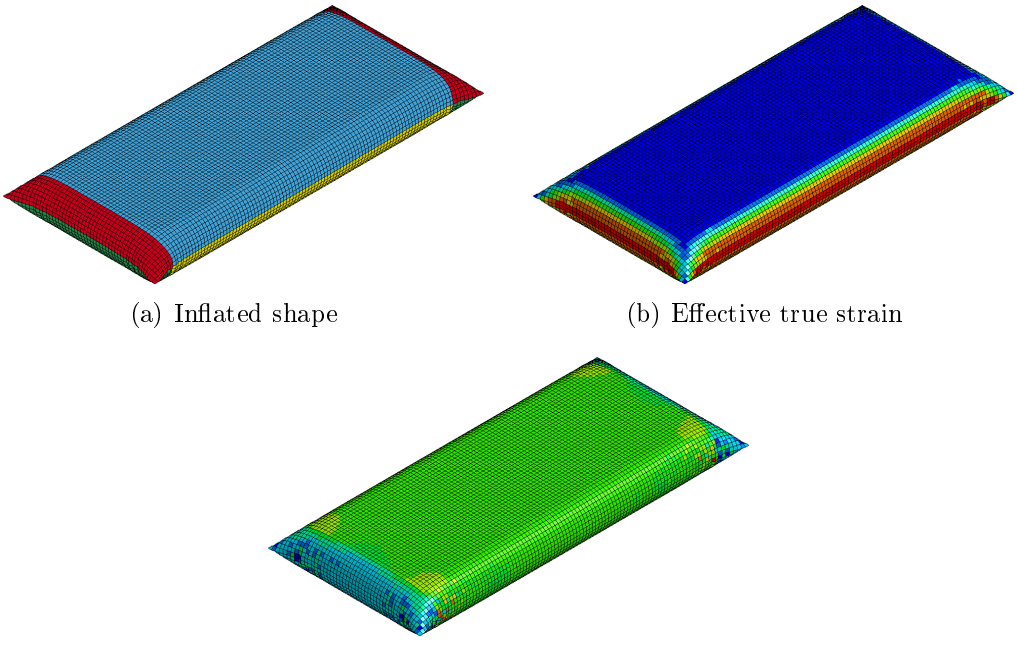

(a) Inflated shape

(b) Effective true strain

(c) Effective stress

Figure 7.13: MAT_108 material simulation results

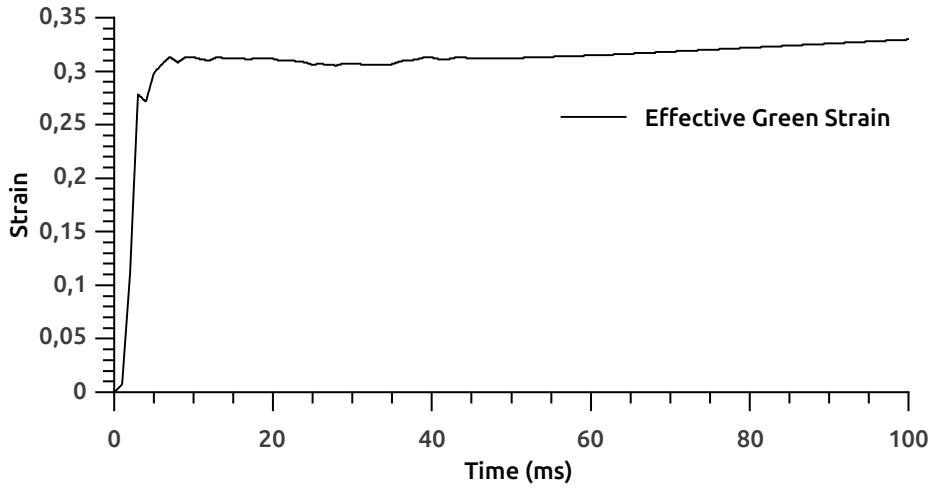

Figure 7.14: MAT_108 material simulation effective strain over time

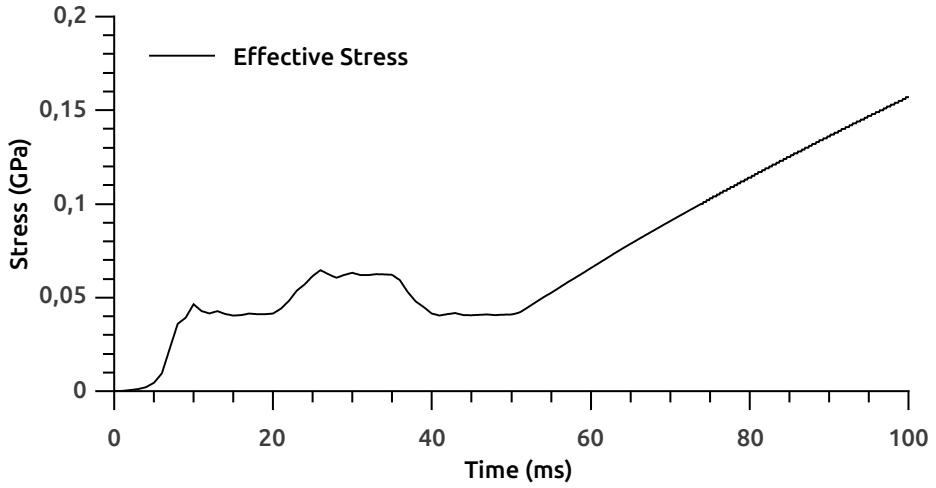

Figure 7.15: MAT_108 material simulation effective stress over time

7.5.2 Prototype with Hybrid Element Material

Figures 7.16, 7.17 and 7.18 show the pressure, restraining load and contained volume of the numerical dunnage bag over time using the hybrid element material. The bag is inflated to 170 kPa(abs) and the void is cycled between 305 and 200 mm. Again pressure increases through mass inflation, then again through the load phase of the compression cycle with constant mass. During the unload phase the pressure decreases. After the compression cycle is completed, the pressure is lower than before the cycle which corresponds to plastic deformation in the material. The load curve has a similar shape to the pressure curve and the restraining load is typically proportional to the internal pressure for constrained bags. The volume curve shows the expected reduction

in internal volume associated with the compression cycle and an increase in volume under the burst inflation at the end of the simulation.

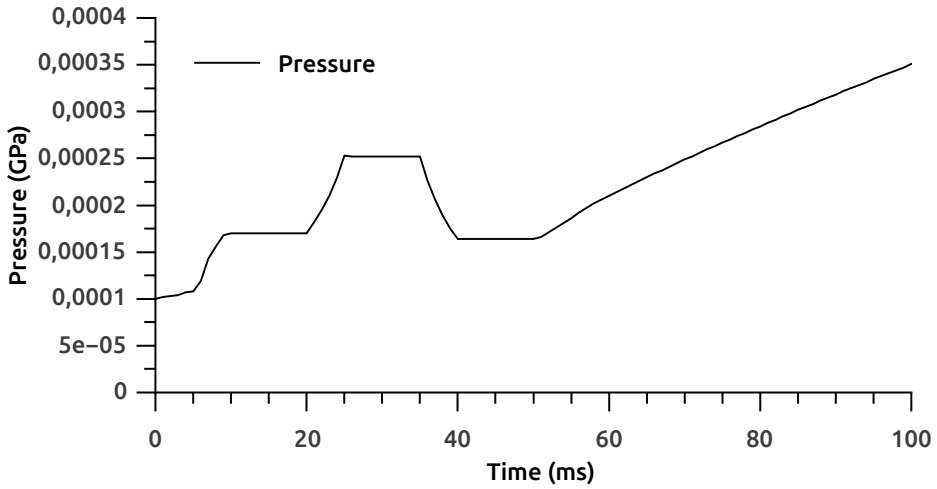

Figure 7.16: Hybrid element material simulation pressure over time

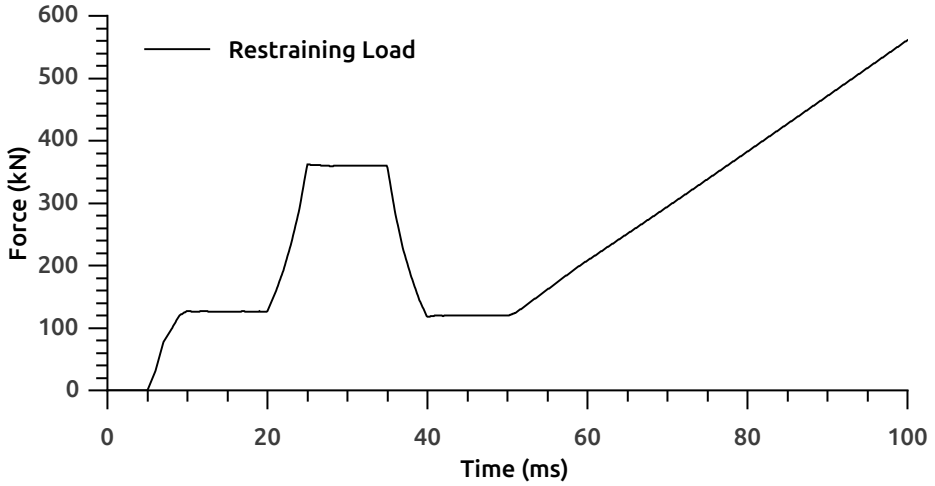

Figure 7.17: Hybrid element material simulation load over time

Figure 7.19 shows the relationships between pressure and void size then restraining load and void size. As before, these curves could be later used in simplified operational simulations.

The comparison of the internal and kinetic energy in the simulation shows internal energy much larger than kinetic energy, figure 7.20. This simulation is again not dominated by dynamic effects and the time scaling is found to be suitable.

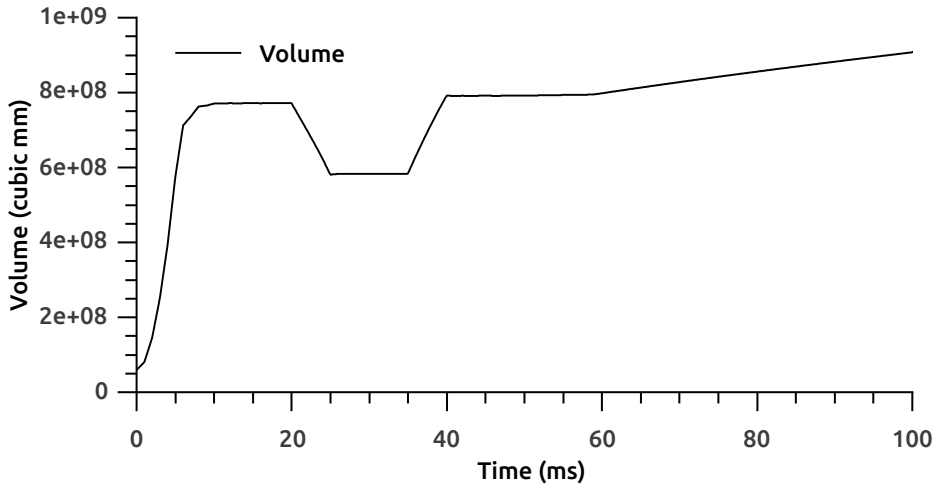

Figure 7.18: Hybrid element material simulation volume over time

The shape of the simulated dunnage bag after the compression cycle is shown in figure 7.21. Also shown are the overlays of effective true strain and effective stress. Again the model captures a high strain along the edge of the inflated bag corresponding to the region where failure is most likely. The hybrid element simulation shows more clearly that the high strain region in the vicinity of the seam is under a similar level of strain. This is confirmed by physical testing where the bag is about as likely to burst along an edge as the seam.

The average strain of the middle third of the bag is presented in figure 7.22. Again the strain is largely constant after inflation making it unsuitable for prediction of failure. Figure 7.23 shows the effective stress over time for the same model, which increases over the burst phase of the test allowing for a suitable failure criteria to be found. The stress in the numerical model at 237 kPa (rel.) was recorded as 240 kPa. This value is three orders of magnitude lower than the stress in the MAT_108 model, illustrating that the stress in a homogenised material is not a physical measure. The stress in the hybrid element is measured on the shell element which is not load bearing in this material.

7.6 Comparison of Test and Simulation Results

A comparison of the results generated by the MAT_108 and hybrid element models show very similar pressure and load characteristics, figures 7.24 and 7.25. The difference in restraining load is explained by the difference in internal volume between the two models, the hybrid element model having more volume, figure 7.26. A comparison of the average effective strain in the middle region of the bag also shows close correlation, figure 7.27. The matching of the

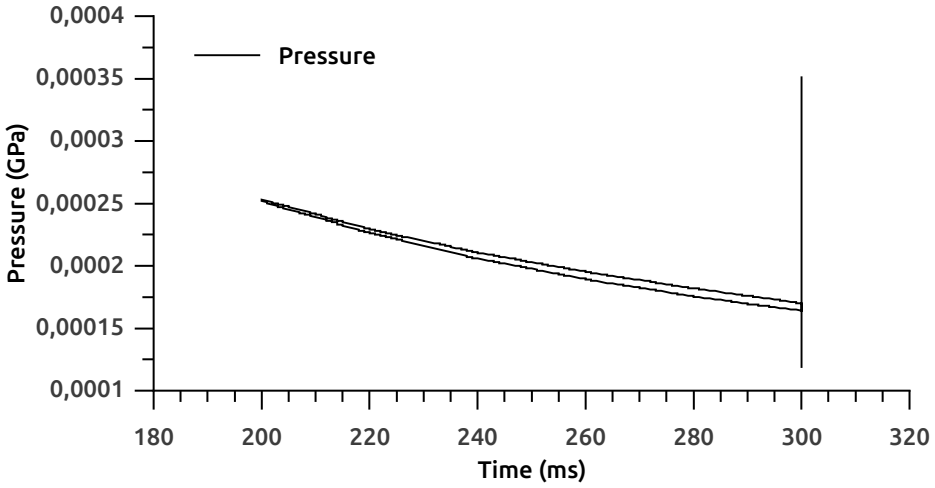

(a) Pressure vs void size

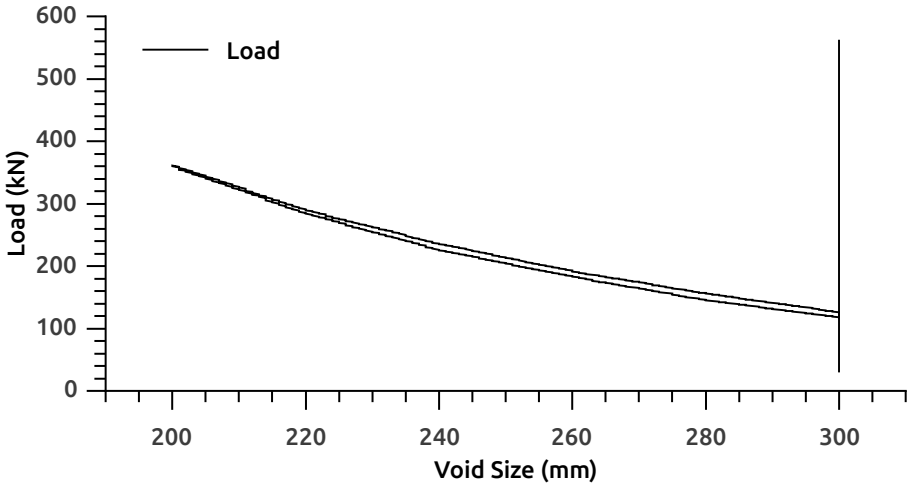

(b) Load vs void size

Figure 7.19: Hybrid element material simulation void cycle results related to void size

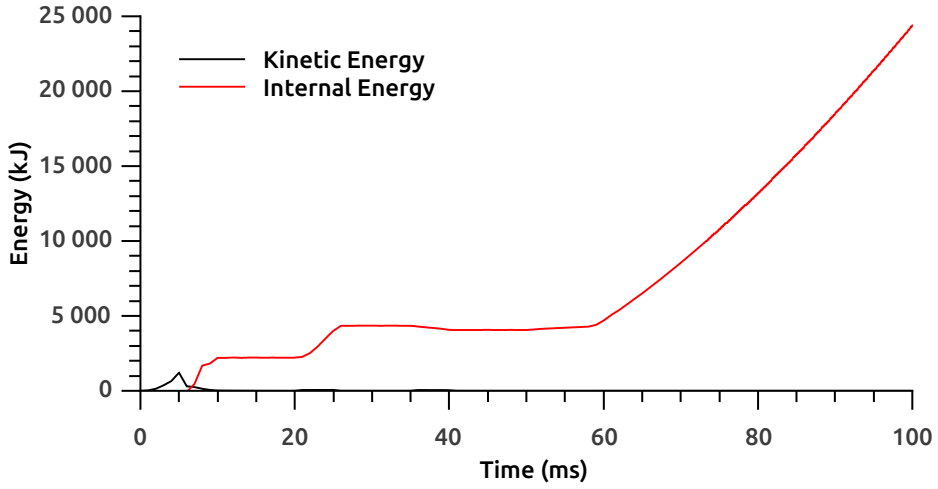

Figure 7.20: Hybrid element material simulation system energy over time

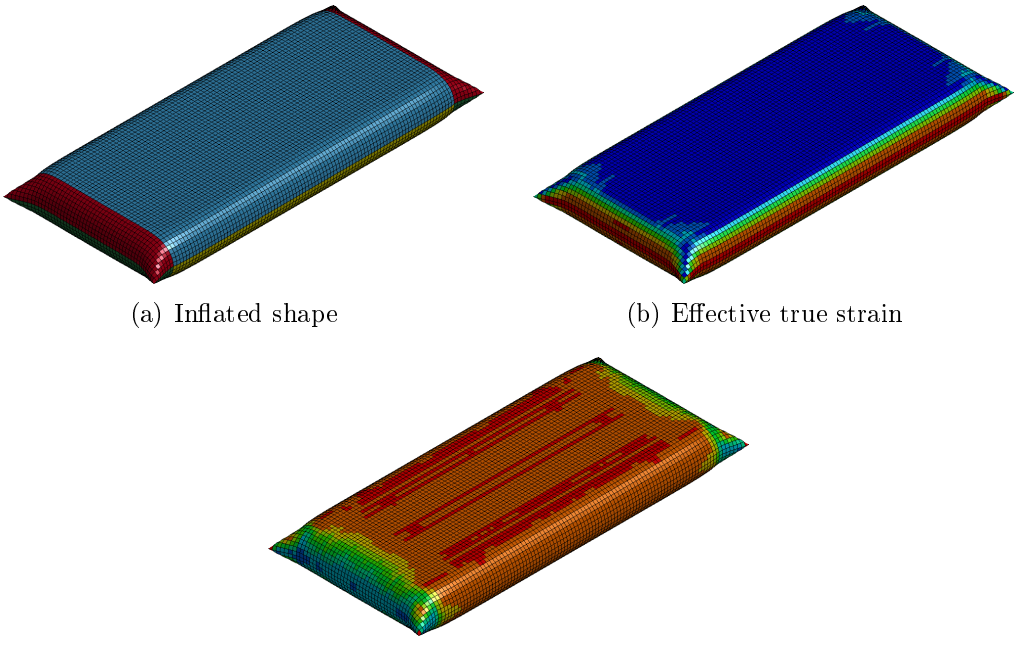

(a) Inflated shape

(b) Effective true strain

(c) Effective stress

Figure 7.21: Hybrid element material simulation results

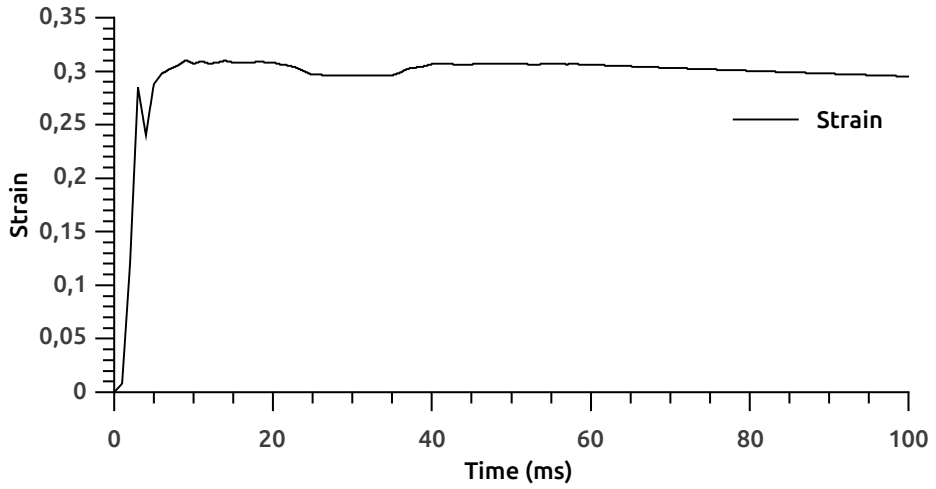

Figure 7.22: Hybrid element material simulation effective strain over time

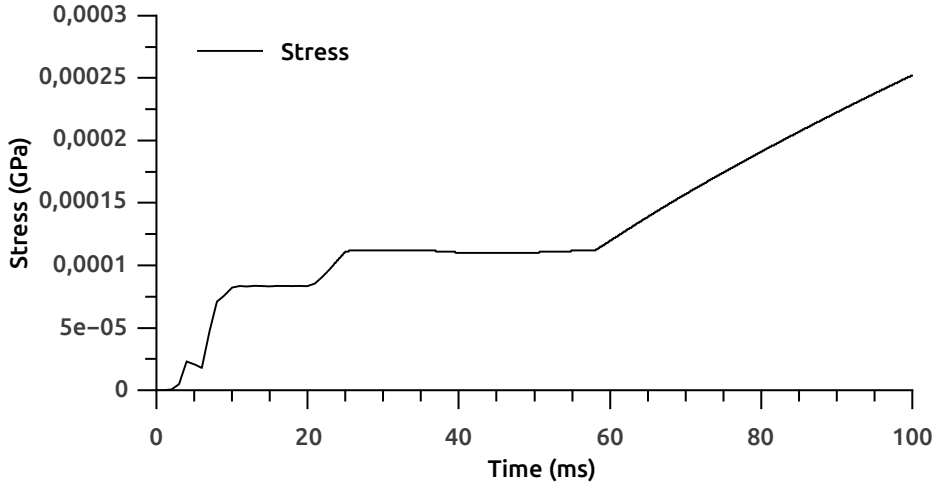

Figure 7.23: Hybrid element material simulation effective stress over time

material strains is not unexpected as it is an indirect input parameter through the material models range calibration.

When comparing the inflated shapes of the inflated bags it can be seen that the hybrid material is deformed to a larger volume matching the physical bags and accounting for the pressure drop, Figure 7.28. Even though there is a very large difference in shape there is not much difference in the strain plots, especially in the high strain regions along the edges of the bag, figure 7.29. This can be very useful in numerical experiments requiring a large number of function evaluations, even though the MAT_108 model does not capture some of the geometric detail it can be used as a high speed surrogate model in optimization. Figure 7.30 shows a comparison of 1^{st} in-plane principal strain

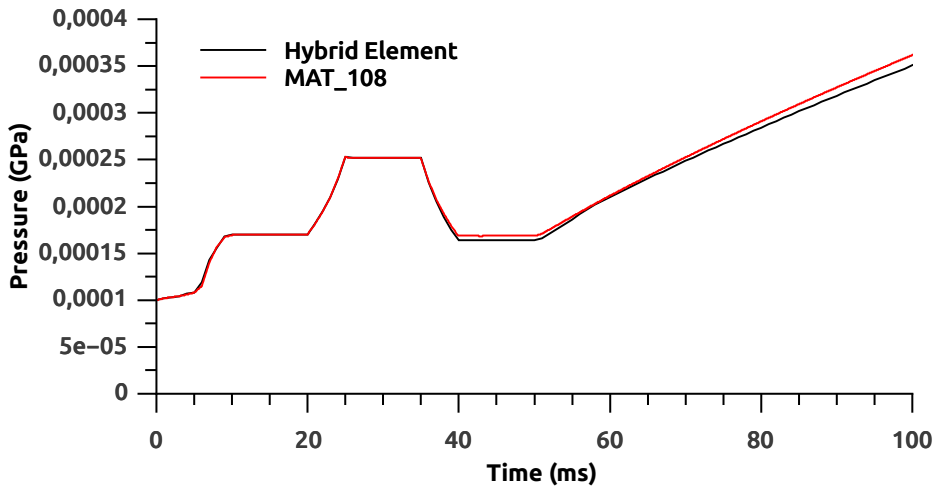

Figure 7.24: Comparison of MAT_108 and hybrid element material simulation pressure over time

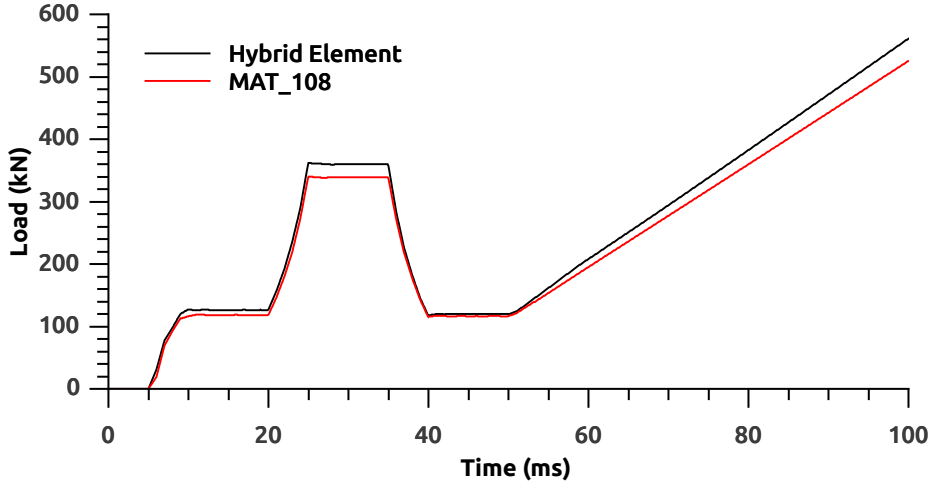

Figure 7.25: Comparison of MAT_108 and hybrid element material simulation load over time

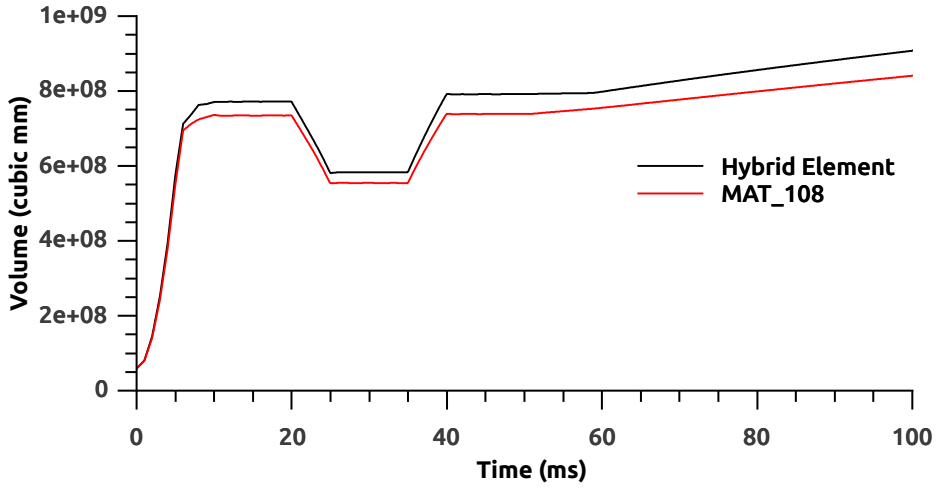

Figure 7.26: Comparison of MAT_108 and hybrid element material simulation volume over time

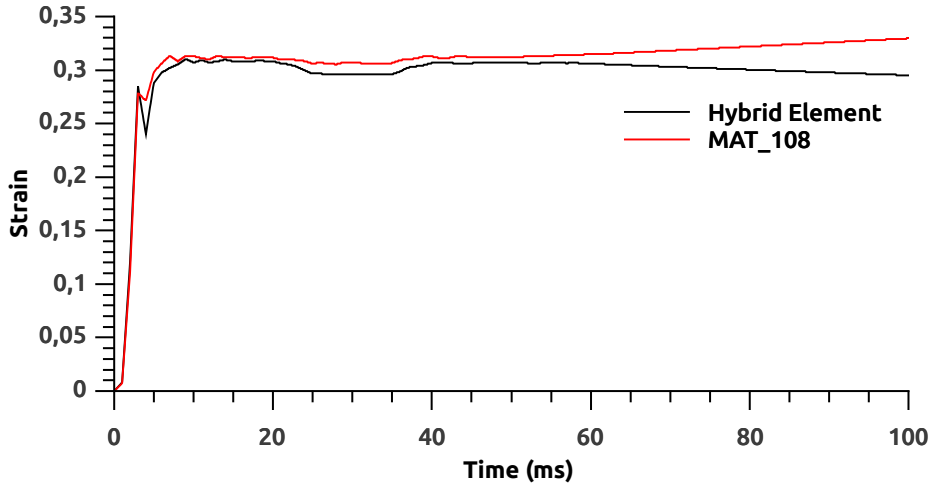

Figure 7.27: Comparison of MAT_108 and hybrid element material simulation effective strain over time

vectors. The figure shows that the MAT_108 model has large areas of shear, indicated by vectors diagonal across the element. As discussed earlier these regions are underutilised as the load is not applied along the fibre directions. This may not be seen in the hybrid model because the shear stiffness of the element is greatly reduced and not especially calibrated. Figure 7.31 shows a comparison of the hoop and lengthwise mid-span cross-sections of the bag. Here it is seen that even though the lengthwise deformation of the two models is approximately the same the hoop section is very different. Which is unexpected given the comparison of the two material swatch test results. The Hybrid element being calibrated on a material test subject to tow interaction and stiffening is unable to replicate that action in the full bag simulation.

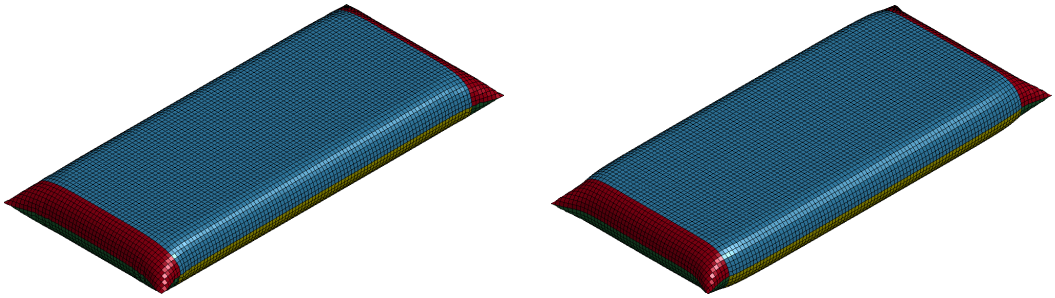

(a) MAT_108 material (b) Hybrid element material

Figure 7.28: Comparison of MAT_108 and hybrid element material simulation inflated shapes, after a single void cycle

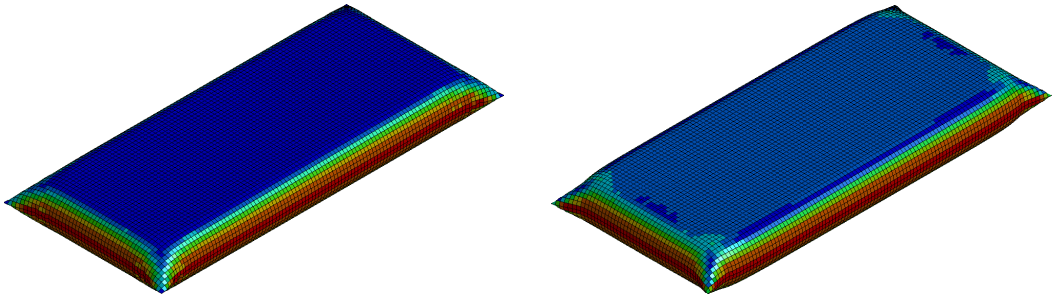

(a) MAT_108 material (b) Hybrid element material

Figure 7.29: Comparison of MAT_108 and hybrid element material simulation effective strain, after a single void cycle

Tables 7.4 and 7.5 compare of the key numerical values associated the modified AAR test. Here the pressure and load recorded in both simulation and testing are compared at the start of the test, at the peak of the compression cycle and at the end of the cycle. The drop in pressure or load for each is then

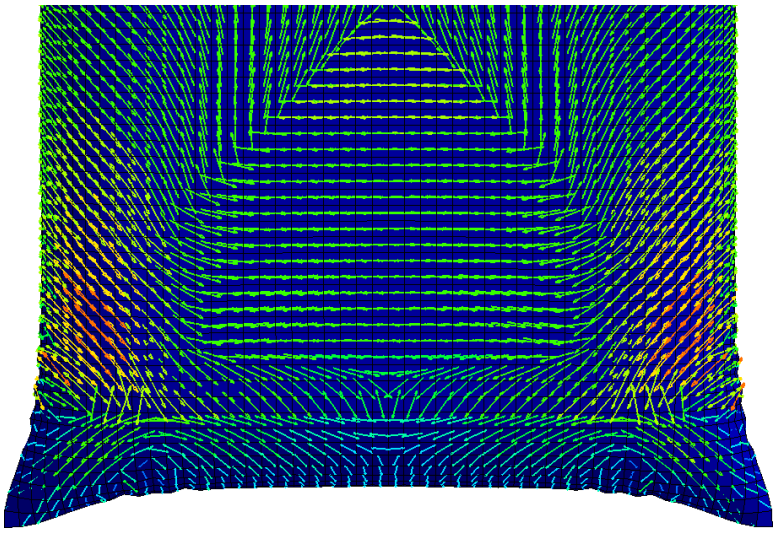

(a) MAT_108 material

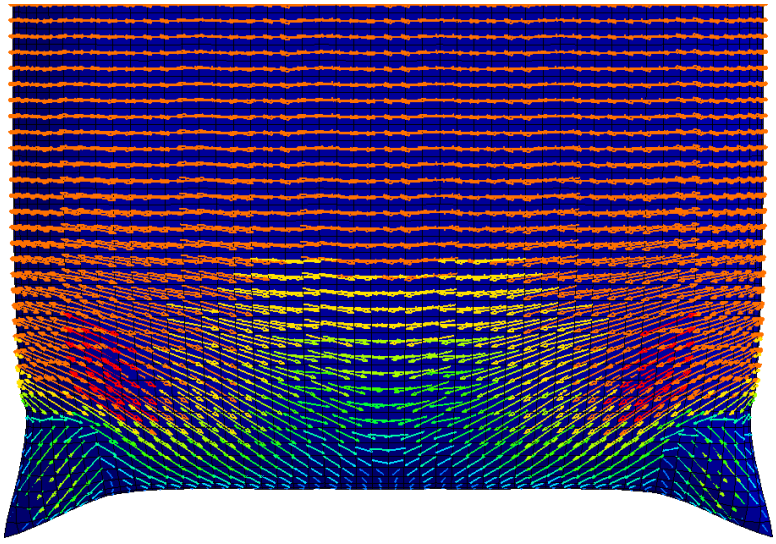

(b) Hybrid element material

Figure 7.30: Comparison of MAT_108 and hybrid element material simulation 1^{st} principal strain vectors, after a single void cycle

(a) Hoop direction

(b) Lengthwise direction

Figure 7.31: Comparison of MAT_108 and hybrid element material simulation cross-section, after a single void cycle. The hybrid element results are shown in red.

stated. A key objective of this project is to match the drop in pressure caused by material deformation. The pressure predicted by the hybrid element model after the compression cycle is within one standard deviation of the physical testing. Similarly the restraining load predicted by the MAT_108 model is within one standard deviation of the physical testing. Both tests over predict both the maximum load at the peak of the compression cycle and the load after the compression cycle.

Table 7.4: Modified AAR test and simulation results for pressure (kPa)

	Start	Maximum	End	Drop
Test	70.1	144.4	62.2	7.9
MAT_108	70	152	68.5	1.5
Hybrid Element	70	152	64	6

Table 7.5: Modified AAR test and simulation results for restraining load (kN)

	Start	Maximum	End	Drop
Test	115.85	307.81	101.08	14.78
MAT_108	118.1	339.3	116.2	1.9
Hybrid Element	126	360	120	6

As a comparison of the use of either model as part of an operational simulation figures 7.32 and 7.33 are shown. Here the pressure and load are related to the void size and are seen to correlate well. All the numerical prototypes proposed can be used to successfully predict the restraining load produced by a dunnage bag at operating pressure and the pressure in a bag after a compression cycle load, based only on simple material data from swatch testing.

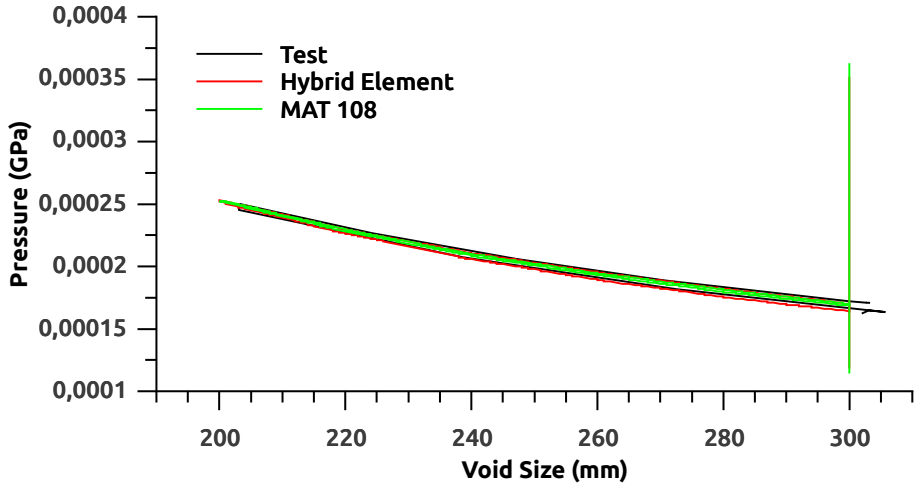

Figure 7.32: Comparison of pressure related to void size for physical test results, MAT_108 and hybrid element material simulation

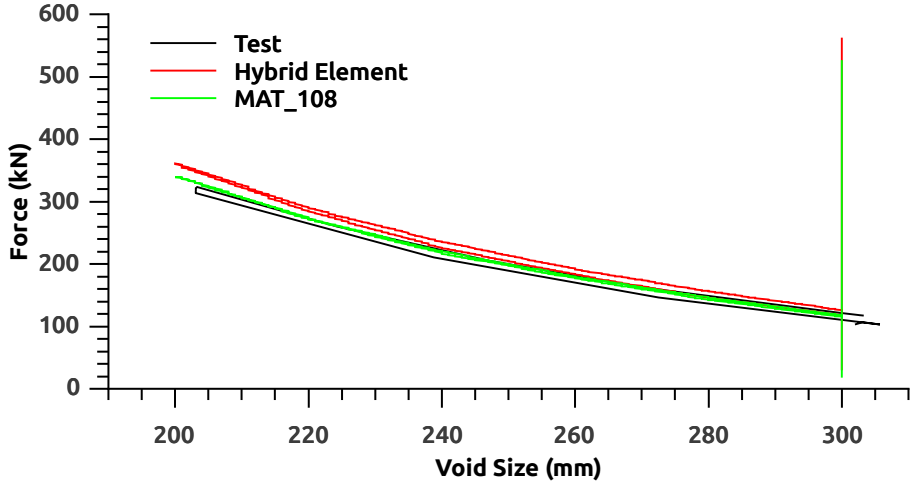

Figure 7.33: Comparison of load related to void size for physical test results, MAT_108 and hybrid element material simulation

Chapter 8

Predictions Using the Prototype Models

Two proposed numerical prototypes have been calibrated and validated for loading of a standard bag in a 305 mm, parallel void. This chapter investigates the use of these two prototypes outside the initial application range. If the model predicts well outside the initial calibration range fewer calibrations will be required to simulate non-standard operating conditions. Two investigations are undertaken. The first is a set of tests to evaluate how well the models predict failure and the second looks at the use of the prototype in non-parallel voids.

8.1 Prediction of Burst Pressure

To investigate the ability of the numerical prototype to predict failure, stress was selected as the indicator metric. In simulations using homogenised material properties the stress values have no physical meaning, but they are consistent within that simulation. This means that areas of high stress in the simulation will still predict areas of high stress in a physical sample, but the value of the stress is not necessarily reasonable. For both numerical models the stress along the mid-span of an edge is recorded during the course of a simulated inflation test. The failure stress is then selected to be the stress at which the numerical model is subjected to the average measured burst pressure observed in the physical tests. The effective stress corresponding to burst is found to be 142 MPa for the model using MAT_108 and 240 kPa for the model using the hybrid element.

The effectiveness of effective stress as a predictor of failure is tested in two different voids: a reduced void of 200 mm and an increased void of 400 mm. The reduced void corresponds to the minimum void in the cycle test and is a common inflation void in industry and the increased void is a potential new market being investigated for markets in Europe. Two new simulations were

performed using each of the two prototype models. The burst pressure in each of the two voids is predicted to be the pressure corresponding to the effective stress defined above.

8.1.1 Parallel 200 mm Void

Figure 8.1 shows a comparison of the effective stress obtained from the two simulations. Both models predict a similar burst pressure and produce similar stress patterns. The results for burst testing in a 200 mm parallel void are compared to the predicted burst pressures in table 8.1. In both cases the numerical models over predicts the burst pressure of the dunnage bag. Using the MAT_108 material the prediction is over by 8.1 % while the hybrid element model over-predicts by 8.7 %.

Table 8.1: Tested and predicted burst pressure results in 200 mm parallel void, the standard deviation for the test set is shown in brackets

	Burst Pressure kPa rel.
Test	320.67 (3.98)
MAT_108	346
Hybrid	348

8.1.2 Parallel 400 mm Void

Figure 8.2 shows a comparison of the effective stress in the two simulations. Both models predict a similar burst pressure and produce similar stress patterns. The results for burst testing in a 400 mm parallel void are compared to the predicted burst pressures in table 8.2. In this case the results are mixed based on the average results. The error of the predicted burst pressure is about 0.5 %, but more variation was found in the test results. There are two burst positions for woven dunnage bags, the lengthwise edge and the seam. In the lengthwise failure the hoop fibres of the woven polypropylene fail while in a seam failure the lengthwise fibres fibres fail. When these two failure positions are separated the data shows two distinct failure pressures. When these two are evaluated separately both models under-predict hoop failure and over-predict seam failure. The MAT_108 model gives a 4.2 % error for hoop failure and 8.3 % error for seam failure, while the hybrid element model gives a 5.2 % error for hoop failure and 7.1 % error for seam failure.

In each of the two test cases the numerical models predicted the burst pressure within 10 % of the tested values. This represents a reasonable prediction

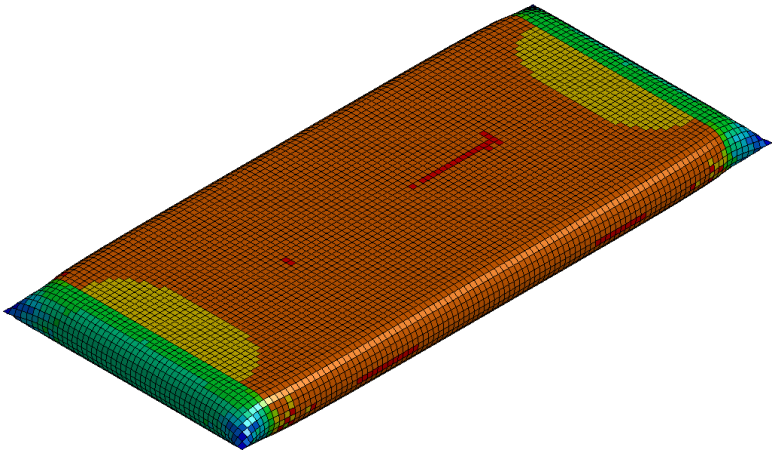

(a) MAT_108 material

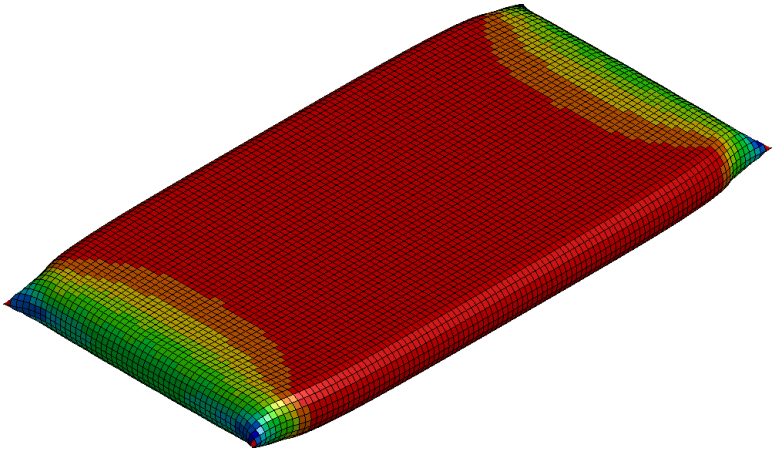

(b) Hybrid element material

Figure 8.1: Effective stress in a 200 mm parallel void at the predicted burst pressure

Table 8.2: Tested and predicted burst pressure results in 400 mm parallel void, the standard deviation for the test set is shown in brackets

	Burst Pressure kPa rel.
Test	182.69 (13.91)
Test Hoop	191.39 (6.15)
Test Length	169.63 (11.43)
MAT_108	183
Hybrid	181

of burst in voids other than the calibration void, suitable for evaluation of new void sizes.

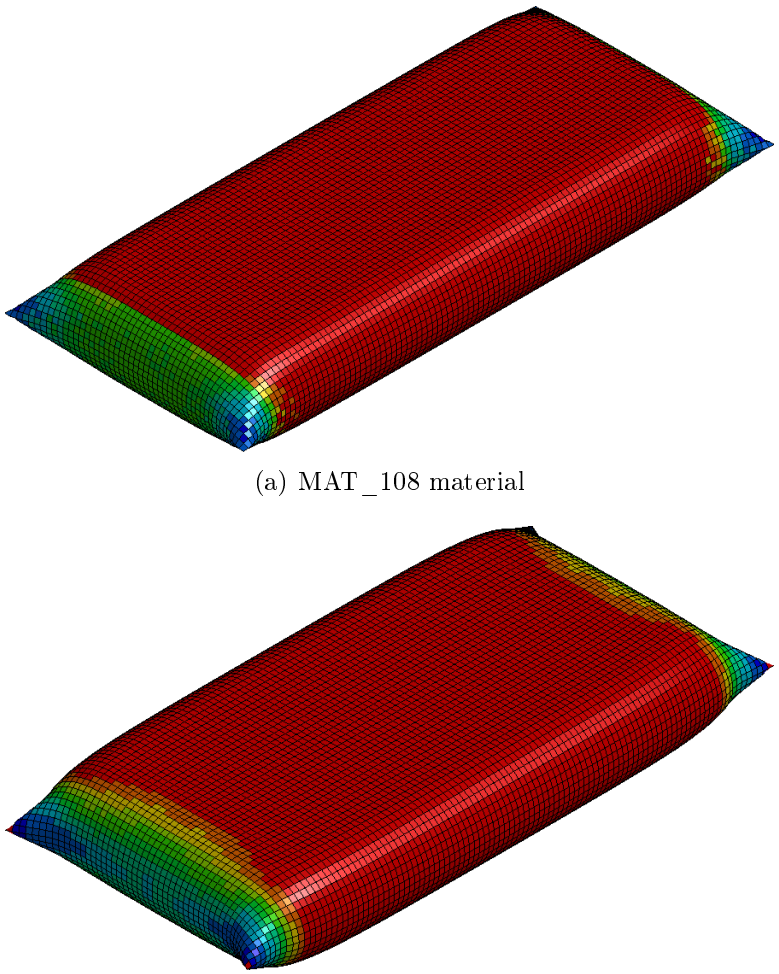

(a) MAT_108 material

(b) Hybrid element material

Figure 8.2: Effective stress in a 400 mm parallel void at the predicted burst pressure

8.2 Prediction of Relative Load in Non-Parallel Voids

One of the objectives of this project is to be able to simulate bags in an arbitrary void in order to evaluate how the bag will respond. To this end a study using the numerical prototype models was conducted. Four simple evaluation cases were simulated. The voids chosen have two voids representing out-of-position (OOP) cases where the bag extends past the restraining void and is partially unconstrained, a cargo misalignment case where the void is non-parallel and the case where inflation between paper rolls is simulated. In each case the bag is inflated to the recommended working pressure of 70 kPa rel. The effective stress recorded in the full bag simulations at working pressure are 41 MPa and 83 kPa for the MAT_108 and Hybrid models respectively. These values correspond to 28 % and 34 % of the stress at burst. The effect of

the void will be evaluated relative to the stress in the bag under recommended operating conditions of 70 kPa and 305 mm parallel void and as a percentage of the expected burst stress.

8.2.1 Paper Roll Humps

A standard L3/4 bag inflated between paper rolls produce effective stresses of 113 MPa and 184 kPa for the MAT_108 and hybrid element simulations respectively, increasing the stress in the bag to 275 % and 221 % of normal operating stress or 79 % and 76 % of predicted burst stress. This shows that a conventional dunnage bag used to restrain paper rolls has less than half the safety margin of a bag used in a conventional application.

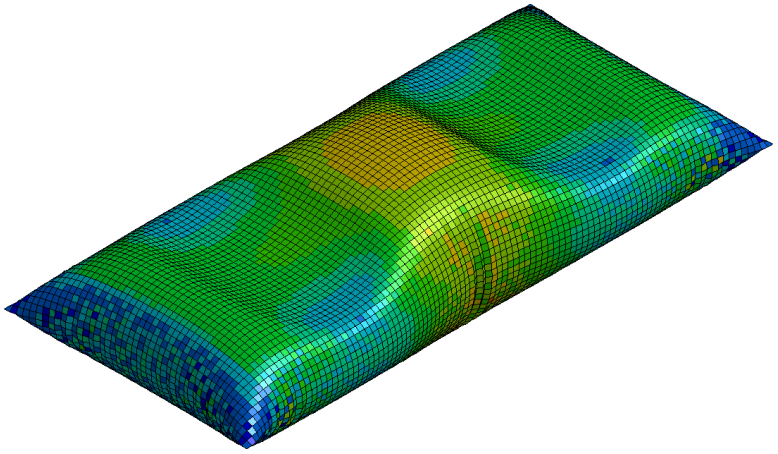

(a) MAT_108 material

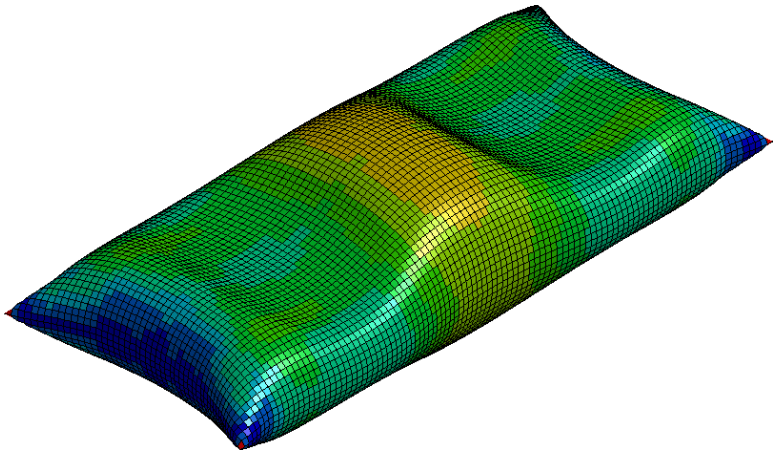

(b) Hybrid element material

Figure 8.3: Effective stress in a 305 mm paper roll void at working pressure

8.2.2 Single Side OOP Void

The single side OOP void occurs when a bag is inflated into a partially parallel void. That is the void is defined as a complete flat plane on one side and a shorter plane on the other, in this case the smaller plane is one third the length of the bag. This OOP inflation occurs when a dunnage bag is inflated between the container wall and a stack of boxes where the bag protrudes from the top of the void. In this case the predicted stress are 104 MPa and 141 kPa for the MAT_108 and Hybrid simulations. The stress in the bag is increased to 253 % and 170 % of operating stress and 73 % and 58 % of predicted failure stress. Again the bag is expected to have a lower margin of safety than a dunnage bag in a conventional application.

8.2.3 Double Side OOP Void

The double side OOP void occurs when a bag is inflated into a parallel void where both bounding surfaces are shorter than the bag. In this case one third shorter. This occurs when a dunnage bag is inflated between two stacks of boxes where the bag protrudes above both stacks. In this case the stress in the MAT_108 and hybrid simulations are 107 MPa and 149 kPa respectively. The stress in the bag increases to 260 % and 179 % of the operating stress and 75 % and 62 % of the predicted burst stress, a significant decrease in the margin of safety provided by the bag.

8.2.4 V-Shape Side Misaligned Void

The V-shaped misaligned void is a void where the space between cargo is not parallel. The case modelled here is a symmetrical V-shaped void reducing from 305 mm to 20 mm over the length of the bag. This can occur if during the inflation of the bag the boxes being restrained are pushed apart at the top while the bottom remains the same distance apart. The stress in the MAT_108 and hybrid simulations are 33 MPa and 56 kPa, decreasing the stress in the bag to 81 % and 67 % of operating stress and both 23 % of predicted burst stress. This is because most of the bag is in a lower stress state reducing the stress in critical areas.

8.2.5 Comparison of Non-Parallel Voids

The ability to predict the effect of using a dunnage bag in a non-conventional void can be very valuable when advising clients on potential risks of using dunnage bags outside their design envelope. In this case the simulations predicted that out of the four test cases inflation of a dunnage bag between paper rolls has the most risk with both simulations predicting that at operating pressure the bag will only have a safety factor of 1.33 as opposed to the recommended

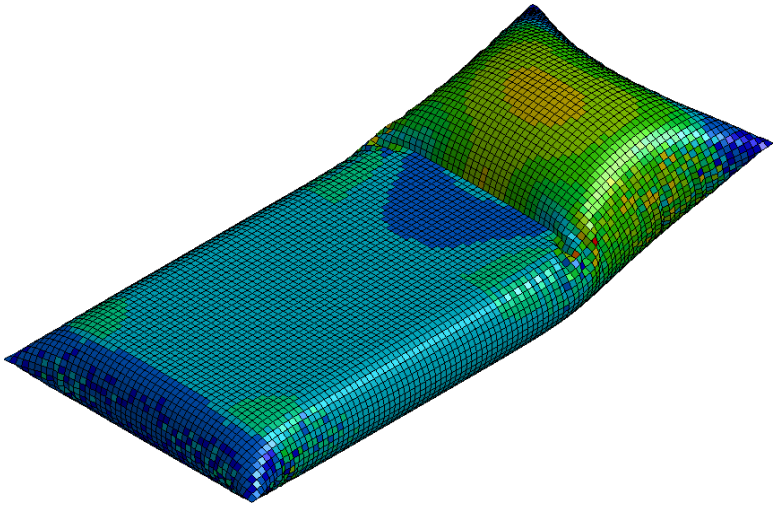

(a) MAT_108 material

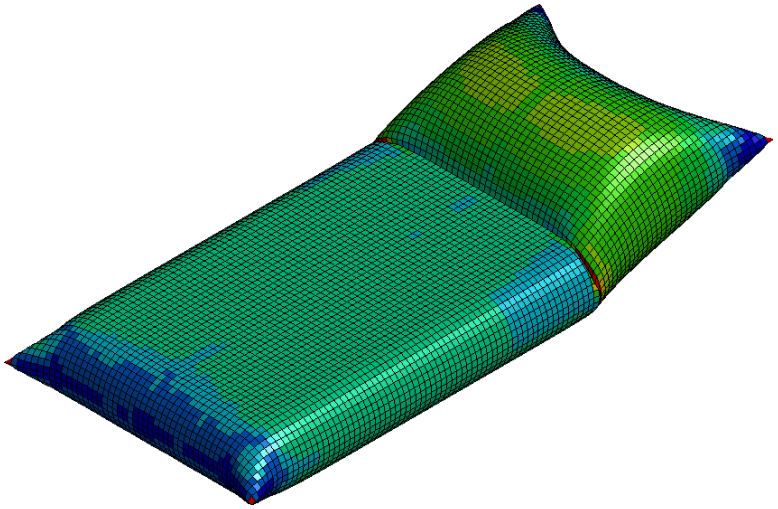

(b) Hybrid element material

Figure 8.4: Effective stress in a 305 mm single sided out of position void at working pressure

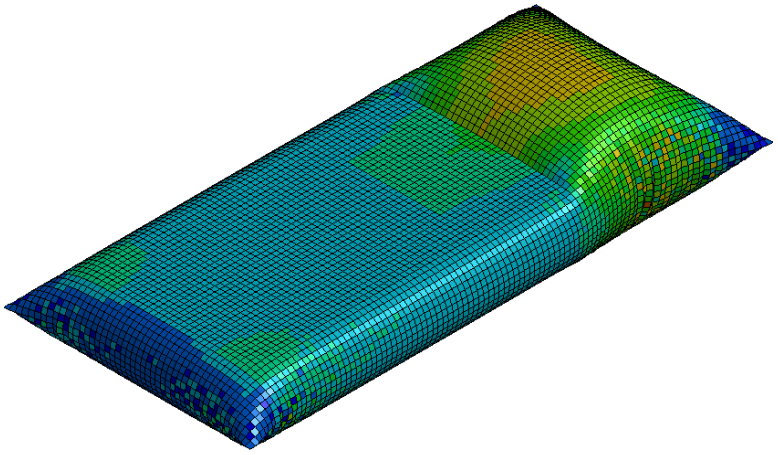

(a) MAT_108 material

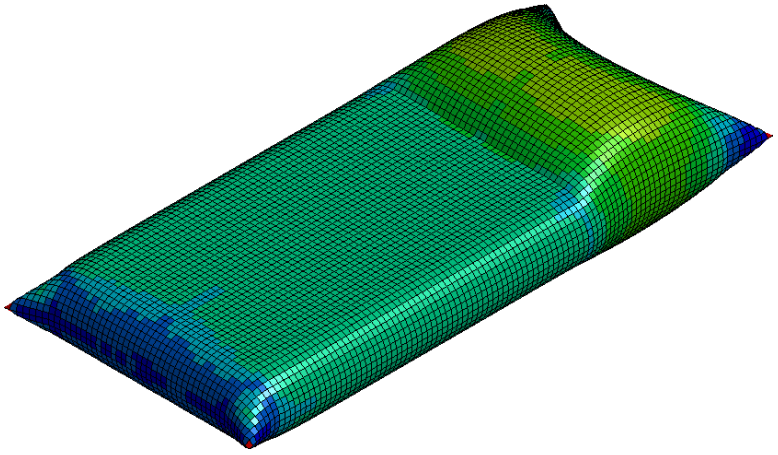

(b) Hybrid element material

Figure 8.5: Effective stress in a 305 mm double sided out of position void at working pressure

factor of 3. The simulations also show that having only a third of the bag unconstrained has a highly detrimental effect on the safety factor of the bag, reducing the factor from between 2.89 and 3.46 to between 1.36 and 1.7, again a significant decrease.

The bag inflated in a V-shaped void showed and increase in safety factor to around 4.37 which is expected of bags inflated into a void smaller than 305 mm. The smaller the void the greater the burst pressure.

Table 8.3 compares the predicted safety factors of dunnage bags inflated into the various voids. The safety factor of a level 4 dunnage bag in a 305 mm parallel void at operating pressure is typically 3. The predictions produced by the simulations in non-parallel voids corresponds well to both theory and experience. In terms of theory it is known that the larger the radius of curvature in the inflated bag the lower the burst pressure. This is matched by the

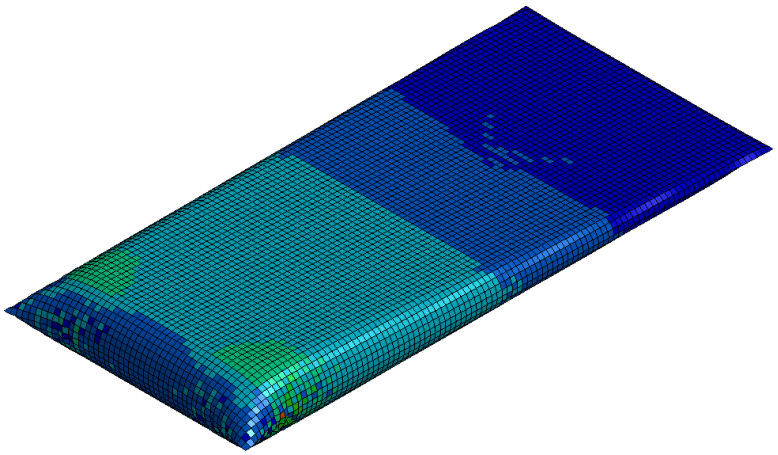

(a) MAT_108 material

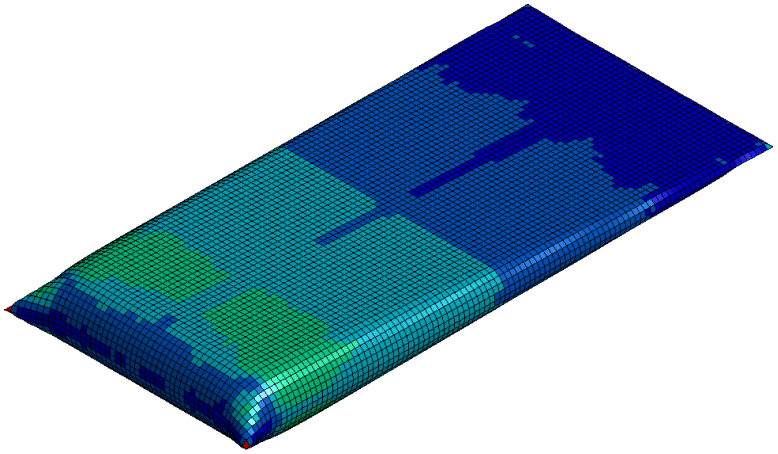

(b) Hybrid element material

Figure 8.6: Effective stress in a V-shaped out of position void at working pressure

simulation in that the order of increasing burst predicted stress is the same as the order of increasing curvature radius: V-shaped void, single side OOP void, double side OOP void and paper humps void.

Experience has also shown this to be the general trend that bags inflated between paper rolls have a low burst pressure while bags in smaller voids have higher burst pressures.

Table 8.3: Safety factors predicted for dunnage bags in non-parallel voids

	MAT_108	Hybrid Element
305 mm parallel	3.46	2.89
Paper roll humps	1.26	1.30
Single side OOP	1.37	1.71
Double Side OOP	1.33	1.61
V-shaped void	4.3	4.29

Chapter 9

Conclusions

This project began with the goal of developing a numerical model for inflatable dunnage bags reinforced with plain-woven polypropylene. The model was required to be suitable for numerical prototyping of new dunnage bags and be able to replicate representative operational load-unload conditions. The following objectives were identified in order to provide a complete methodology for the development of the numerical models:

1. Develop a test method for characterising the material properties of plain-woven polypropylene.
2. Parametrise woven polypropylene in terms of engineering parameters and select an appropriate material model.
3. Find a method that accounts for the work done by the inflation gas under loading.
4. Build a numerical model of an inflatable dunnage bag under cyclic loading.
5. Simulate a certification test for dunnage bags and validate the results with physical testing.

The approach taken for this project was to investigate the methods used to analyse other tensile structures in literature and adapt those methods to work for inflatable dunnage bags. A key component was found to be the material response of the plain-woven polypropylene used to reinforce and protect the dunnage bags. A new test device was designed and built to test woven swatches under bi-axial loading and material strain measurements were taken using DIC. With the measured material response in hand, the response of a numerical replica of the swatch test was mapped to the test data. This mapping made use of a numerical optimiser to provide the solution to the inverse problem. Two material models were calibrated using this method and applied to the numerical dunnage bag model.

A simple inflation model was chosen from those available in LS-DYNA that makes use of the Ideal Gas Law to calculate the pressure in the dunnage bag given the mass of air in the bag at any given time. This method was found to produce identical results to the simple pressure load previously used, but gave additional functionality to the model. Using the gas inflation model the pressure in the bag is recalculated for different volumes allowing simulations of void cycling to be run.

A modified version of the AAR Product Performance Profile for Pneumatic Dunnage was used to evaluate the response of the numerical prototypes to operational loading. Two numerical models were created, one for each material model calibrated, each making use of the inflation model. The results of the numerical simulations were compared to physical test results. The ability of the model to evaluate bags inflated in non-parallel voids as well as their ability to predict burst pressure in various voids was then investigated.

Dunnage bags were found to be tensile structures with full gas volumes, somewhat overlapping with other pressure rigidized and inflatable structures such as air-beams and Tensairity structures. It was found that for structures with components requiring inflation based pre-tension as the primary stiffening mechanism the material pre-tension is coupled to the pressure in the contained volume. Even with simple structures such as balloons and beams finite element methods are required to reasonably predict the response of the structure to the pre-tensioning when loading. For this class of structure, where deployment simulations are required, an explicit finite element code is required. When wrinkling occurs there are abrupt changes in the geometry, similar to a rigid body mode, which causes the simulations using implicit integration not to converge. The software package chosen for this project was LS-DYNA.

Investigation of plain-woven polypropylene showed that the material is both non-homogeneous and non-continuous with a highly non-linear orthotropic response where the shear response is decoupled. DIC was used to detect the strain ranges in the material hoop and lengthwise directions when the bag is subjected to a full void cycle. This data was then used to define the ranges for bi-axial tests performed on cruciform swatches cut directly from sample bags. The load-elongation response of the woven material was then evaluated and an average load-unload curve was determined for the material hoop and lengthwise directions (MD and CD).

The material models available were evaluated in terms of their ability to match the material load response recorded in physical testing. Two options were found suitable, an orthotropic elastic plastic material model native to LS-DYNA and a hybrid element that combined a linear elastic membrane with non-linear elastic springs. The parameter values for these two materials were calibrated by means of an inverse problem. The inverse problem statement makes use of a numerical replica of the bi-axial swatch test for each material. The numerical replica tests are then subjected to the displacements measured in the physical test. LS-OPT is used to minimise the difference between the

load-elongation curve measured in the swatch tests and the load-elongation curves generated by the numerical prototype models. Good correlations were found in each case.

The SIMPLE_AIRBAG_MODEL available in LS-DYNA was chosen for the full bag simulations. This model itself is a hybrid inflation model making use of a combination of the uniform pressure method and a simple equation of state. The internal cavity of the dunnage bag is defined as a control volume filled with a user defined mass of air. The Ideal Gas Law is then applied to the control volume to calculate the pressure, uniformly applied to the inner surface of the bag at each time-step. The software calculates the volume of the bag and the mass in the bag is defined as input data by the user, $PV = mRT$ is used to calculate the pressure. Alternative methods including the ALE method and CP methods which were found to be too complex for this simulation and the additional computational effort, was not warranted.

On the recommendation of the industry partner the AAR Product Performance Profile for Pneumatic Dunnage was used as the basis for the operational testing of the numerical models. The AAR is the certification agency for all rail transport in the United States of America. All dunnage bag designs destined for sale in the USA are required to be certified according to this AAR standard. The test breaks down into three components: a leak test, a cycle test and a burst test. Simulation of leakage and the post failure characteristics of dunnage bags were beyond the scope of this project. As a result, the simulations focussed on the cyclic loading of dunnage bags. A modified version of the AAR test was then developed that was more suitable for the test equipment available and suitable for numerical simulation.

A series of bags were inflated to 70 kPa in a 305 mm initial void. The void was then cycled down to 200 mm and returned to 305 mm over 10 seconds. The bag inflation was then continued in the 305 mm void until it burst. The average pressure in the bag after cycling was 62.2 kPa and the average burst pressure was 237 kPa.

The results for the same test performed on the two numerical prototype models produced pressures after cycling of 68.5 and 64 kPa for the model using MAT_108 and the hybrid element material respectively, a less than 3 % error when the hybrid element material is used. The numerical prototype using the hybrid element material was found to more accurately predict the pressure in the bag while the prototype using MAT_108 was found to more accurately predict the restraining load produced by the bag. The MAT_108 and hybrid element material models predict operational restraining loads of 118.1 and 126 kN respectively, compared to the average result of physical testing of 115.85 kN. A less than 2 % error for the model using material model MAT_108 was found. Both models were found to be useful and the choice of which model to use should be driven by the results desired from the model.

The ability of the models to predict the effect of deployment into various voids was split into two components: an evaluation of the ability of each model

to predict the burst pressure of a bag in a larger or smaller void and the relative material loading of the same bag in different void configurations. In order to test burst pressure prediction of the prototype models the effective stress in each model was found corresponding to the average burst pressure recorded for bags burst in the 305 mm void. The bags were then inflated into a 200 and 400 mm void. The predicted burst pressure in the new voids were estimated to be the pressure at which the same effective stress recorded in the 305 mm void is seen in that model. In the 200 mm void the prototype using MAT_108 over-predicted the burst pressure by 8.1 % while the prototype using the hybrid element material over-predicted the burst pressure by 8.9 %. In the 400 mm void the MAT_108 prototype predicted the burst pressure between 4.3 and 7.9 % while the hybrid element material prototype predicted the burst pressure between 5.5 and 6.7 %. In all cases the prototypes were within 10 % of the values recorded during physical testing. This means that the two models are suitable for predicting whether the burst pressure in an arbitrary void will be higher or lower that the recommended operating void.

Several out of position cases were then investigated, two cases where the bag protrudes from its intended void, one where the void is no longer parallel and one where the void is defined by cylindrical surfaces instead of flat surfaces. The results from these tests predicted that bags inflated between the cylindrical surfaces are most likely to fail prematurely. At operating pressure the effective stress in the simulated bag is nearest the stress recorded in the simulation at failure. The two out of position cases were found to be the next most likely to fail while the non-parallel V-shaped void showed a reduction in burst likelihood. These last three cases match the experience of the industry partner, making the prototype models suitable for evaluating the response of a dunnage bag to non-standard voids.

This research provides several novel contributions to the existing body of knowledge pertaining to inflatable tensile structures especially to inflatable dunnage bags. This research makes use of a new simplified method to map accurate material load-unload characteristics from physical testing to material models in LS-DYNA. This research also makes use of a hybrid element material to overcome some of the limitations of the native material models and improve the unload characteristic of the material. The models presented captures the combined effects of internal PV-work and externally applied load capturing the loss in pressure caused by a cycled void load on a fully inflated bag.

This project has met all of its objectives and produced two novel models that make use of only simple material tests and standard commercial software to replicate an operational load case for inflatable dunnage bags reinforced with plain-woven polypropylene. A test method was developed to characterise the response of plain-woven polypropylene to bi-axial loading. The material was parametrised in terms of parameters suitable for engineering problems. An accurate inflation model was added to the existing model for kraft paper reinforced bags. The two prototype models are suitable for cyclic loading and

were validated against physical tests. The results of the validation showed that the new models are capable of predicting the reduced pressure after a cycle load and the operational restraining load within 5 %. The models were found to be suitable for predicting the response of a full bag even in voids outside of the initial calibration envelope.

The methods presented here are suitable for the development of numerical models suitable for prototyping inflatable dunnage bag under conventional operating conditions.

Chapter 10

Recommendations for Further Research

10.1 Update and Improve Material Models

During the course of this project it was found that a key component in the development of a numerical prototype is to have accurate material data and models that can effectively match the material response. Two methods were used, each with limitations. It is recommended that as future work improvements to material testing methods and numerical models occur.

The first step will be to develop more capable testing equipment. The current equipment only allows for conventional uni-axial tests and bi-axial tests at a constant displacement ratio. A new test device should be developed that captures more of the material response by allowing for variable load, displacement and and shear states. A simple test with increasing popularity is the bubble test where a circular sample is clamped to a circular fixture and pressure is applied to one side of the fabric sheet producing a bubble. DIC is then used to measure the strain in the sheet. A finite element replica of the test is created and the material parameters are then optimised to match the response of the material tests.

An alternative material test is also available that has more flexibility to produce various bi-axial and shear states. The shear ramp test discussed in chapter 4 allows for any combination of bi-axial tension and shear to be applied to a cruciform sample. The benefit of this device is that shear can be directly tested as opposed to indirectly using the bubble test. Shear response can also be evaluated when the material is subjected to a pre-tension.

Once test equipment is available that is capable of measuring a wider material response more representative material models can be calibrated and evaluated. The addition of a diagonal cross-member to the hybrid element already implemented could give the element the ability to more accurately match the shear response of the material. With the addition of more test data the calibra-

tion procedure by Dubois and Forsberg (2013) can be implemented to calibrate the MAT_034 material model to be suitable under bi-axial loading. With an accurate material response model a project can be undertaken to develop a user-defined material model that captures the key responses of plain-woven polypropylene.

In addition to improving the material properties of the reinforcing material of a dunnage bag, work should be done to capture the effect of the seam on the bag. In the current model the seam is not accounted for at all. It is known that about half of failures in the Level 3/4 bags are caused by seam failures rather than reinforcing material failure. Test equipment must be put in place that can evaluate the characteristics of the seam itself so that failure in that region can be predicted in new models.

10.2 Numerical Sensitivity Study

With the numerical models in place we now have the opportunity to perform various sensitivity analyses. The numerical model is suitable for investigating the effects of over and under-inflation of the bag on the restraining load and to investigate the effect of manufacturing errors on the material. Further sensitivity analysis can be performed to investigate more specific variables such as the relationship between the MD and CD material stiffness, and the effect of surface friction. Preliminary investigations should also be done on the aspect ratio of the bag.

10.3 New Prototype Designs

The numerical prototype is intended to allow new concepts to be evaluated. Some initial ideas generated during this project include: adding a compression element or cable reinforcement to the bag, increasing the number of folds along the stitched seam to improve the seam strength, using double bags in larger voids so that the void for each bag is reduced, adding cable reinforced gussets to existing bags and changing the shape of the seam to improve material engagement.

10.4 Topology and Shape Optimization

A further field to be investigated is the use of optimisation software to run through various prototypes and evaluate their relative merit. Topology optimisation can be used to identify the areas that would most benefit from material addition and reinforcement. Size optimization could be used to estimate the thickness required in various regions of the material to achieve an overall material mass reduction.

A more complex analysis can be used to perform shape optimization of the dunnage bag. The most likely place to start is with the shape of the seam. At the moment the seam is stitched perpendicular to the main body of the bag, but the degree of material engagement could be improved by switching to a curved seam. This will reduce the unused material near the seam of the bag improving the overall strength of the bag.

Appendices

Appendix A

Material Test Procedures

A.1 Bi-Axial Test Method

The set-up for the bi-axial tensile test requires an the MTS-Criterion, HBM Spider DAQ, LaVision DaVis DIC software and two LaVission E-Lite cameras and programmable timing unit (PTU) and analogue to digital converter (ADC). The setup procedure follows;

1. Mount the bi-axial tensile test device in the MTS-Criterion, figure A.1.
2. Connect the four load-cells of the bi-axial device to the HBM Spider DAQ.
3. Connect the cross-head displacement output from the MTS-Criterion to the Spider DAQ.
4. Connect the PTU, DAC and two E-Light cameras to the PC running the DaVis software, figure A.2.
5. Connect a second cross-head displacement output from the MTS-Criterion to the ADC connected to the DaVis PC.
6. Displace the MTS-Criterion cross-head 2 mm to take up any slack in the bi-axial device.
7. Mount a generic cruciform sample to the bi-axial device.
8. Position and focus the cameras so that the entire 100 x 100 mm area of interest is in view. Also ensure that the bit rage of the cameras are maximized, figure A.3.
9. Calibrate the cameras at the desired range using a calibration plate. Ensure that the average position error for calibration is less than 0.5 pixels, figure A.4.

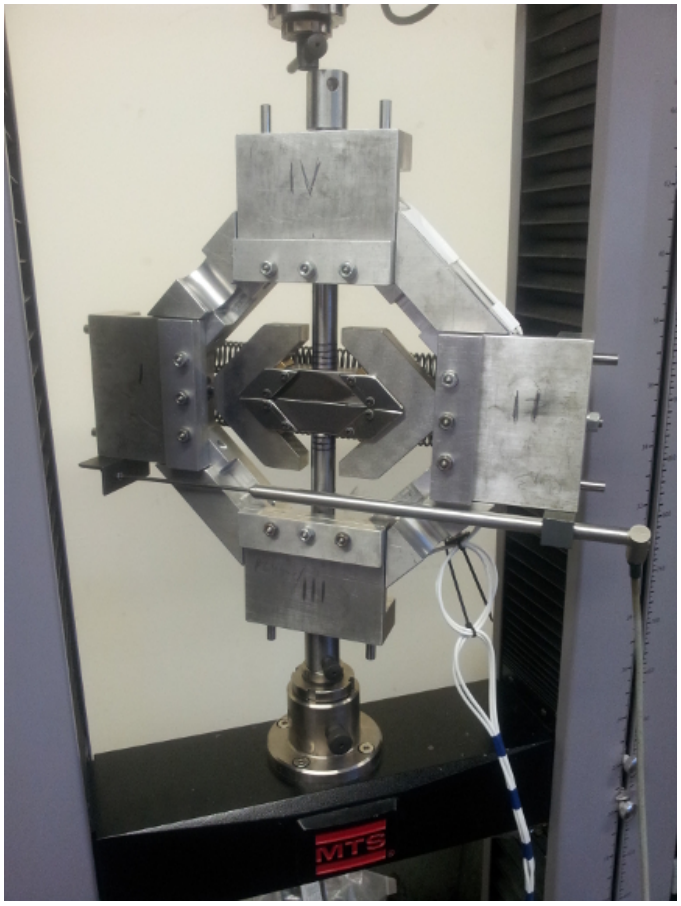

Figure A.1: Bi-axial test fixture mounted on the MTS Criterion tensile test device

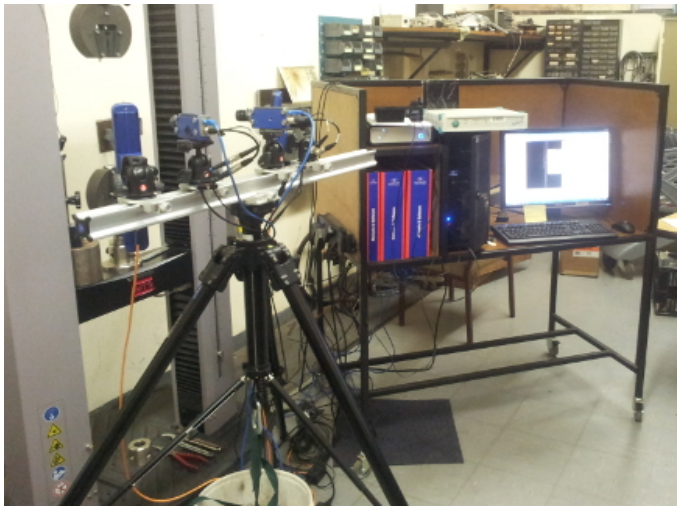

Figure A.2: Digital image correlation setup with Spider 8 data logger

Figure A.3: Digital image correlation camera set up

Figure A.4: Digital image correlation calibration plate

With the set-up complete a series of bi-axail tests can be performed without needing to re-calibrate the DIC set-up. The test procedure is as follows;

1. Mount a cruciform sample to the bi-axial device.
2. Using the DaVis system take 5 images of the static sample and run the DIC software.
3. Confirm that the DIC software is able to find correlation between images.
4. Evaluate the deformation registered by the DIC software. The RMS of the average deformation will be used as a measure of the noise floor for the test.
5. Start recording images with the DaVis software and load-cell data with the HBM Spider.
6. Start the load cycle on the MTS-Criterion.
7. Once the load cycle is complete stop all devices.
8. Save the load-time and MTS cross-head displacement-time data on the HBM-Spider.
9. Run image correlation on the the recored images.
10. Export the MTS cross-head-displacement - time data from DaVis.
11. Use the virtual strain gauge option in DaVis to export the average xx and yy surface strain for a 50 x 50 mm central region. These correspond to the material MD and CD.

A.2 Data Processing

The data required as a result of these tests are the load-elongation curves in the MD and CD for a 50 x 50 mm central region of interest. The load in each material direction is taken from the HBM spider data and the elongation is calculated using the strain data output by the DIC system. This data needs to be calibrated and synchronized.

1. Scale the load-cell data from the HBM-Spider converting the mV/V output to kN.
2. Pre-multiply the average material strain data from the DIC system to get the elongation of a 50 x 50 mm square.
3. Using the common MTS cross-head data field from each data source, synchronize the data.

4. Export a two-column data set with the load (kN) and elongation (mm)for each test.

5. Take the average of all the tests to generate the final load-elongation curve for that material.

Appendix B

Reduced Input Decks for Full Bag Models: MAT_108

```
*KEYWORD
*PARAMETER
I endtim         100R termt    100.00000R inflatem  0.245719R endmass   0.130000
*TITLE
$# title
M190 48x102 L3/4 170 kPa(abs) 300-200mm void,9e-7 density(kg,mm,ms,kN,GPa,kN-m)
*CONTROL_ACCURACY
$#     osu       inn    pidosu
         1         2         0
*CONTROL_ENERGY
$#    hgen      rwen    slnten     rylen
         2         2         2         2
*CONTROL_TERMINATION
$#  endtim    endcyc     dtmin    endeng    endmas
&endtim            0     0.000     0.000     0.000
*CONTROL_TIMESTEP
$#  dtinit    tssfac      isdo    tslimt     dt2ms      lctm     erode     ms1st
     0.000  0.500000         0     0.000     0.000         0         0         0
$#  dt2msf   dt2mslc     imscl    unused    unused     rmscl
     0.000         0         0                         0.000
*DATABASE_ABSTAT
*DATABASE_BNDOUT
*DATABASE_ELOUT
*DATABASE_MATSUM
*DATABASE_NCFORC
*DATABASE_NODFOR
*DATABASE_NODOUT
*DATABASE_RCFORC
*DATABASE_RWFORC
*DATABASE_SLEOUT
*DATABASE_SPCFORC
*DATABASE_TRHIST
$#      dt    binary      lcur     ioopt
  1.000000         3         0         1
*DATABASE_BINARY_D3PLOT
$#      dt      lcdt      beam     npltc    psetid
  1.000000         0         0         0         0
$#   ioopt
         0
*DATABASE_EXTENT_BINARY
$#   neiph     neips    maxint    strflg    sigflg    epsflg    rltflg    engflg
         0         0         3         1         1         1         1         1
$#  cmpflg    ieverp    beamip     dcomp      shge     stssz    n3thdt   ialemat
         0         0         0         1         2         3         2         1
$# nintsld   pkp_sen      sclp    unused     msscl     therm    intout    nodout
         0         0  1.000000                   2         0ALL       ALL
$#    dtdt    resplt
         0         0
*BOUNDARY_SPC_SET_ID
$#      id                                                              heading
         0Hold-mid-x-in-y
$#    nsid       cid      dofx      dofy      dofz     dofrx     dofry     dofrz
         1         0         0         1         0         1         0         1
*SET_NODE_LIST_TITLE
mid-x
$#     sid       da1       da2       da3       da4    solver
         1     0.000     0.000     0.000     0.000MECH
$#    nid1      nid2      nid3      nid4      nid5      nid6      nid7      nid8
        26        84       195       201       277       289       360       374
*BOUNDARY_SPC_SET_ID
$#      id                                                              heading
         0Hold-mid-y-in-x
$#    nsid       cid      dofx      dofy      dofz     dofrx     dofry     dofrz
         2         0         1         0         0         0         1         1
*SET_NODE_LIST_TITLE
mid-y
$#     sid       da1       da2       da3       da4    solver
         2     0.000     0.000     0.000     0.000MECH
$#    nid1      nid2      nid3      nid4      nid5      nid6      nid7      nid8
      1014      1154      1386      1389      1658      1669      1914      1925
      2158      2169      2412      2423      2634      2648      2868      2879
      3082      3093      3292      3303      3494      3505      3684      3695
```

```
*CONTACT_AIRBAG_SINGLE_SURFACE_ID
$#     cid                                                         title
         1SELFCONTACT
$#    ssid      msid     sstyp     mstyp    sboxid    mboxid       spr       mpr
         1         0         2         0         0         0         0         0
$#      fs        fd        dc        vc       vdc    penchk        bt        dt
     0.000     0.000     0.000     0.000     0.000         0     0.0001.0000E+20
$#     sfs       sfm       sst       mst      sfst      sfmt       fsf       vsf
  1.000000  1.000000     0.000     0.000  1.000000  1.000000  1.000000  1.000000
*SET_PART_LIST_TITLE
ALLPARTS
$#     sid       da1       da2       da3       da4    solver
         1     0.000     0.000     0.000     0.000MECH
$#    pid1      pid2      pid3      pid4      pid5      pid6      pid7      pid8
         1         2         3         4         0         0         0         0
*PART
$# title
TOPSIDE
$#     pid     secid       mid     eosid      hgid      grav    adpopt      tmid
         1         2         1         0         0         0         0         0
*SECTION_SHELL_TITLE
double thick
$#   secid    elform      shrf       nip     propt   qr/irid     icomp     setyp
         2         9  1.000000         2         3         0         0         1
$#      t1        t2        t3        t4      nloc     marea      idof    edgset
  0.460000  0.460000  0.460000  0.460000     0.000     0.000     0.000         0
*MAT_ORTHO_ELASTIC_PLASTIC_TITLE
MAT108
$#     mid        ro        ea        eb       gab      prba      prca      prcb
         1 9.0000E-7  3.500000  2.000000  0.500000  0.010000  0.010000  0.010000
$#    sigy      lcss        q1        c1        q2        c2
     0.000         1     0.000     0.000     0.000     0.000
$#      ra        rb        rc       rab
  1.000000  3.000000  1.000000  1.000000
$#    aopt      beat
     0.000     0.000
$#      xp        yp        zp        a1        a2        a3
     0.000     0.000     0.000     0.000  1.000000     0.000
$#      v1        v2        v3        d1        d2        d3
     0.000     0.000     0.000     0.000     0.000     0.000
*PART
$# title
TOPMID
$#     pid     secid       mid     eosid      hgid      grav    adpopt      tmid
         2         1         1         0         0         0         0         0
*SECTION_SHELL_TITLE
single thick
$#   secid    elform      shrf       nip     propt   qr/irid     icomp     setyp
         1         9  1.000000         2         3         0         0         1
$#      t1        t2        t3        t4      nloc     marea      idof    edgset
  0.230000  0.230000  0.230000  0.230000     0.000     0.000     0.000         0
*PART
$# title
BOTSIDE
$#     pid     secid       mid     eosid      hgid      grav    adpopt      tmid
         3         2         1         0         0         0         0         0
*PART
$# title
BOTMID
$#     pid     secid       mid     eosid      hgid      grav    adpopt      tmid
         4         1         1         0         0         0         0         0
*RIGIDWALL_GEOMETRIC_FLAT_MOTION
$#    nsid    nsidex     boxid     birth     death
         0         0         1     0.0001.0000E+20
$#      xt        yt        zt        xh        yh        zh      fric
     0.000     0.000 150.00000     0.000     0.000     0.000     0.000
$#    xhev      yhev      zhev      lenl      lenm
     0.000     0.000     0.000     0.000     0.000
$#    lcid       opt        vx        vy        vz
         3         1     0.000     0.000 -1.000000
         0         0         1     0.0001.0000E+20
     0.000     0.000-150.00000     0.000     0.000     0.000     0.000
```

```
     0.000     0.000     0.000     0.000     0.000
         3         1     0.000     0.000  1.000000
*DEFINE_BOX_TITLE
Bounding Box
$#   boxid       xmn       xmx       ymn       ymx       zmn       zmx
        1-1295.0000 1295.0000-610.00000 610.00000-301.00000 301.00000
*DEFINE_CURVE_TITLE
MAT108-Plastic
$#    lcid      sidr       sfa       sfo      offa      offo    dattyp
         1         0  0.100000  1.000000     0.000     0.000         0
$#              a1                  o1
              0.000             0.020000
           1.000000             0.300000
*DEFINE_CURVE_TITLE
Inflation mass
$#    lcid      sidr       sfa       sfo      offa      offo    dattyp
         2         0&endtim   &inflatem      0.000     0.000         0
$#              a1                  o1
              0.000                0.000
           0.050000             1.000000
           0.100000                0.000
           0.500000                0.000
           0.510000&endmass
           1.100000&endmass
*DEFINE_CURVE_TITLE
Motion
$#    lcid      sidr       sfa       sfo      offa      offo    dattyp
         3         0&endtim     1.000000     0.000     0.000         0
$#              a1                  o1
              0.000                0.000
           0.200000                0.000
           0.250000            50.000000
           0.350000            50.000000
           0.400000                0.000
           0.800000                0.000
           1.100000                0.000
*AIRBAG_SIMPLE_AIRBAG_MODEL
$#     sid    sidtyp      rbid      vsca      psca      vini       mwd      spsf
         1         1         0  1.000000  1.000000     0.000     0.000     0.000
$#      cv        cp         t      lcid        mu         a        pe        ro
 717.00000 1004.0000 300.00000         2  0.700000     0.000 1.0000E-4 1.1640E-9
$#     lou      text         a         b        mw      gasc
         0     0.000     0.000     0.000     0.000     0.000
*DAMPING_GLOBAL
$#    lcid    valdmp       stx       sty       stz       srx       sry       srz
         0  0.500000     0.000     0.000     0.000     0.000     0.000     0.000
*ELEMENT_SHELL
$#   eid     pid      n1      n2      n3      n4      n5      n6      n7      n8
       1       1      50      51      52     117       0       0       0       0
       2       1     109     110     118     108       0       0       0       0
       3       1      58      59      60     119       0       0       0       0
       4       1     116       1       2     120       0       0       0       0
*NODE
$#   nid               x               y               z      tc      rc
       1       1095.5000       609.50000      -10.000000       0       0
       2       1095.5000       585.12000       -5.000000       0       0
       3       1095.5000       560.73999           0.000       0       0
       4       1095.5000       536.35999           0.000       0       0
*END
```

Appendix C

Reduced Input Decks for Full Bag Models: Hybrid Element

```
*KEYWORD
*PARAMETER
I endtim         100R termt    100.00000R inflatem  0.259283R endmass   0.130000
*TITLE
$# title
M191 48x102, L3/4, 170 kPa(abs), 300-200mm void, 9e-7 density(kg,mm,ms,kN,GPa,)
*CONTROL_ACCURACY
$#     osu       inn    pidosu
         1         2         0
*CONTROL_ENERGY
$#    hgen      rwen    slnten     rylen
         2         2         2         2
*CONTROL_TERMINATION
$#  endtim    endcyc     dtmin    endeng    endmas
&endtim            0     0.000     0.000     0.000
*CONTROL_TIMESTEP
$#  dtinit    tssfac      isdo    tslimt     dt2ms      lctm     erode     ms1st
     0.000  0.500000         0     0.000     0.000         0         0         0
$#  dt2msf   dt2mslc     imscl    unused    unused     rmscl
     0.000         0         0                         0.000
*DATABASE_BNDOUT
*DATABASE_ELOUT
*DATABASE_MATSUM
*DATABASE_NCFORC
*DATABASE_NODFOR
*DATABASE_NODOUT
*DATABASE_RCFORC
*DATABASE_RWFORC
*DATABASE_SPCFORC
*DATABASE_TRHIST
$#      dt    binary      lcur     ioopt
  1.000000         3         0         1
*DATABASE_BINARY_D3PLOT
$#      dt      lcdt      beam     npltc    psetid
  1.000000         0         0         0         0
$#   ioopt
         0
*DATABASE_EXTENT_BINARY
$#   neiph     neips    maxint    strflg    sigflg    epsflg    rltflg    engflg
         0         0         3         1         1         1         1         1
$#  cmpflg    ieverp    beamip     dcomp      shge     stssz    n3thdt   ialemat
         0         0         0         1         2         3         2         1
$# nintsld   pkp_sen      sclp    unused     msscl     therm    intout    nodout
         0         0  1.000000                   2         0ALL       ALL
$#    dtdt    resplt
         0         0
*BOUNDARY_SPC_SET_ID
$#      id                                                                heading
         0Hold-mid-x-in-y
$#    nsid       cid      dofx      dofy      dofz     dofrx     dofry     dofrz
         1         0         0         1         0         1         0         1
*SET_NODE_LIST_TITLE
mid-x
$#     sid       da1       da2       da3       da4    solver
         1     0.000     0.000     0.000     0.000MECH
$#    nid1      nid2      nid3      nid4      nid5      nid6      nid7      nid8
        26        84       195       201       277       289       360       374
*BOUNDARY_SPC_SET_ID
$#      id                                                                heading
         0Hold-mid-y-in-x
$#    nsid       cid      dofx      dofy      dofz     dofrx     dofry     dofrz
         2         0         1         0         0         0         1         1
*SET_NODE_LIST_TITLE
mid-y
$#     sid       da1       da2       da3       da4    solver
         2     0.000     0.000     0.000     0.000MECH
$#    nid1      nid2      nid3      nid4      nid5      nid6      nid7      nid8
      1014      1154      1386      1389      1658      1669      1914      1925
*CONTACT_AIRBAG_SINGLE_SURFACE_ID
$#     cid                                                                title
         1SELFCONTACT
$#    ssid      msid     sstyp     mstyp    sboxid    mboxid       spr       mpr
```

```
         1         0         2         0         0         0         0         0
$#      fs        fd        dc        vc       vdc    penchk        bt        dt
     0.000     0.000     0.000     0.000     0.000         0     0.0001.0000E+20
$#     sfs       sfm       sst       mst      sfst      sfmt       fsf       vsf
  1.000000  1.000000     0.000     0.000  1.000000  1.000000  1.000000  1.000000
*SET_PART_LIST_TITLE
ALLPARTS
$#     sid       da1       da2       da3       da4    solver
         1     0.000     0.000     0.000     0.000MECH
$#    pid1      pid2      pid3      pid4      pid5      pid6      pid7      pid8
         1         2         3         4         0         0         0         0
*PART
$# title
TOPSIDE
$#     pid     secid       mid     eosid      hgid      grav    adpopt      tmid
         1         2         2         0         0         0         0         0
*SECTION_SHELL_TITLE
double thick
$#   secid    elform      shrf       nip     propt   qr/irid     icomp     setyp
         2         9  1.000000         2         3         0         0         1
$#      t1        t2        t3        t4      nloc     marea      idof    edgset
  0.460000  0.460000  0.460000  0.460000     0.000     0.000     0.000         0
*MAT_ELASTIC_TITLE
Elastic
$#     mid        ro         e        pr        da        db  not used
         2 9.0000E-7  0.001000  0.490000     0.000     0.000         0
*PART
$# title
TOPMID
$#     pid     secid       mid     eosid      hgid      grav    adpopt      tmid
         2         1         2         0         0         0         0         0
*SECTION_SHELL_TITLE
single thick
$#   secid    elform      shrf       nip     propt   qr/irid     icomp     setyp
         1         9  1.000000         2         3         0         0         1
$#      t1        t2        t3        t4      nloc     marea      idof    edgset
  0.230000  0.230000  0.230000  0.230000     0.000     0.000     0.000         0
*PART
$# title
BOTSIDE
$#     pid     secid       mid     eosid      hgid      grav    adpopt      tmid
         3         2         2         0         0         0         0         0
*PART
$# title
BOTMID
$#     pid     secid       mid     eosid      hgid      grav    adpopt      tmid
         4         1         2         0         0         0         0         0
*PART
$# title
CDTOP
$#     pid     secid       mid     eosid      hgid      grav    adpopt      tmid
         5         3         7         0         0         0         0         0
*SECTION_DISCRETE_TITLE
Spring
$#   secid       dro        kd        v0        cl        fd
         3         0     0.000     0.000     0.000     0.000
$#     cdl       tdl
     0.000     0.000
*MAT_SPRING_GENERAL_NONLINEAR_TITLE
SPringCDdouble
$#     mid      lcdl      lcdu      beta       tyi       cyi
         7        12        13     0.000     0.000     0.000
*PART
$# title
CDBOT
$#     pid     secid       mid     eosid      hgid      grav    adpopt      tmid
         6         3         7         0         0         0         0         0
*PART
$# title
MDTOP
$#     pid     secid       mid     eosid      hgid      grav    adpopt      tmid
         7         3         6         0         0         0         0         0
```

```
*MAT_SPRING_GENERAL_NONLINEAR_TITLE
SPringMDdouble
$#     mid      lcdl      lcdu      beta       tyi       cyi
         6        14        15     0.000     0.000     0.000
*PART
$# title
MDBOT
$#     pid     secid       mid     eosid      hgid      grav    adpopt      tmid
         8         3         6         0         0         0         0         0
*PART
$# title
CDTOPMID
$#     pid     secid       mid     eosid      hgid      grav    adpopt      tmid
         9         3         4         0         0         0         0         0
*MAT_SPRING_GENERAL_NONLINEAR_TITLE
SPringCD
$#     mid      lcdl      lcdu      beta       tyi       cyi
         4         4         5     0.000     0.000     0.000
*PART
$# title
CDBOTMID
$#     pid     secid       mid     eosid      hgid      grav    adpopt      tmid
        10         3         4         0         0         0         0         0
*PART
$# title
MDTOPMID
$#     pid     secid       mid     eosid      hgid      grav    adpopt      tmid
        11         3         3         0         0         0         0         0
*MAT_SPRING_GENERAL_NONLINEAR_TITLE
SPringMD
$#     mid      lcdl      lcdu      beta       tyi       cyi
         3         6         7     0.000     0.000     0.000
*PART
$# title
MDBOTMID
$#     pid     secid       mid     eosid      hgid      grav    adpopt      tmid
        12         3         3         0         0         0         0         0
*RIGIDWALL_GEOMETRIC_FLAT_MOTION
$#    nsid    nsidex     boxid     birth     death
         0         0         1     0.0001.0000E+20
$#      xt        yt        zt        xh        yh        zh      fric
     0.000     0.000 150.00000     0.000     0.000     0.000     0.000
$#    xhev      yhev      zhev      lenl      lenm
     0.000     0.000     0.000     0.000     0.000
$#    lcid       opt        vx        vy        vz
         3         1     0.000     0.000 -1.000000
         0         0         1     0.0001.0000E+20
     0.000     0.000-150.00000     0.000     0.000     0.000     0.000
     0.000     0.000     0.000     0.000     0.000
         3         1     0.000     0.000  1.000000
*DEFINE_BOX_TITLE
Bounding Box
$#   boxid       xmn       xmx       ymn       ymx       zmn       zmx
        1-1295.0000 1295.0000-610.00000 610.00000-301.00000 301.00000
*DEFINE_CURVE_TITLE
MAT108-Plastic
$#    lcid      sidr       sfa       sfo      offa      offo    dattyp
         1         0  0.100000  1.000000     0.000     0.000         0
$#                a1                  o1
             0.000            0.046340
          1.000000            0.447000
*DEFINE_CURVE_TITLE
Inflation mass
$#    lcid      sidr       sfa       sfo      offa      offo    dattyp
         2        0&endtim   &inflatem     0.000     0.000         0
$#                a1                  o1
             0.000               0.000
          0.050000            1.000000
          0.100000               0.000
          0.500000               0.000
          0.510000&endmass
          1.100000&endmass
```

```
*DEFINE_CURVE_TITLE
Motion
$#    lcid      sidr       sfa       sfo      offa      offo    dattyp
         3         0&endtim     1.000000     0.000     0.000         0
$#               a1                  o1
             0.000                0.000
          0.200000                0.000
          0.250000           50.000000
          0.350000           50.000000
          0.400000                0.000
          0.800000                0.000
          1.100000                0.000
*DEFINE_CURVE_TITLE
LCDL CD
$#    lcid      sidr       sfa       sfo      offa      offo    dattyp
         4         0  0.375000  0.486800     0.000     0.000         0
$#               a1                  o1
          -4.000000           -0.600000
          -3.500000           -0.540000
          -3.000000           -0.480000
          -2.500000           -0.410000
          -2.000000           -0.360000
          -1.500000           -0.290000
          -1.000000           -0.225000
          -0.133300           -0.050000
              0.000               0.000
           0.133300            0.050000
           1.000000            0.225000
           1.500000            0.290000
           2.000000            0.360000
           2.500000            0.410000
           3.000000            0.480000
           3.500000            0.540000
           4.000000            0.600000
*DEFINE_CURVE_TITLE
LCDU CD
$#    lcid      sidr       sfa       sfo      offa      offo    dattyp
         5         0  0.425000  0.486800     0.000     0.000         0
$#               a1                  o1
          -3.000000           -2.500000
          -2.500000           -0.500000
          -2.000000           -0.320000
          -1.500000           -0.220000
          -1.000000           -0.150000
          -0.500000           -0.070000
              0.000               0.000
           0.500000            0.070000
           1.000000            0.150000
           1.500000            0.220000
           2.000000            0.320000
           2.500000            0.500000
           3.000000            2.500000
*DEFINE_CURVE_TITLE
LCDL MD
$#    lcid      sidr       sfa       sfo      offa      offo    dattyp
         6         0  0.125000  0.487600     0.000     0.000         0
$#               a1                  o1
          -4.000000           -1.000000
          -3.500000           -0.250000
          -3.000000           -0.150000
          -2.500000           -0.110000
          -2.000000           -0.070000
          -1.500000           -0.045000
          -1.000000           -0.018000
          -0.250000      -5.000000e-04
              0.000               0.000
           0.250000        5.000000e-04
           1.000000            0.018000
           1.500000            0.045000
           2.000000            0.070000
           2.500000            0.110000
           3.000000            0.150000
```

```
           3.500000           0.250000
           4.000000           1.000000
*DEFINE_CURVE_TITLE
LCDU MD
$#    lcid      sidr       sfa       sfo      offa      offo    dattyp
         7         0  0.100000  0.487600     0.000     0.000         0
$#              a1                  o1
          -3.000000          -0.500000
          -2.900000          -0.120000
          -2.000000          -0.045000
          -1.500000          -0.020000
          -1.000000          -0.010000
          -0.500000          -0.003000
              0.000              0.000
           0.500000           0.003000
           1.000000           0.010000
           1.500000           0.020000
           2.000000           0.045000
           2.900000           0.120000
           3.000000           0.500000
*DEFINE_CURVE_TITLE
LCDL CD D
$#    lcid      sidr       sfa       sfo      offa      offo    dattyp
         8         0  0.375000  1.000000     0.000     0.000         0
$#              a1                  o1
          -4.000000          -1.500000
          -3.500000          -1.250000
          -3.000000          -1.125000
          -2.500000          -0.900000
          -2.000000          -0.750000
          -1.500000          -0.550000
          -1.000000          -0.450000
          -0.700000          -0.300000
              0.000              0.000
           0.700000           0.300000
           1.000000           0.450000
           1.500000           0.550000
           2.500000           0.900000
           3.000000           1.125000
           3.500000           1.250000
           4.000000           1.500000
*DEFINE_CURVE_TITLE
LCDU CD D
$#    lcid      sidr       sfa       sfo      offa      offo    dattyp
         9         0  0.500000  1.280000     0.000     0.000         0
$#              a1                  o1
          -3.000000          -1.500000
          -2.700000          -0.750000
          -2.000000          -0.400000
          -1.500000          -0.200000
          -1.000000          -0.050000
          -0.500000          -0.010000
              0.000              0.000
           0.500000           0.010000
           1.000000           0.050000
           1.500000           0.200000
           2.000000           0.400000
           2.700000           0.750000
           3.000000           1.500000
*DEFINE_CURVE_TITLE
LCDL MD D
$#    lcid      sidr       sfa       sfo      offa      offo    dattyp
        10         0  0.500000  1.280000     0.000     0.000         0
$#              a1                  o1
          -4.000000          -2.000000
          -3.500000          -1.750000
          -3.000000          -1.500000
          -2.500000          -1.250000
          -2.000000          -1.000000
          -1.500000          -0.750000
          -1.000000          -0.500000
          -0.500000          -0.250000
```

```
               0.000              0.000
            0.500000           0.250000
            1.000000           0.500000
            1.500000           0.750000
            2.000000           1.000000
            2.500000           1.250000
            3.000000           1.500000
            3.500000           1.750000
            4.000000           2.000000
*DEFINE_CURVE_TITLE
LCDU MD D
$#    lcid      sidr       sfa       sfo      offa      offo    dattyp
        11         0  0.500000  1.280000     0.000     0.000         0
$#              a1                 o1
           -3.000000          -7.000000
           -2.140000          -1.375000
           -2.000000          -1.250000
           -1.500000          -0.800000
           -1.000000          -0.500000
           -0.500000          -0.200000
               0.000              0.000
            0.500000           0.200000
            1.000000           0.500000
            1.500000           0.800000
            2.000000           1.250000
            2.140000           1.375000
            3.000000           7.000000
*DEFINE_CURVE_TITLE
LCDL CD D
$#    lcid      sidr       sfa       sfo      offa      offo    dattyp
        12         0  0.375000  1.000000     0.000     0.000         0
$#              a1                 o1
           -4.000000          -0.600000
           -3.500000          -0.540000
           -3.000000          -0.480000
           -2.500000          -0.410000
           -2.000000          -0.360000
           -1.500000          -0.290000
           -1.000000          -0.225000
           -0.133300          -0.050000
               0.000              0.000
            0.133300           0.050000
            1.000000           0.225000
            1.500000           0.290000
            2.000000           0.360000
            2.500000           0.410000
            3.000000           0.480000
            3.500000           0.540000
            4.000000           0.600000
*DEFINE_CURVE_TITLE
LCDU CD D
$#    lcid      sidr       sfa       sfo      offa      offo    dattyp
        13         0  0.425000  1.000000     0.000     0.000         0
$#              a1                 o1
           -3.000000          -2.500000
           -2.500000          -0.500000
           -2.000000          -0.320000
           -1.500000          -0.220000
           -1.000000          -0.150000
           -0.500000          -0.070000
               0.000              0.000
            0.500000           0.070000
            1.000000           0.150000
            1.500000           0.220000
            2.000000           0.320000
            2.500000           0.500000
            3.000000           2.500000
*DEFINE_CURVE_TITLE
LCDL MD D
$#    lcid      sidr       sfa       sfo      offa      offo    dattyp
        14         0  0.125000  0.995400     0.000     0.000         0
$#              a1                 o1
```

```
          -4.000000           -1.000000
          -3.500000           -0.250000
          -3.000000           -0.150000
          -2.500000           -0.110000
          -2.000000           -0.070000
          -1.500000           -0.045000
          -1.000000           -0.018000
          -0.250000       -5.000000e-04
              0.000                0.000
           0.250000        5.000000e-04
           1.000000            0.018000
           1.500000            0.045000
           2.000000            0.070000
           2.500000            0.110000
           3.000000            0.150000
           3.500000            0.250000
           4.000000            1.000000
*DEFINE_CURVE_TITLE
LCDU MD D
$#    lcid      sidr       sfa       sfo      offa      offo    dattyp
        15         0  0.100000  0.995400     0.000     0.000         0
$#              a1                  o1
          -3.000000           -0.500000
          -2.900000           -0.120000
          -2.000000           -0.045000
          -1.500000           -0.020000
          -1.000000           -0.010000
          -0.500000           -0.003000
              0.000               0.000
           0.500000            0.003000
           1.000000            0.010000
           1.500000            0.020000
           2.000000            0.045000
           2.900000            0.120000
           3.000000            0.500000
*AIRBAG_SIMPLE_AIRBAG_MODEL
$#     sid    sidtyp      rbid      vsca      psca      vini       mwd      spsf
         1         1         0  1.000000  1.000000     0.000     0.000     0.000
$#      cv        cp         t      lcid        mu         a        pe        ro
 717.00000 1004.0000 300.00000         2  0.700000     0.000 1.0000E-4 1.1640E-9
$#     lou      text         a         b        mw      gasc
         0     0.000     0.000     0.000     0.000     0.000
*DAMPING_GLOBAL
$#    lcid    valdmp       stx       sty       stz       srx       sry       srz
         0  0.500000     0.000     0.000     0.000     0.000     0.000     0.000
*ELEMENT_SHELL
$#   eid     pid      n1      n2      n3      n4      n5      n6      n7      n8
       1       1      50      51      52     117       0       0       0       0
       2       1     109     110     118     108       0       0       0       0
       3       1      58      59      60     119       0       0       0       0
       4       1     116       1       2     120       0       0       0       0
*NODE
$#   nid               x               y               z      tc      rc
       1       1095.5000       609.50000      -10.000000       0       0
       2       1095.5000       585.12000       -5.000000       0       0
       3       1095.5000       560.73999           0.000       0       0
       4       1095.5000       536.35999           0.000       0       0
*END
```

List of References

AAR (2004 November). Product Performance Profile for Pneumatic Dunnage.

AAR (2012 January). Product Performance Profile for Pneumatic Dunnage.

Amiot, F., Bornert, M., Doumalin, P., Dupré, J.C., Fazzini, M., Orteu, J.J., Poilâne, C., Robert, L., Rotinat, R., Toussaint, E., Wattrisse, B. and Wienin, J.S. (2013). Assesment of digital image correlation measurement accuracy in the ultimate error regime: mainresults of a collaborative benchmark. *Strain: An International Journal for Experimental Mechanics*, vol. 49, pp. 483–496.

Apedo, K.L., Ronel, S., Jacquelin, E., Bennani, A. and Massenzio, M. (2010). Nonlinear finite element analysis of iflatable beams made from orthotropic woven fabric. *International Journal of Solids and Structures*, vol. 47, pp. 2017–2033.

Blandino, J.R., Johnston, J.D. and Dharamsi, U.K. (2002). Corner wrinkling of a square membrane due to symmetric mechanical loads. *Journal of Spacecraft and Rockets*, vol. 39, pp. 717–724.

Bletzinger, K.U., Jarasjarungkiat, A. and Wüchner, R. (2007). Wrinkling as multiscale phenomenon in numerical analysis of membranes. In: *ECCOMAS Thematic Conference on Multi-scale Computational Methods for Solids and Fluids*.

Boisse, P., Borr, M., Buet, K. and Cherouat, A. (1997). Finite element simulations of textile composite forming including the biaxial fabric behaviour. *Composites: Part B*, vol. 28B, pp. 453–464.

Boisse, P., Gasser, A. and Hivet, G. (2001). Analysis of fabric tensile behaviour: determination of the biaxial tension-strain surfaces and their use in forming simulations. *Composites: Part A*, vol. 32, pp. 1395–1414.

Boisse, P., Hamila, N., Helenon, F., Hagege, B. and Cao, J. (2008). Different approaches for woven composite reinforved from simulation. *International Journal of Materaterial Forming*, vol. 1, pp. 21–29.

Breuer, J.C.M. and Luchsinger, R.H. (2010). Inflatable kites using the concept of tensairity. *Aerospace Science and Technology*, vol. 14, pp. 557–563.

Bridgens, B.N. and Gosling, P.D. (2008). A predictive model for membrane structure design. In: *Textile Composites and Inflatable Structures II*. Springer.

Brueggert, M. and Tanov, R.R. (2002). An LS-DYNA user defined material model for loosely woven fabric with non-orthogonal varying weft and warp angle. In: *7th International LS-DYNA User Conference: Material Technology*.

Cao, J., Akkerman, R., Boisse, P., Chen, J., Cheng, H., de Graaf, E., Gorczyca, J., Harrison, P., Hivet, G., Launay, J., Lee, W., Liu, L., Lomov, S., Long, A., de Luycker, E., Morestin, F., Padvoiskis, J., Peng, X., Sherwood, J., Stoilova, T., Tao, X., Verpoest, I., Willems, A., Wiggers, J., Yu, T. and Zhu, B. (2008). Characterization of mechanical behavior of woven fabrics: Experimental methods and benchmark results. *Composites: Part A*, vol. 39, pp. 1037–1053.

Cao, Z., Yan, J., Fan, F. and Zhang, X. (2011). Experimental research on tensairity. In: *International Conference on Electronic Technology and Civil Engineering (ICETCE)*.

Cavallaro, P.V. (2005 March). Combined in-plane shear and multi-axial tension or compression testing apparatus.

Cavallaro, P.V. (2006). Technology & Mechanics Overview of Air-Inflated Fabric Structures. Tech. Rep., Naval Undersea Warfare Center Division - Newport, Rhode Island.

Cavallaro, P.V., Johnson, M.E. and Sadegh, A.M. (2003). Mechanics of plain-woven fabrics for inflated structures. *Composite Structures*, vol. 61, pp. 375–393.

Cavallaro, P.V. and Quigley, A.M.S.C.J. (2007). Contributions of strain energy and pv-work on the bending behavior of uncoated plain-poven fabric air beams. *Journal of Engineering Fibers and Fabrics*, vol. 2, pp. 16–30.

Cavallaro, P.V., Sadegh, A.M. and Quigley, C.J. (2007). Decrimping behavior of uncoated plain-woven fabrics to combined biaxial tension and shear stresses. *Textile Research Journal*, vol. 77, pp. 403–416.

Cerda, E. and Mahadevan, L. (2003). Geometry and physics of wrinkling. *Physical Review Letters*, vol. 90, pp. 074302–1–074302–4.

Chen, J., Lussier, D.S., Cao, J. and Peng, X.Q. (2002). Materials characterization methods and material models for stamping of plain woven composites. *International Journal of Forming Processes*, vol. 4, pp. 3–4.

Chung, P.W. and Tamma, K.K. (1999). Woven fabric composites - developments in engineering bounds, homogenization and applications. *International Journal for Numerical Methods in Engineering*, vol. 45, pp. 1757–1790.

D'Amato, E. (2001). Finite element modeling of textile composites. *Composite Structures*, vol. 54, pp. 467–475.

Davids, W.G. and Zhang, H. (2008). Beam finite element for nonlinear analysis of pressurized fabric beam-columns. *Engineering Structures*, vol. 30, pp. 1969–1980.

Dridi, S., Morestin, F. and Dogui, A. (2012). Use of digital image correlation to analyse the shearing deformation in woven fabric. *Experimental Techniques*, vol. 36, pp. 46–52.

Drozdov, A.D. and Dusunceli, N. (2013). Modeling of multi-cycle deformation of polymers with various deformation programs. *Multidiscipline Modeling in Materials and Structures*, vol. 9, pp. 4–22.

Dubois, D. and Forsberg, J. (2013). Using LS-OPT for parameter identification and MAT_FABRIC with FORM=-14. In: *9th European LS-DYNA Conference 2013*.

Durville, D. (2008). Finite element simulation of the mechanical behaviour of textile composites at the mesoscopic scale of individual fibers. In: *Textile Composites and Inflatable Structures II*. Springer.

Ehlers, S. and Varsta, P. (2009). Strain and stress relation for non-linear finite element simulations. *Thin Walled Structures*, vol. 47, pp. 1203–1217.

Fichter, W.B. (1966). A theory of inflated thin-wall cylindrical beams. Tech. Rep., NASA, Washington.

Forestier, R., Massoni, E. and Chastel, Y. (2002). Estimation of constitutive parameter using an inverse method coupled to a 3D finite element software. *Journal of Materials Processing Technology*, vol. 125-126, pp. 594–601.

Fuller, R.B. (1975). *Synergetics*. MacMillan.

Galliot, C. and Luchsinger, R.H. (2009). A simple model describing the non-linear biaxial tensile behavior of PVC-coated polyester fabrics for use in finite element analysis. *Composite Structures*, vol. 90, pp. 438–447.

Galliot, C. and Luchsinger, R.H. (2010*a*). The shear ramp: A new test method for the investigation of coated fabric shear behavior - part II: Experimental validation. *Composites: Part A*, vol. 41, pp. 1750–1759.

Galliot, C. and Luchsinger, R.H. (2010*b*). The shear ramp: A new test method for the investigation of coated fabric shear behaviour - part I: Theory. *Composites: Part A*, vol. 41, pp. 1743–1749.

Galliot, C. and Luchsinger, R.H. (2011). Uniaxial and biaxial mechanical properties of ETFE foils. *Polymer Testing*, vol. 30, pp. 356–365.

Garbowski, T., Maier, G. and Novati, G. (2012). On calibration of orthotropic elastic-plastic constitutive models for paper foils by biaxial tests and inverse analysis. *Structural multidisciplinary optimization*, vol. 46, pp. 111–128.

Gorczyca, J.L., Sherwood, J.A., Lussier, D.S. and Chen, J. (2002). Incorporation of material model into LS-DYNA implicit to model the shear behavior of uncured woven-fabric composite materials. In: *7th International LS-DYNA User Conference: Material Technology*.

Grujicic, M., Bell, W., He, T. and Cheeseman, B. (2008). Development and verification of a meso-scale based dynamic material model for plain-woven single-ply ballistic fabric. *Journal of Materials Science*, vol. 43, pp. 6301–6323.

Gründig, L., Moncrieff, E. and Schewe, H. (1995). On the feasibility of using large scale photogrammetry to accurately determine in-service strain distribution across three-dimensional textile roofs. In: *Textile Composites and Textile Structures*. EUROMECH.

Hallquist, J.O. (2006). *LS-DYNA Theory Manual*. Livermore software Technology corporation.

Haßler, M. and Schweirzerhof, K. (2008). Nonlinear finite element analysis of inflatable prefolded membrane structures under hydrostatic loading. In: *Textile Composites and Inflatable Structures II*. Springer.

Hirth, A., Haufe, A. and Olovsson, L. (2007). Airbag simulation with LS-DYNA past - present - future. In: *6th European LS-DYNA User's Conference*.

Holland, D.B., Virgin, L.N., Tinker, M.L. and Slade, K.N. (2002). Geometric scaling properties of inflatable structures for use in space solar power generation. Tech. Rep., American Institute of Aeronautics and Astronautics.

Husain, A., Sehgal, D.K. and Pandey, R.K. (2004). An inverse finite element procedure for the determination of constitutive tensile behavior of materials using miniature specimen. *Computational Materials Science*, vol. 31, pp. 84–92.

Jetteur, P. and Bruyneel, M. (2008). Advanced capabilities for the simulation of membrane and inflatable space structures using SAMCEF. In: *Textile Composites and Inflatable Structures II*. Springer.

Jin, L., Sun, B. and Gu, B. (2011). Finite element simulation of three-dimensional angle-interlock woven fabric undergoing ballistic impact. *The Journal of The Textile Institute*, vol. I, pp. 1–12.

Kajberg, J. and Lindkvist, G. (2004). Characterization of materials subjected to large sstrain by inverse modelling based on in-plaine displacement fields. *International Journal of Solids and Structures*, vol. 41, pp. 3439–3459.

Kolling, S., Haufe, A., Feucht, M. and Bois, P.A.D. (2005). SAMP-1: a semi-analytical model for the simulation of polymers. In: *LS-DYNA Anwenderforum, Bamberg*, pp. 27–52.

Kröplin, B. (2005). Inflated membrane structures on the ground, in the air and in space - a classification. In: *Textile Composites and Inflatable Structures*. Springer.

Lampani, L. and Gaudenzi, P. (2010). Numerical simulation of the behaviour of inflatable structures for space. *Acta Astronautica*, vol. 67, pp. 362–368.

Lecompte, D., Smits, A., Bossuyt, S., Sol, H., Vantomme, J., Hemelrijck, D.V. and Habraken, A.M. (2006). Quality assessment of speckle patterns for digital image correlation. *Optics and Lasers in Engineering*, vol. 44, pp. 1132–1145.

Lee, J.K., Ha, W.P., Lee, J.H., Chae, D.B. and Kim, J.H. (2009). Validation methodology on airbag deployment process of driver side airbag. In: *The 21st International Ttechnical Conference on the Enhanced Safety of Vehicles.*

Lin, H., Cliford, M.J., Long, A.C. and Sherburn, M. (2009). Finite element modeling of fabric shear. *Modeling and Simulation in Materials Science and Engineering*, vol. 17, p. 015008(16pp).

Linhard, J., Wüchner, R. and Bletzinger, K.U. (2008). Introducing cutting patterns in form finding and structural analysis. In: *Textile Composites and Inflatable Structures II.* Springer.

Lomov, S.V., Huysmans, G., Lou, Y., Parnas, R.S., Prodromou, A., Verpoest, I. and Phelan, F.R. (2001). Textile composite: Modelling strategies. *Composites: Part A*, vol. 32, pp. 1379–1394.

Lomov, S.V., Ivanov, D.S., Verpoest, I., Zako, M., Kurashiki, T., Nakai, H. and Hirosawa, S. (2007*a*). Meso-FE modelling of textile ccomposite: road map, data flow and algorithms. *Composites Science and Technology*, vol. 67, pp. 1870–1891.

Lomov, S.V., Ivanov, D.S., Verpoest, I., Zako, M., Kurashiki, T., Nakai, H., Molimard, J. and Vautrin, A. (2007*b*). Full-field strain measurement for validation of meso-FE analysis of textile composeites. *Composites: Part A*, vol. 39, pp. 1218–1231.

Luchsinger, R.H. (2006). Adaptable Tensairity. In: *International Conference on Adaptable Building Structures.*

Luchsinger, R.H., Pedretti, A., Pedretti, M. and Steingruber, P. (2004*a*). The new structural concept Tensairity: Basic principals. In: *Proceedings of the Second International Conference of Structural Engineering, Mechanics and Computation.*

Luchsinger, R.H., Pedretti, M. and Reinhard, A. (2004*b*). Pressure induced stability: From pneumatic structures to Tensairty. *Journal of Bionics Engineering*, vol. 1(3), pp. 141–148.

Luchsinger, R.H., Sydow, A. and Crettol, R. (2011). Structural behaviour of asymmetric spindle-shaped Tensairity girders under bending loads. *Thin-Walled Structures*, vol. 49, pp. 1045–1053.

Maurin, B. and Motro, R. (2005). Fabric membranes cutting pattern. In: *Textile Composites and Inflatable Structures.* Springer.

Milani, A.S. and Nemes, J.A. (2004). An intelligent inverse method for characterization of textile reinforced thermoplastic ccomposite using a hyperelastic constitutive model. *Composites Science and Technology*, vol. 64, pp. 1565–1576.

Mohammed, U., Lekakou, C., Dong, L. and Bader, M.G. (2000). Shear deformation and micromechanics of woven fabrics. *Composites: Part A*, vol. 31, pp. 299–308.

Moncrieff, E. (2005). Systems for lightweight structure design: The state-of-the-art and current developments. In: *Textile Composites and Inflatable Structures*. Springer.

Nilakantan, G., Keefe, M., Bogetti, T.A., Adkinson, R. and Gillespie, J.W. (2010). On the finite element analysis of a woven fabric impact using multiscale modeling techniques. *International Journal of Solids and Structures*, vol. 47, pp. 2300–2315.

Pauletti, R.M.O. (2008). Static analysis of taut structures. In: *Textile Composites and Inflatable Structures II*. Springer.

Pedretti, M. (2004). Tensairity. In: *European Congress on Computational Methods in Applied Sciences and Engineering*.

Peng, X.Q. and Cao, J. (2005). A continuum mechanics-based non-orthogonal constitutive model for woven composite fabrics. *Composites: Part A*, vol. 36, pp. 859–874.

Plagianakos, T.S., Teutsch, U., Crettol, R. and Luchsinger, R.H. (2009). Static response of a spindle-shaped Tensairity column to axial compression. *Engineering Structures*, vol. 31, pp. 1822–1831.

Pronk, A.C.D. and Houtman, R. (2005). Making Blobs With a Textile Mould. In: *Textile Composites and Inflatable Structures*. Springer.

Rumpel, T., Schweizerhof, K. and Haßler, M. (2005). Efficient finite element modelling and simulation of gas and fluid support membrane and shell structures. In: *Textile Composites and Inflatable Structures*. Springer.

Stander, N., Roux, W., Goel, T., Eggleston, T. and Craig, K. (2012). *LS-OPT User's Manual - A Design Optimization and Probabalistic Analysis Tool for the Engineering Analyst*. Livermore software Technology corporation.

Stein, M. and Hedgpeth, J.M. (1961). Analysis of partly wrinkled membranes. Tech. Rep., NASA, Washington.

Stimpfle, B. (2008). Structural air - pneumatic structures. In: *Textile Composites and Inflatable Structures*. Springer.

Suhey, J.D., Kim, N.H. and Niezrecki, C. (2005). Numerical modeling and design of inflatable structures - application to open-ocean-aquaculture cages. *Aquaculture Engineering*, vol. 33, pp. 285–303.

Sutton, M.A., Wolters, W.J., Peters, W.H., Ranson, W.F. and McNeill, S.R. (1983). Determination of displacement using an improved digital correlation method. *Image and Vision Computing*, vol. 1, no. 3, pp. 133–139.

Tan, P., Tong, L. and Steven, G.P. (1997). Modeling for predicting the mechanical properties of textile composites - a review. *Mechanical Properties of Textile Composites*, vol. 28A, pp. 903–922.

Tarczewski, R. (2005). Post-tension modular inflated structures. In: *Textile Composites and Inflatable Structures*. Sprnger.

Tarfaoui, M., Drean, J.Y. and Akesbi, S. (2001). Predicting the stress-strain behavior of woven fabrics using the finite element method. *Textile Research Journal*, vol. 71, pp. 790–795.

Tripathi, D. (2002). *Practical Guide to Polypropylene*. Rapra technologhy LTD.

Venter, M.P. (2011). *Development and Validation of a Numerical Model for an Inflatable Paper Dunage Bag Using Finite Element Methods*. Master's thesis, Department of Mechanical and Mechatronic Engineering, Stellenbosch University.

Venter, M.P. and Venter, G. (2012). Overview of the development of a numerical model for an inflatable paper dunage bag. *Packaging Technology and Science*, vol. 25 (8), pp. 467–483.

Wagner, R. (2005). On the design process of tensile structures. In: *Textile Composites and Inflatable Structures*. Springer.

Wagner, R. (2008). Kinematics in tensioned structures. In: *Textile Composites and Inflated Structures II*. Springer.

Wang, C.G., Du, H.F.T.X.W. and Wan, Z.M. (2007). Wrinkling prediction of rectangular shell-membrane under transverse in-plane displacement. *International Journal of Solids and Structures*, vol. 44, pp. 6507–6516.

Wang, J. (2010). Corpuscular method for airbag deployment simulations in LS-DYNA. In: *LSTC Training*.

Wang, J.T. and Johnson, A.R. (2003). Deployment simulation methods for ultra-lightweigh inflatable structures. Tech. Rep., NASA and US Army Research Laboritory.

West, A.C. and Adams, D.O. (1997). Investigating fiber tow crimping effcts in braided composite materials. *Experimental Techniques*, vol. September, pp. 15–18.

Wever, T.E., Plagianakos, T.S., Luchsinger, R.H. and Marti, P. (2010). Effect of fabric webs on the static response of spindle-shaped Tensairity columns. *Journal of Structural Engineering*, vol. 4, pp. 410–418.

Witowski, K., Feucht, M. and Stander, N. (2011). An effect curve matching metric for parameter identification using partial mapping. In: *8th European LS-DYNA Users Conference, Strasbourg*.

Wong, Y.W. and Pellegrino, S. (2005). Wrinkling in square membranes. In: *Textile Composites and INflatable Structures*. Springer.

Wong, Y.W. and Pellegrino, S. (2006). Wrinkled membranes part III: Numerical simulations. *Mechanics of Materials and Structures*, vol. 1, pp. 63–95.

Zhou, J.M., Qi, L.H. and Chen, G.D. (2006). New inverse method for identification of constitutive parameters. *Transactions of Nonferrous Metals Society of China*, vol. 16, pp. 148–152.